PLACER GOLD PROVENANCE IN THE BLACK HILLS CREEK, WEST-CENTRAL YUKON: INSIGHT FROM GRAIN MORPHOLOGY AND GEOCHEMISTRY

Mark Higgins

Submitted in Partial Fulfilment of the Requirements

For the Degree of Bachelor of Sciences, Honours

Department of Earth Sciences

Dalhousie University, Halifax, Nova Scotia

April 19 2012

Distribution License

DalSpace requires agreement to this non-exclusive distribution license before your item can appear on DalSpace.

NON-EXCLUSIVE DISTRIBUTION LICENSE

You (the author(s) or copyright owner) grant to Dalhousie University the non-exclusive right to reproduce and distribute your submission worldwide in any medium.

You agree that Dalhousie University may, without changing the content, reformat the submission for the purpose of preservation.

You also agree that Dalhousie University may keep more than one copy of this submission for purposes of security, back-up and preservation.

You agree that the submission is your original work, and that you have the right to grant the rights contained in this license. You also agree that your submission does not, to the best of your knowledge, infringe upon anyone's copyright.

If the submission contains material for which you do not hold copyright, you agree that you have obtained the unrestricted permission of the copyright owner to grant Dalhousie University the rights required by this license, and that such third-party owned material is clearly identified and acknowledged within the text or content of the submission.

If the submission is based upon work that has been sponsored or supported by an agency or organization other than Dalhousie University, you assert that you have fulfilled any right of review or other obligations required by such contract or agreement.

Dalhousie University will clearly identify your name(s) as the author(s) or owner(s) of the submission, and will not make any alteration to the content of the files that you have submitted.

If you have questions regarding this license please contact the repository manager at dalspace@dal.ca.

Grant the distribution license by signing and dating below.

_____ _____

Name of signatory Date

ABSTRACT

Bedrock gold sources for rich placer gold deposits in West Central Yukon have been elusive since the 1898 Klondike gold rush. Poor bedrock exposure in an area that escaped Cenozoic glaciation has hindered the effectiveness of traditional exploration techniques. This study applies morphological and geochemical analysis to determine the provenance of gold grains at six placer gold operations in the Black Hills Creek (BHC) watershed, a south-flowing tributary of the Stewart River, to help identify local gold sources. The flatness index = [(a + b)/2c] of gold particles was determined using a binocular microscope and imaging software in which the long (a), intermediate (b), and short (c) axes were measured. Bulk-gold fineness is defined by the ratio of [Au/(Ag + Au)*1000] and provides information about source-rock. Fineness values were measured using microprobe analysis. Flatness has been shown to increase with downstream transport, e.g. high measured flatness values (>7.0) would suggest reworking of grain shape during transport. Contributing areas for each placer site were determined by ArcGIS watershed analysis.

Grains from the four northern placers (Sites 1 to 4) have similarly low flatness indices with averages of 5.0, 4.8, 5.4, and 4.3, suggesting short to moderate transport distances (less than 10 km). Local bedrock sources are implied and fineness values, generally less than 800 are similar to published data from the Eureka Dome. In contrast, grains from the southern two placer deposits show a broad range of flatness indices from 3.9 to 24.0, and a range of fineness values (650 to 900) which indicate provenance from multiple sources. Proximal sources were found to contribute significant portions of grains to the southern sites, and the geochemical signature of these short travelled grains has helped to better understand the mineralization style of bedrock exploration targets unique to the catchment areas of sites 5 and 6.

Keywords: Yukon Tanana Terrane, Tintina Gold Province, Particle flatness, electron microprobe, gold fineness, geochemical fingerprinting

Table of Contents

LIST OF FIGURES

LIST OF TABLES

ACKNOWLEDGEMENTS

I am very appreciative to the exploration team at Smash Minerals Corp, Adrian Fleming, Dennis Arne, Chris Pennimpede and Chris Siron for providing the funding and geological material to complete this project. Their on-going interest in the study and requests for monthly updates helped move this project forward. I would also like to thank Kyle Landry, Gordan Brown and Dan Macdonald for their advice and technical expertise in grain imaging, sample preparation and EMP analysis. Co-supervisor Richard Cox, Honours co-ordinator Martin Gibling and my sister Jenna are thanked for their guidance and timely feedback on chapters throughout the writing process. Additionally my peers in the Honours 2012 class for valuable feedback and motivation throughout the year. Finally I would express a sincere thanks to my supervisor Mike Young for suggesting the project and mentoring me throughout this experience.

CHAPTER 1: INTRODUCTION

1.1 Problem Statement

The central Yukon, located within the Tintina Gold Belt (Fig. 1.1) has a long history of prolific placer gold mining, where grains of gold are eroded from bedrock sources and accumulate in river channels. This type of segregation is due primarily to the high specific gravity of gold (19.3 g/cm^3), and has played a major role in the mining history of the Yukon, with estimated production of over 300 tonnes since the Klondike gold rush of 1898 (Lowey, 2006). However, few bedrock gold discoveries of equivalent scale have been discovered, prompting numerous explanations of this unusual abundance. Earlier studies suggested that the gold was sourced from hydrothermally enriched sediments, which were then re-concentrated into placer deposits (Tempelmen-Kluit, 1982). The theory of hypogene (near surface) alteration was again proposed by Dusfrene et al. (1987), and even supported by Knight et al. (1999b). The new hypothesis for formation of the gold-rich placer systems suggests deep in situ weathering of disseminated, low gold-grade bedrock sources with subsequent fluvial concentration of resistant material (quartz and gold) as the primary mechanism (Lowey, 2006). Recent studies south of the Klondike (Dumula and Mortensen, 2002; Mortensen et al., 2004; Mackenzie and Craw, 2009) suggest that the bedrock sources exist, are potentially economic, and are just recently being discovered, such as the newly defined White Gold District (Fig. 1.2; Mackenzie et al., 2009). The White Gold District occurs 80 km south of the Klondike region in a separate drainage system where the bedrock geology remains poorly understood due to limited bedrock exposure. (<2%).

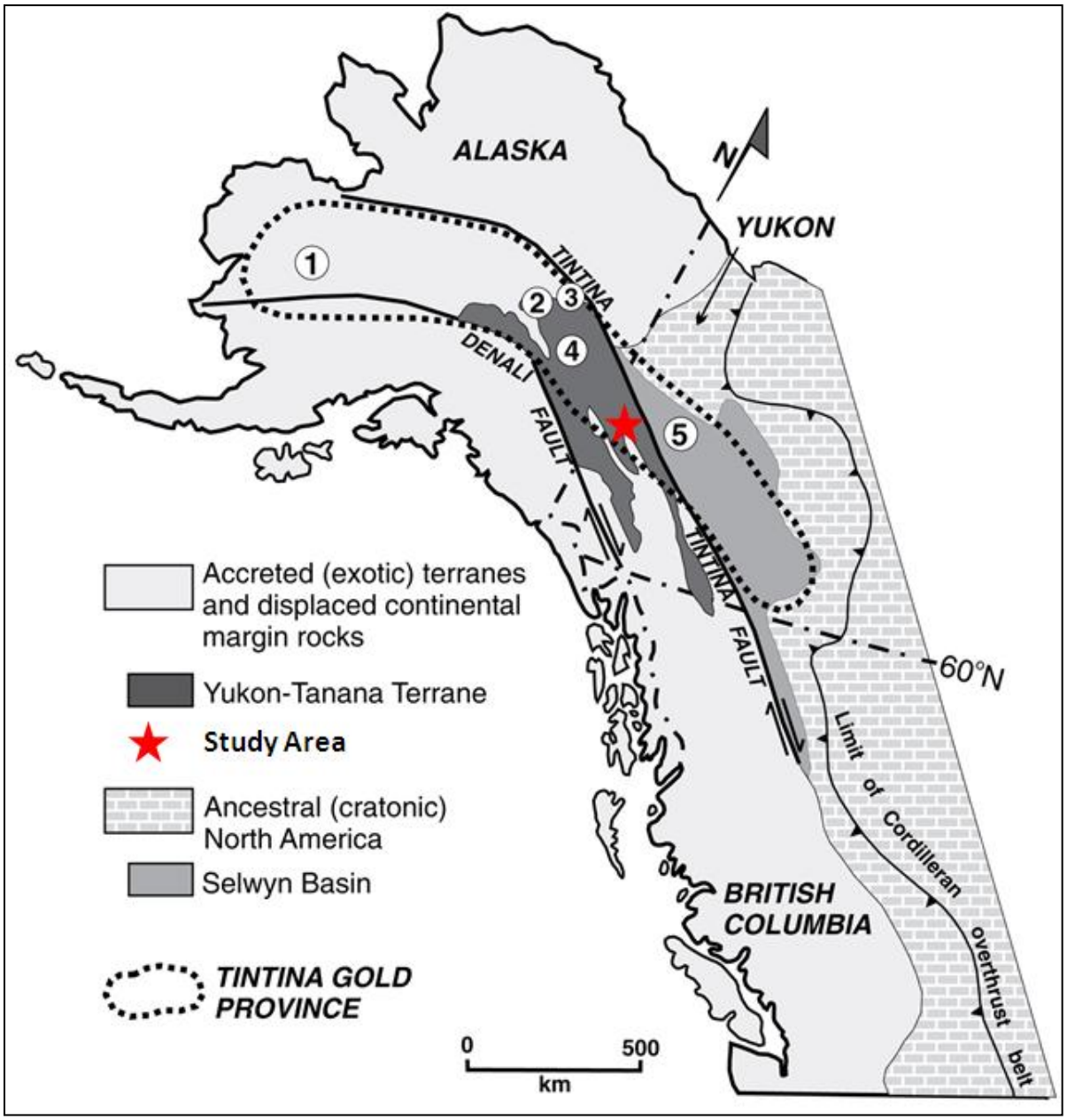

Figure 1.1 Geological Setting of the Tintina Gold Province and the Yukon Tanana Terrane. Modified from Mair et al (2006). Circled number indicate significant gold deposits (>1Moz).

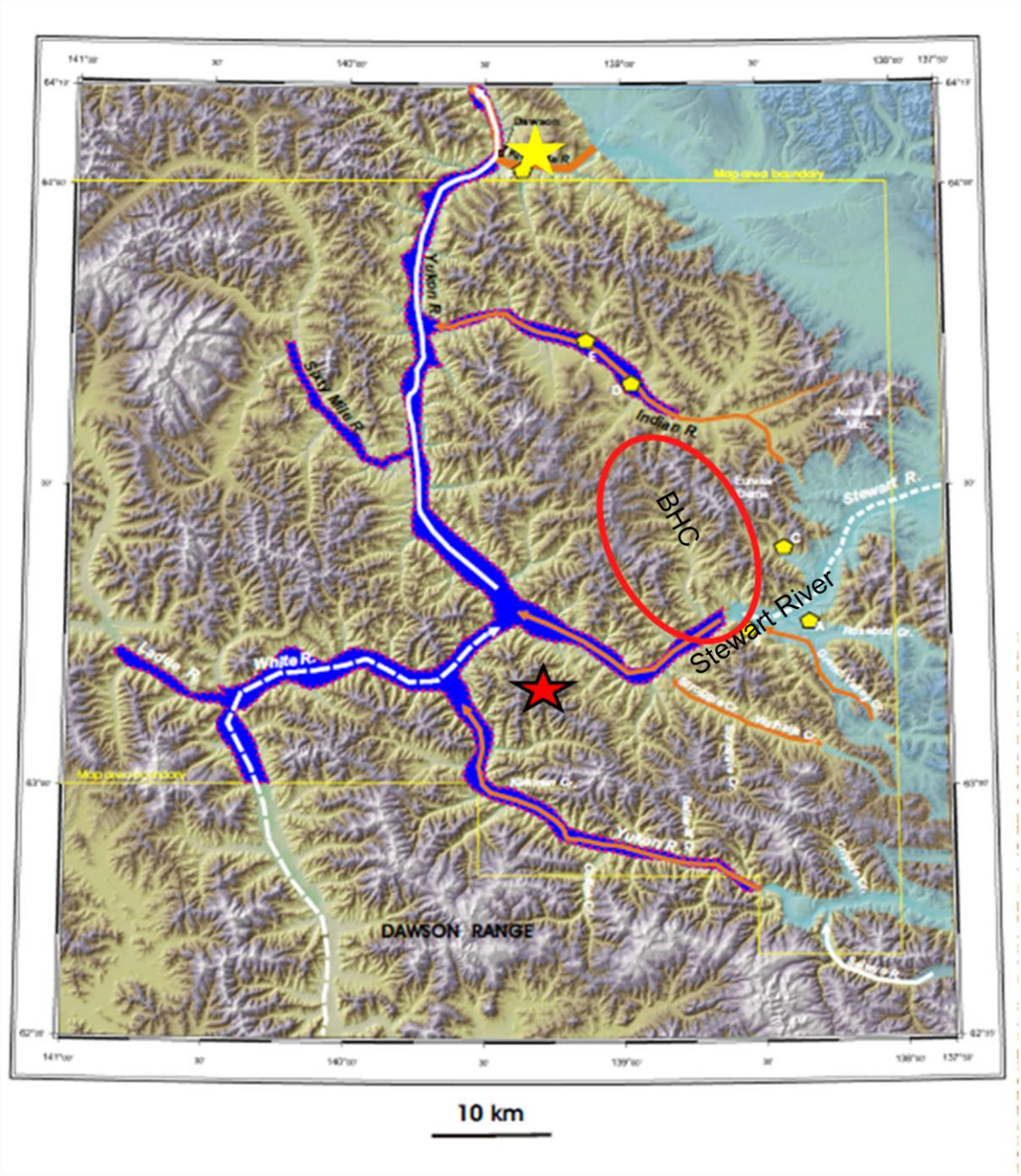

Figure 1.2 Geography of the West-Central Yukon. Modified from Jackson et al.(2009). Light blue indicated the limit of Cenozoic Glaciation, proposed by Jackson et al. (2009). Dark Blue is "Glacial Lake Yukon". Highlighted in red is the Study Area, the Black Hills Creek (BHC) Watershed, a south flowing tributary of the Stewart River. Note that while valley glaciers in the Stewart River approached the study area, no evidence of glaciation is present in the BHC. Yellow star highlights Dawson City, the center of the famous 1898 gold Rush, approx. 60 to 80 km north of the study area. Highlighted with the red star is the recently discovered Golden Saddle Deposit (>1 M oz), sparking the new Yukon Gold Rush, in the area south of the Klondike.

Specifically, the Black Hills Creek watershed (Fig. 1. 2) has produced over 100,000 oz of placer gold since 1970 (Chapman et al., 2011). In the Klondike where the source of placer gold has been attributed to small, mesothermal gold-bearing quartz vein systems formed during Paleozoic to Mesozoic orogenesis with little economic potential (Chapman et al., 2010). In contrast, recent exploration projects in the White Gold District have discovered at least two deposits of mineable scale (Fig 1.2), the Golden Saddle deposit in 2008 (>1Moz) (Mackenzie and Craw, 2009), and the Coffee deposit in 2009 (Wainwright et al., 2010). These discoveries were made using systematic soil sampling along the ridge tops with follow-up tightly spaced grid soil sampling, highlighting the effectiveness of unconventional exploration techniques in this type of covered terrain.

Compositional studies of placer gold grains in the west-central Yukon have shown that the alloy composition, (Au-Ag-Hg-Cu-Pb) reflects that of the source from which it was liberated and can be used to identify the geochemical signature of the source of the placer gold grains (Knight et al., 1999b; Mortensen et al., 2004; Dumula and Mortensen 2002; Chapmanet al., 2010; Chapman, 2011). Additionally, the relationship between gold grain morphology (flatness, roundness, overall shape and texture) and distance of fluvial transport has been well established in various geographic settings, including the Yukon (Knight et al., 1999a), New Zealand (Youngson and Craw, 1999), South Africa (Hallbauer and Utter, 1977) and Chile/Bolivia (Townley et al., 2003). These studies have resulted in semi-quantitative values which allow for estimates of fluvial transport distances based on morphological analysis of gold grains.

Building on recent and ongoing regional placer gold studies in the central Yukon (Chapman et al., 2011; Chapman et al., 2010; Dumala et al., 2002; Knight et al., 1999b,), this study aims to use geochemical fingerprinting coupled with distance to source estimates from the physical characteristics of gold grains and to investigate the provenance of placer gold from a single watershed, the Black Hills Creek (BHC). In order to determine the source of the placer gold, samples from six active placer operations along the BHC and some of its northern tributaries have been purchased by the sponsoring company, Smash Minerals Corp. The technique of extracting gold at each of these operations is proprietary. Knight et al. (1999a) suggested that bulk sampling directly from the miners is preferred, as it minimizes the possibility of grain sorting and stratigraphic bias. The objectives of this study are twofold: 1) to trace the provenance of placer gold grains from each operation using transport distance estimates and geochemical correlations between alloy compositions in the gold grains and geochemical compositions in soil, rock and stream sediment samples, and 2) using this data, provide insight into the mineralization style(s?) of the gold deposits contributing to the placer operations in the BHC watershed.

1.2 Regional Geology

1.2.1 Bedrock Geology

The goldfields of the west-central Yukon are located in the Tintina Gold Province, host to numerous world class gold deposits. Northeast of the study area, the Tintina Fault, which shows dextral strike (Fig. 1.1) responsible for 450 km of offset since the mid Cretaceous (Ryan and Gordey, 2002). Basement rocks in the study area, near the northern extent of the Stewart River, are metasedimentary, metaplutonic and metavolcanic Paleozoic rocks, and form part of Yukon Tanana Terrane (YTT) (Ryan and Gordy, 2002). The largest terrane in

the NW Cordillera (Nelson and Colpron, 2007), the YTT is composed predominantly of early Paleozoic clastic sedimentary rocks subsequently intruded by felsic and mafic plutonic rocks all of which were variably deformed and metamorphosed into quartz and mica schists and mafic and felsic orthogneisses (Ryan and Gordy, 2002). The YTT was accreted to the North American craton during the Permian during which time peak metamorphic conditions reached greenshist to upper amphibolite facies. Extensive recrystallization and metamorphism of the basement rocks produces a series of gneisses and schists. Thrust stacking continued until the mid-Cretaceous, followed by regional extension, in the form of brittle normal faulting, and the initiation of the Tintina Fault (Lowey, 2006).

A wide range of bedrock gold occurrences are thought to exist close to the study area, including: early Jurassic orogenic quartz-carbonate veins throughout the region but most common in the Klondike (Chapman et al., 2010), intrusion-related mineralization in the Moosehorn range to the east (Dumula and Mortensen 2002) and late Cretaceous fault breccias and related high-level hydrothermal mineralization in the Eureka Dome and Golden Saddle (Mackenzie and Craw, 2009). All of the basement rocks are unconformably overlain by post-accretionary, gold-bearing conglomerates and sandstones of the Tantalus Formation, in turn overlain by the upper Cretaceous basalts and rhyolites of the Carmacks Group (Ryan and Gordy, 2003; Lowey, 2006).

1.2.2 Cenozoic Landscape Evolution

The late Cenozoic history of the Stewart River area has been described by numerous workers (Jackson et al., 2009; Duk-Rodkin et al., 2004). Jackson et al. (2009) concluded that the gentle topography of the Klondike plateau is part of a formerly low-lying erosional surface which has been experiencing long term uplift of approximately 0.9cm/ka. This has resulted in deep valley incision of up to 600m since the deposition of the Carmacks Group in the late Cretaceous. Systematic mapping was carried out on Cenozoic sediments, including the classification of gravels as fluvial or glacio-fluvial to determine the extent of Cenozoic glaciations. The results indicated that the extent of glaciation was less than previously proposed by Duk-Rodkin et al. (2004) (Fig. 1.2). Gravel samples within the BHC are made up of a variety of clast lithologies all sourced from within the BHC watershed and no evidence of glacial input was determined (Jackson et al., 2009). The Cenozoic stratigraphy of placer pits in the BHC suggests that the maximum extent of glaciation during the late Pliocene and early Pleistocene extended just east of the confluence of the BHC and the Stewart River (Fig 1.2). Jackson et al. (2009) concluded that the BHC watershed escaped glaciation and sedimentation was dominated by alluvial and colluvial processes, and that the drainage pattern of the BHC (north-to-south) was also unaffected.

1.2.3 Previous Work on Regional Gold Composition

Previous regional studies have used placer gold grain composition to establish placer-lode gold correlations (Knight et al., 1999b; Dumula and Mortensen 2002; Mortensen et al., 2004; Chapman et al. 2010; 2011). While the effects of surface processes is known to change the composition on the rims of gold grains, either by the removal of silver, or by addition of new gold, the affected rim accounts for a very small volume of the grain. Silver

leaching occurs under surface conditions, and varies in different climatic and temperate settings. Results of these studies suggest that the alloy composition (Au, Ag, Cu and Hg) of the core of gold grains reflects the composition of its lode source. Previous workers in western-Yukon have generated geochemical signatures from gold occurrences in the Klondike, the White River area and the Eureka Dome (Fig 1.5). The details of these geochemical fingerprints are outlined in Chapter 4, and are used in an attempt to identify the bedrock sources of individual placers.

1.2.4 Placer Formation

A model for placer formation in the Klondike was proposed by Lowey (2006) and has been extended to this study area based on similarities in bedrock geology and Cenozoic geomorphic history. Lowey (2006) suggested that the dominant mechanisms controlling placer formation were tectonic uplift and climate variations associated with glacial cycles. In this model, the bedrock undergoes deep chemical weathering of the micas and feldspars, producing a thick residual saprolite chemically enriched in resistant minerals such as quartz and gold. Formation of the saprolites could have initiated soon after the late Cretaceous gold mineralization, when the Yukon was situated further to the south. These warmer climatic conditions may have impacted the degree to which silver leaching of grain rims. This change would have a regional effect, and does not complicate comparisons with other regional placer gold grains. This enriched saprolite is then eroded and concentrated in river beds during uplift and fluvial incision (Fig 1.3 A to D). The placer gold-rich White Channel Gravels in the Klondike are likely a product of enrichment process (Lowey, 2006). This period of deep chemical weathering was facilitated by a warmer climate which culminated at 5 Ma as the climate cooled entering cyclical glacial advances during the

Pliocene-Pleistocene (Lowey, 2006). Subsequent cycles of deep stream incision, and isostatic uplift re-concentrated the high-level gravels into low-level gravels of Pleistocene-Holocene age (Fig 1.3E and F).

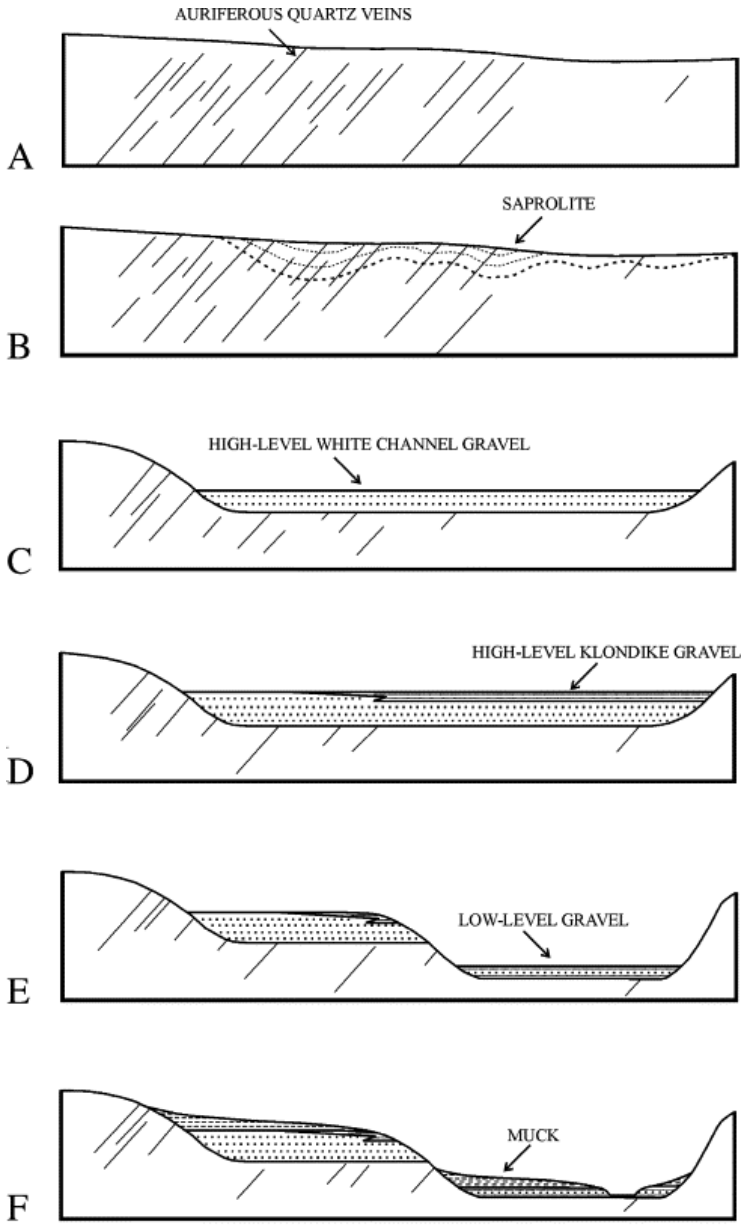

Figure 1.3 Placer formation model from Lowey (2006), describing how gold is first concentrated in high level gravels by chemical weathering (A to D), and then physically re-concentrated into lower level placer deposits by uplift, stream incision. Gold particles are left behind, as less dense material is carried away in stream suspension.

Within the stream itself, gold particles are concentrated by a combination of factors including transport sorting, density sorting and changes in stream gradient. Additionally, bed roughness is the most important process, with coarse gravel bars, and the large void spaces between clasts, ideally suited for trapping heaving minerals. If the bedload being transported is smooth surface gold particles are less likely to be caught (Lowey, 2006). While the processes of formation can be extended to the White Gold District based on similarities of climate and topography, the gravel clasts in the BHC are locally derived, dominated by gneiss and schist, distinct from the quartz-rich White Channel Gravels. This localised variation is likely the result of less intense weathering and shorter transport distances within the BHC watershed.

1.3 Local Geology

Local geology of the BHC was described by MacKenzie and Craw (2011) and is shown in Figure 1.4 and summarized schematically in Figure 1.5. The bedrock of the BHC study area consists of four predominant lithological units. The oldest unit is the Late Devonian-Mississippian quartzite metasediments, a banded, locally fissile, quartz-muscovite schist, interlayered with biotite gneiss and schist. These metasediments were intruded first by Mississippian–Permian hornblende gneiss, which locally can be found inter-layered with minor amounts of pyroxenite, and later by felsic orthogneiss, defined by biotite-quartz-feldspar mineralogy. These units contain a strong southeast-striking, shallow to moderately dipping tectonic fabric, formed in the late Permian during northeast-directed ductile shortening and reactivated in the Jurassic. Numerous NW-NE trending steeply dipping brittle faults cut across all rocks and typically mantle the creek beds including the main Black Hills Creek (Fig 1.4).

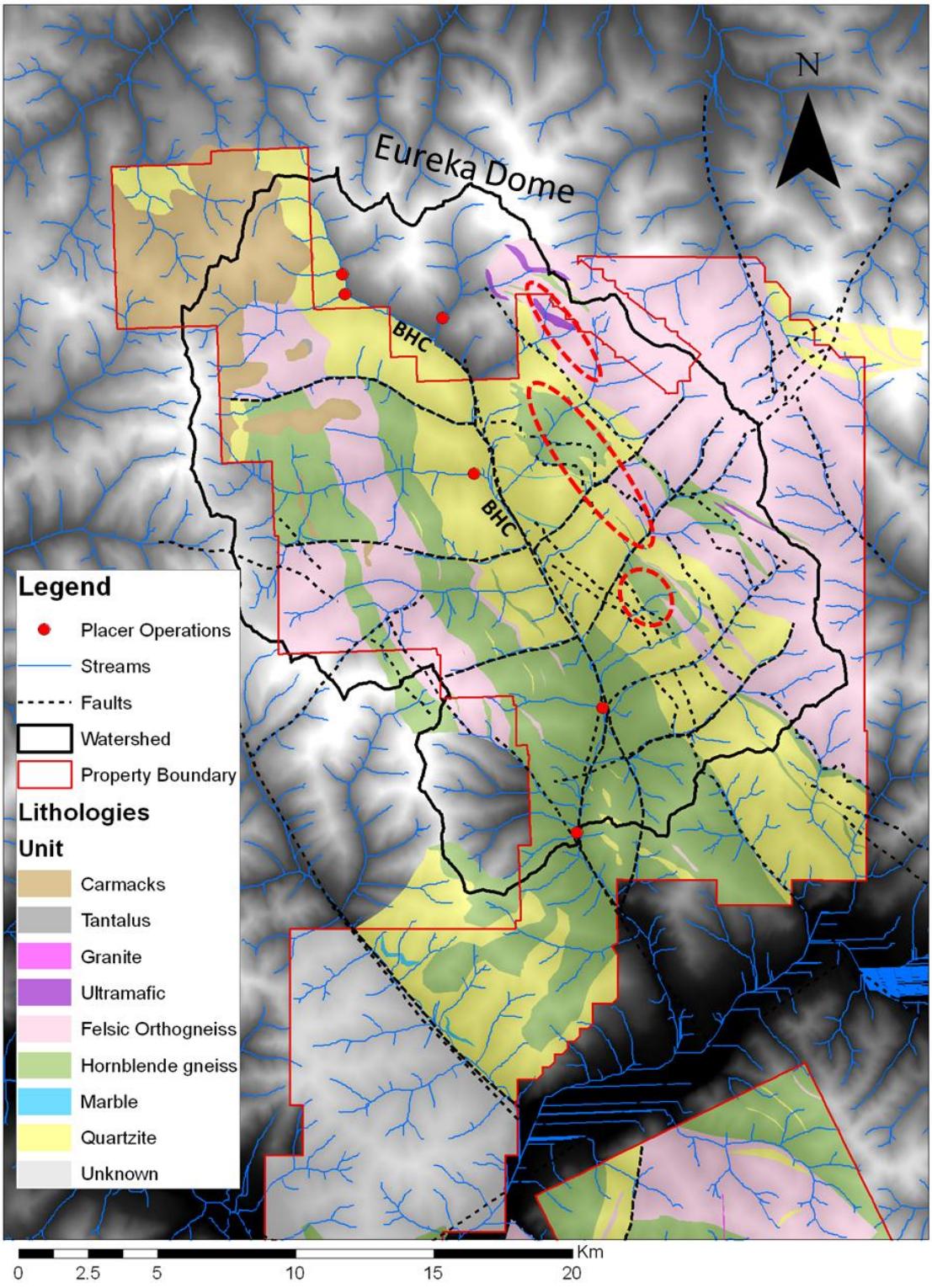

Figure 1.4 Local Geology of the Black Hills Creek watershed. See legend and text for structural and lithological descriptions. Red dots indicate the 6 placer sample locations, while red circles indicate target areas identified by Smash Minerals, and discussed in text. Mapped faults in the BHC are often the sites of modern streams, including the main valley

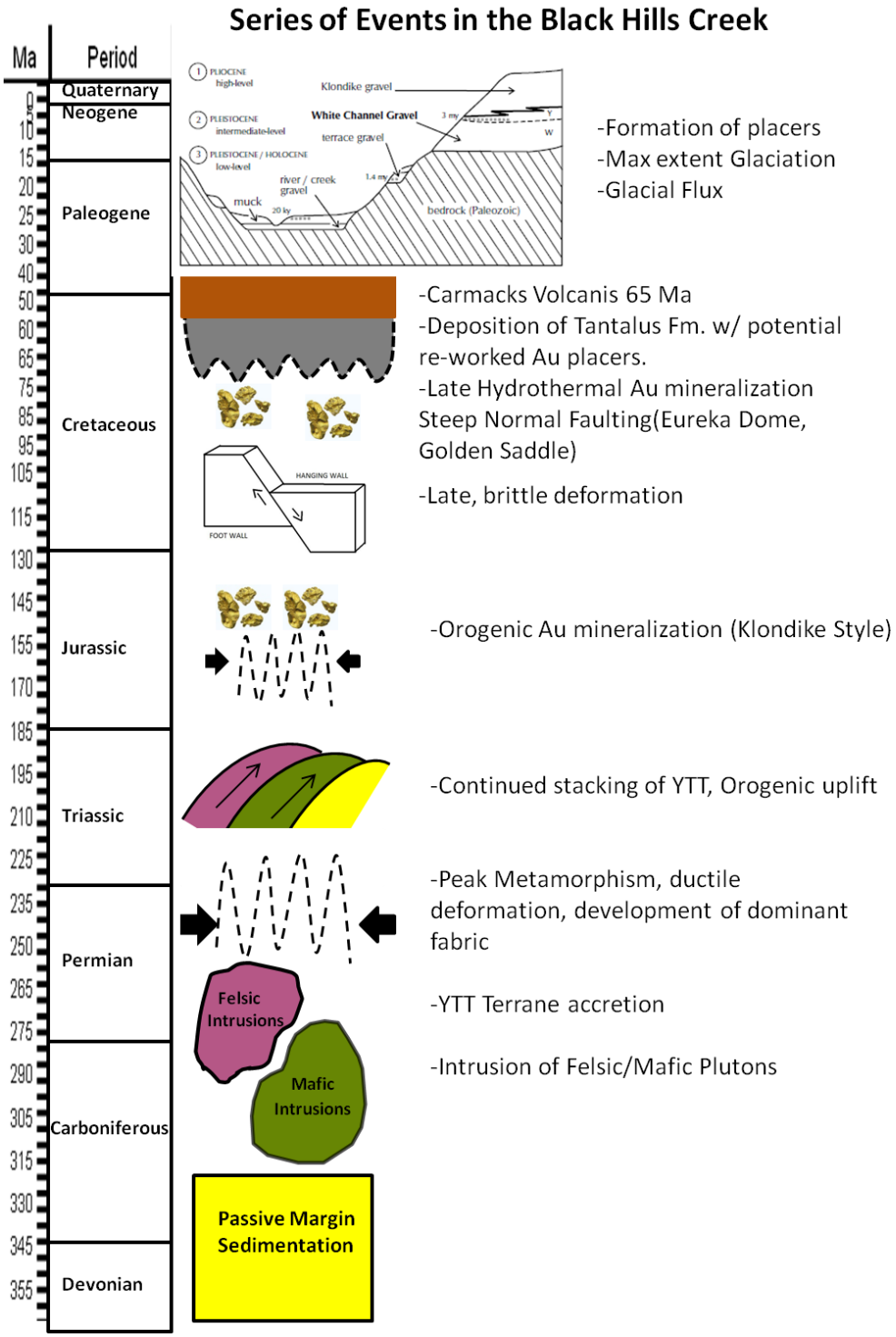

Figure 1.5 Schematic composite stratigraphic column depicting important geological events in the BHC area. Events from Devonian to Late Cretaceous are taken from Mackenzie and Craw (2011), while the Cenozoic events are summarized from Lowey (2006) and Jackson et al. (2009). Uppermost figure showing concentration of low level placers taken from Lowey (2006).

Unconformably overlying all rock types and exposed in the northwest part of the study area are the Cretaceous Tantalus Formation and Carmacks Group, exposed in the northwest part of the study area (Fig 1.4).

1.4 Mineralization in the Black Hills Creek

MacKenzie and Craw (2011) summarized the controls on mineralization within the BHC, highlighting several structural and contact zones with good potential to host gold-bearing hydrothermal zones. These targets were identified by anomalous gold in soil samples, determined by tightly spaced grid soil sampling. The most promising of these targets are the contact zones between the metaplutonic rocks (both mafic and felsic) and the metasedimentary rocks. As a result of the competence contrast, these contact zones were strongly deformed during the Permian compressional deformation resulting in highly sheared and fissile contact zones. As regional compression gave way to extension in the mid Cretaceous, these structurally prepared weakened zones were brittlely faulted and hydrothermally altered. Locally, quartz veins filling fractures and fault breccias formed in these weakened zones, and contain hematite, magnetite, pyrite and gold mineralization. The weakened zones were continuously reactivated by an unknown number of brittle deformation events through to the late Cretaceous (MacKenzie and Craw, 2011). These structural controls on mineralization in the BHC compare favourably with Cretaceous hydrothermal mineralization in the Golden Saddle and Coffee deposits to the southeast (Fig 1.2). In the Golden Saddle deposit, late Cretaceous normal faults were used as pathways for hydrothermal mineralization, best developed in felsic gneisses and metasediments (MacKenzie and Craw, 2010).

Chapman et al. (2011) completed a microgeochemical characterization of placer gold grains in the Stewart River area, including several samples from placer operations in the BHC. They concluded that two distinct geochemical signatures define placer gold grains found in the BHC. The first is a low sulphidation epithermal style of mineralization characterized by the presence of sulphide, sulfotellurides and sulfosalt inclusions, attributed to epithermal sources in the Eureka Dome (Fig. 1.4). The second signature is for grains which only rarely contain simple pyrite and base metal sulphide inclusions. The authors attributed these grains to orogenic style mineralization similar to that found in the Klondike. This approach of characterising placer grains based on inclusions suite may develop improved geochemical signatures, but has some limitations. Inclusions are easily removed by surface processes and were found in a very small proportion, between 2 and 9%, of grains in from five sites in the BHC. Chapman et al. (2011) characterized the second mineralization style (including identified exploration targets) in the BHC as orogenic based primarily on the absence of sulfotellurides and sulfosalt inclusions. In contrast, this study utilizes a multidisciplinary approach, using distance to source estimates, combined with mapping and trenching of known gold occurrences in order to associate geochemical signatures with mineralization styles inferred from the field observations.

1.6 Scope of the Study

The objectives of this project are to systematically characterize placer gold grain morphologies and geochemical composition of gold grains from the six different placer operations in the BHC (Fig 1.4). Physical characteristics provide information on the degree of physical weathering, a proxy for the distance of fluvial transport. Examining the range in

grain morphologies within each sample permits the determination of transport distances. The transport distance estimates and an extensive database containing whole-rock geochemistry of soil, rock and stream sediments throughout the study are used in order to identify potential contributing bedrock sources. Geochemical signatures associated with contributing bedrock sources may be characterized, in terms of their Ag, Au, Hg and Cu concentrations. This in turn may provide insight into the mineralization style, and distinguish between bedrock sources outside the Smash Property (Eureka Dome), and potential deposits inside the claim boundary.

CHAPTER 2: METHODOLOGY

The following chapter outlines the methods used in this study of the gold grain provenance. In attempting to characterize the source of the gold grains, analyses of grain morphology and geochemistry are combined with a detailed geographic analysis of the Black Hills Creek watershed.

2.1 Grain Morphology

Gold is a malleable native element whose morphological features evolve more rapidly than silicates in response to physical weathering. Very little shape modification is attributed to the mass transport of colluvial gold, significant morphological changes in gold particles is attributed to distance of travel, or time spent in fluvial systems (Youngson and Craw, 1999). Changes in particle morphology are attributed to two physical weathering processes. The most important is hammering, the re-distribution of mass caused by contact with other grains, and abrasion, scraping, or re-working, of the surface by moving particles. Several classification schemes have been developed to characterize the morphological evolution of gold grains, notably Knight et al. (1999a) and refined by Youngson and Craw (1999). Methods set out in these studies were used in order to characterize placer deposits based on the number of, and proximity to, bedrock gold sources.

When gold grains are released from their rock source by weathering they are assumed to be undeformed and display a considerable variability in shape (three dimensional) and outline (two dimensional). Hammering and abrasion are the two mechanisms by which the shape of gold particles is transformed in the fluvial environment (Knight et al., 1999a). The factors which have been used to establish relationships between grain morphology and

distance of fluvial transport are as (1) particle outline, (2) particle roundness, (3) surface textures, (4) particle folding and (5) particle flatness.

2.1.1 Particle Outline

In the case of gold particles, outline refers to the dimensional description of a grain lying flat with its short axis perpendicular to the surface. Outline was chosen rather than shape as there is no classification scheme capable of accurately describing grains in three dimensions as there are infinite possibilities (Knight et al., 1999a). Close to the source, gold grains typically have complex or branched outlines (Fig. 2.1). Within the first few kilometers of transport, rounding of particles by abrasion gradually transforms branched outlines to complex, and eventually equant outlines. Further downstream, rounding and flattening continue to change the outline, and proportions of equant and elongate grains are much higher.

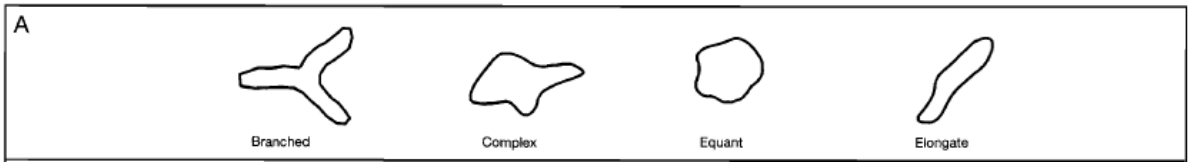

Figure 2.1 Examples of typical shape outlines of grains. From left to right, the outlines represent morphological evolution in the fluvial environment. From Youngson and Craw (1999)

2.1.2 Particle Roundness

Particle roundness does not refer to a measure of grain sphericity (3-D), but rather the degree to which angular edges have been "smoothed out". Rounding of gold grains begins as soon as they enter the fluvial environment, and is achieved by hammering and abrasion. Studies in New Zealand concluded that only some rounding occurs within the first 10 km

(Youngson and Craw, 1999), however similar studies in the Klondike (Knight et al., 1999a) suggest that grain roundness increases rapidly and is the most sensitive measure of transportation distance during the first 5 km, after which it remains essentially unchanged. Coarse gold particles, where the a-axis is > 3 mm, are found to be more rounded than smaller particles with identical transport histories (Youngson and Craw, 1999), as they tend to more difficult to suspend, resulting in more travel time and *in situ* abrasion than smaller grains. This observation suggests that rounding is an accurate indicator of transport distance only when comparing grains of similar sizes. The degree of roundness was determined visually under binocular microscope.

2.1.3 Surface textures

Primary gold particles display original crystal habit and surface features. Close to the source, liberated gold grains display angular edges and crystalline surface texture. With increased transportation distance, abrasion has the largest actively erasing these primary surface textures as grains become smoother and more polished in appearance. The latest event tends to be preferentially preserved and must be carefully interpreted. Surface textures are best observed using high-resolution secondary electron images not possible within the scope of this study. However observations were made through binocular microscope.

2.1.4 Folding

Particle folding is attributed to extreme "flattening" and is an indicator of significant fluvial transportation (Youngson and Craw, 1999). It can be difficult to observe as the evidence is often removed by subsequent flattening and particle breaking. A broken fold

can be identified by the presence of an extremely flat and sharp edge. The presence of folded particles was recorded when observed in some samples.

2.1.5 Flatness

Knight et al. (1999a) concluded that flatness was the best indicator of transport distance of more than 3 km, but becomes less reliable within 3 km of the source. In the Klondike, flatness was seen to increase rapidly within the first 5 km and more slowly afterward. Flattening is achieved primarily by "hammering", the collision of other particles into the malleable gold. This re-distribution of mass increases the surface area and decreases the thickness of gold particles. Eventually, once the grain has been sufficiently flattened, it increases the entrainment potential to a critical value where fluvial transport is much easier (Youngson and Craw, 1999).

2.2 Sampling Strategy

Over 500 gold grains from six placer operations from the study area (Fig 1.4) were analysed with the methodology outlined in this chapter. Samples from each placer pit were obtained from the operators and subdivided into different groups on the basis of morphology. For each of the 6 sites, subsamples of "A" type grains refer to those with irregular shapes and angular edges (the least morphologically evolves). "B" type grains refer grains with edges that have experienced some rounding, but still with irregular shapes (more evolved morphological features). "C" type grains were identified on the basis of well rounded edges, and polished, smooth, surfaces (the most morphologically evolved). Representative samples were selected from each subsample, and a detailed analysis of the physical characteristics (flatness and roundness) of each grain was recorded, resulting in a

morphological data set of about 150 grains. From there, approximately 100 grains were prepared for geochemical analysis.

2.3 Microscope Methods

A Zeiss binocular microscope was used to record the three principal axes of gold grains. While the grain was lying on its "preferred surface" (Fig. 2.2a), the long (a) and intermediate (b) axes were imaged and measured using PAXit imaging software. Grains were then turned and rested on the edge of a petrie dish to allow for imaging and measurement of the short (c) axis (Fig. 2.2b). These measurements allowed for the calculation of Cailleux flatness index [(a+b)/2c]. In simple terms, the length, width and thickness of gold grains produces a numerical classification of grain flatness. This is a simple method for determining the mass redistribution and flattening of a gold grain during fluvial transport. A margin of error for this measurement is estimated at 5 to 10 μm, only becoming an issue where grains are extremely thin (<100 μm), and calculated flatness indices are quite high. The increasing uncertainty with increasing flatness was considered when interpreting the results. Several limitations need to be considered when calculating

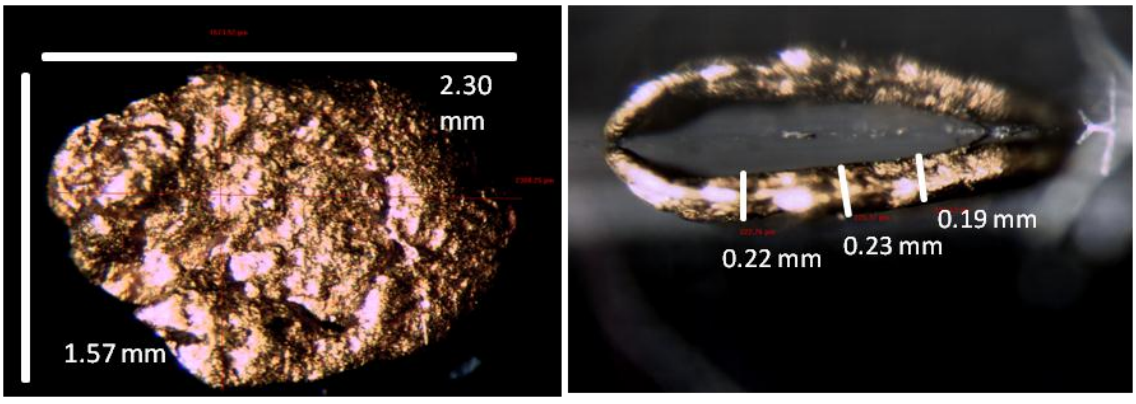

Figure 2.2 Example of grain measurement technique achieved using a binocular microscope and PAXit imaging software. Measurements of the three major axis are used to calculate the Cailleux flatness index = [(a+b)/2c].

flatness of a gold particle. Although Knight et al. (1999a) stated that the majority of new gold in the Klondike is cubic/spherical (i.e Cailleux flatness=1) in some cases flatness can be inherited from the primary crystal shape (Youngson and Craw, 1999). To avoid this possible source of error, flatness was considered only when grains showed some evidence of rounding and deviated from the primary crystal habit. Alternatively, grain armoring, a process where placer gold grains are transported within mineral aggregates can protect a grain from the effects of hammering and abrasion, allow for grains to appear primitive, or proximal in nature, when in fact they have travelled much greater distances. This is a potential source of outliers when calculating grain flatness, and needs to be considered when interpreting the results.

Previous studies in the Yukon (Knight et al., 1999a), the Otago region of New Zealand (Youngson and Craw 1999), and the Andes (Townley et al., 2003) have examined the relationship between grain flatness and distance from source. These studies have resulted in semi-quantitative curves relating both the Shilo [((a+b)/2c)-1] and the Cailleux flatness index [(a+b)/2c)] to distance of fluvial transport. These studies have notable differences. Knight et al. (1999a) confined their analysis to grains between 0.5 and 1.5 mm and concluded that grains flatten rapidly within the first 5 km of fluvial transport. Youngson and Craw (1999) measured the flatness of grains with a-axis length of up to 3 mm and argued that significant flattening occurs only after transport of at least 10 km. They proposed critical flatness values of 3 and 7 to constrain transport distances to less than 1 and less than 10 km, respectively. Ideally, grains between 0.5 and 1.5 mm in maximum length were characterized, but in some samples, the availability of these grain sizes was limited, and measurements were performed on larger grains as well. The flatness-distance

curves from these two studies (Fig. 2.3), as well as the critical flatness values defined by Youngson and Craw (1999), should be adequate to make first-order estimations of transport distances, especially in instances where high values of gold targets have already been identified and soil anomalies suggest the presence of potential sources.

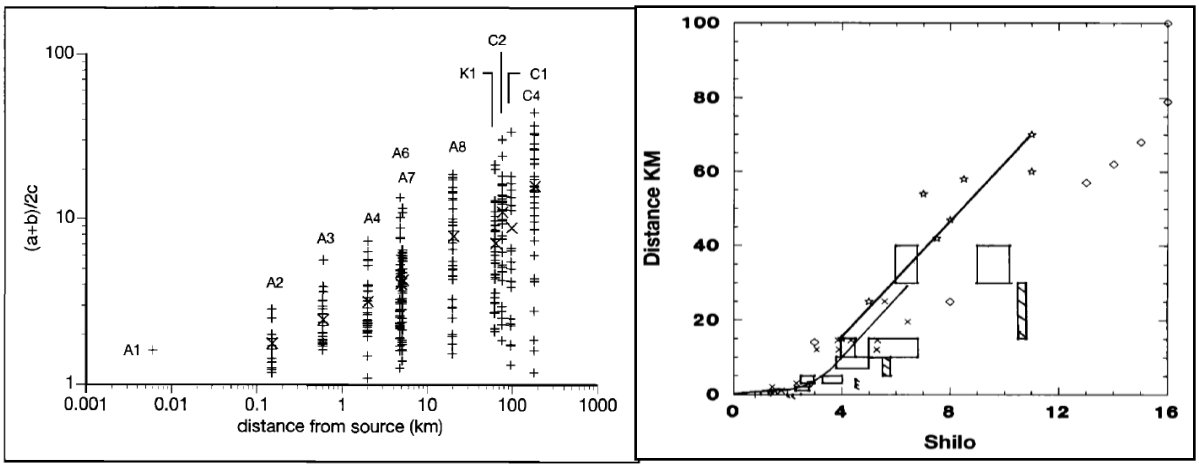

Figure 2.3 Flatness-Distance relationship established in New Zealand by Youngson and Craw (1999), left, and a Yukon curve from Knight et al. (1999). Note the log scale in the New Zealand example. The Yukon curve (right) references the Shilo shape factor in the x axis, which is the same as the Cailleux flatness index, except minus 1. Cailleux = (a+b)/2c, and Shilo = [(a+b)/2c]-1.

Finally, one needs to consider that placer gold deposits often host grains from multiple sources, with different morphological characteristics. These subgroups may include particles from both proximal and distal sources, particles eroded from different levels of the same source, particles recycled from paleo-placers (e.g Tantalus Formation) and folded particles, which have re-thickened, been hammered, and may appear unfolded.

2.3 Geochemical Signatures

2.3.1 Electron Microprobe (EMP)

Microprobe chemical analysis and back-scattered electron images (BSE) were obtained using the JEOL 8200 electron microprobe at Dalhousie University. The instrument is equipped with 5 wavelength dispersive spectrometers and an energy dispersive detector (EDS). Representative gold grains from each of the sample site were mounted in 2.5 cm epoxy slides and carbon coated. BSE Images were obtained using a beam current of 2.0 x 10^{-8} nA and acceleration voltage of 15 kV. These images were used to identify weathered zones, silver leached rims, and were helpful to select specific point for EMP analysis. Elemental concentrations of Au, S, As, Fe, Hg, Sb, Ni, Pb, Ag and Cu were determined. Particular X-rays used were as follows: Au, Hg and Pb used Mα X-Ray. S, Fe, Cu, Ni were determined with Kα X-ray line, and As, Ag and Sb used Lα X-rays. Calibrations were performed before each analytical run using PETJ spectrometer crystal (Sb, Pb, Ag, Au, S and Hg), LIFH crystal (As, Ag, Sb), and TAPH crystal for As. Gold and silver were standardized with pure standards of each metal. Mercury and copper were standardized to cinnabar and chalcopyrite standards respectively. Count times for each element were 20 000 ms. Average detection limits for unknown gold samples were as follows: Au=0.13 Ag=0.03 Cu=0.042 wt% and Hg= 0.12 wt%. Approximately 100 grains were mounted in thin section for microprobe analysis. A minimum of two points were analysed from each grain to test for data re-producibility, or any compositional zoning within individual grains. Duplicate points were taken every 10 to 15 points. Standards of 80% Au and 20% Ag were analysed three times and were found to have 81.44, 81.99, 81.9 Au, and 17.98, 17.91 and 17.95 Ag, respectively. Standards of 100% Ag were run three times and found to have 100.7, 101.0

and 101.1 respectively. The underestimation of silver during analysis of gold/silver standards has been attributed to the ZAF correction. Following the methods of Dumula and Mortensen (2002), only analyses totalling to more than 95% were considered of good quality and considered in the discussion. A total of 63 grains yielded 115 quality point analyses, 11 grains from site 1, 6 from site 2, 12 from site 3, 11 from site 4, 16 from site 5, and 6 from site 6. Low totals from EPMA analyses were likely due to sample preparation (e.g. scratches on the slide). Additionally, 2-D WDS elemental maps and line scans were performed to analyze compositional zoning due to weathering.

2.3.2 Interpreting geochemical signatures

Compositional studies of placer gold grains are a common exploration strategy in covered areas. In the Western Yukon, several researchers (Knight et al., 1999b; Chapman et al., 2001, 2010, 2011; Dumula and Mortensen 2002; Mortensen et al., 2004, 2005) have demonstrated some of the ways in which geochemistry can effectively link placer gold grains to bedrock sources and styles of mineralization. In his extensive study of placer gold composition in the Klondike, Knight et al. (1999b) showed that the major (Au, Ag, Hg, Cu) element core composition of placer grains is unaffected by fluvial transport and reflects the composition of the bedrock source from which it was liberated. Bulk-gold fineness is used to characterize the gold to silver ratio of a particular grain. It is defined by the ratio of [Au/(Ag + Au)*1000] with values reported in weight percent. Pure gold has a fineness of 1000, and pure silver has a fineness value of 0. Totals of EMP analyses were typically between 95 to 97 wt%. The 3 to 5 % discrepancy is less than ideal, and may have a small effect when calculating gold fineness. Recent studies (Mortensen et al., 2004; Chapman et al., 2010, 2011) have applied additional geochemical techniques to improve correlations

between placer gold grains, bedrock sources and mineralization styles. Micro inclusions, within individual placer grains, are thought to reflect the ore and gangue mineralogy of their bedrock source. This technique requires a large sample size and extensive EMP analyses. Inclusions are also known to be removed due to abrasion and hammering, so are much less common in far-travelled grains.

The removal of silver from the rims of gold grains is common in placer gold grains, and is a product of chemical weathering, and can result in rims between 1 and 20 microns in thickness. Rim thickness was investigated by Knight et al. (1999b) as a potential indicator of transport distance. The author concluded that the leached rims are much less reliable as transport indicators than flatness and roundness. The processes which remove silver from the rims of gold grains begin immediately after the liberation of the grain from bedrock, and are active while the particle is in a colluvial or soil horizon. By the time the grain enters the fluvial system, some leaching may already have occurred. Additionally, once the grain enters the fluvial system, physical erosion begins. The same factors which control the morphology of the grains (mentioned above) are actively re-working the outer edges of the grain, removing the silver leached rim, or introducing some compositional variation from sediment load. While there is a positive relationship between rim thickness and transport, it is a much less reliable indicator than morphological characteristics mentioned earlier.

2.4 Watershed Analysis

In attempting to find the source of placer gold grains sampled from the Black Hills Creek, it is necessary to have some understanding of the stream network. With the use of ArcGIS, we were able to determine which tributary streams of the Black Hills Creek are

contributing to each placer pit, as well as the total area from which the sediments in each location could be derived.

2.4.1 Digital Elevation Model (DEM)

A digital elevation model (DEM) is defined as any numeric or digital representation of the elevation of a surface (Tarboton et al., 1991). The data are displayed in regular square grids, or cells, where each grid is surrounded by eight adjacent cells. The resolution of a DEM depends on the distance between sample points. Before using a DEM for quantitative analysis, "sinks" must first be removed from the dataset. Some sinks are natural and represent an area of internal drainage, while some are simply errors within the DEM. They are corrected digitally by filling in the sinks with the lowest neighbouring elevation value.

The next step involves assigning flow direction for each cell. The flow direction is defined as the direction in which water will flow out of a cell (Jenson and Domingue, 1988). This means that the direction of flow will be into a surrounding cell with the lowest elevation. In ArcGIS, the flow direction tool automatically calculates flow direction for each cell. Flow direction data sets are then converted to flow accumulation datasets, which calculate the number of cells contributing flow to any particular cell. Each contributing cell is assigned a value of one. If the number of contributing cells exceeds an assigned threshold value, then the cell in question is deemed part of a drainage network.

With the stream network defined, further information can be obtained using GIS tools such as Stream Order and Stream Link, designed to classify streams based on their number on tributaries. First-order streams are drainages which consist entirely of overland flow, and have no component of upstream concentrated flow. If two first-order streams

intersect, then the result is a second-order stream. When two second-order streams converge, they result in a third-order stream.

2.4.2Calculating contributing Area

ArcGIS records the flow direction of each cell, and combines that information with the stream network. Every cell which may contribute sediment to a particular point in a stream can be outlined using the Watershed tool. Due to continued incision and uplift, the placer sites are located on the banks of modern streams so the point of the stream closest to the placer operation was used to calculate the contributing area.

In order to constrain the source area requires that assumptions about the Cenozoic history of the study area are true. While fluvial systems have deeply incised the Klondike Plateau, the region has not experienced significant tectonic deformation since the Late Cretaceous (Jackson et al., 2009). With no tectonic re-arrangement, and the absence of glacial landscape evolution, the geographic outline of watersheds and drainage divides are assumed to be stable since fluvial incision began. Thus, sediments in the modern streams and placer deposits are locally sourced, with no evidence of glacial input during the Cenozoic.

At this stage, we are able to select any point along a stream, and calculate which cells in the DEM, and thus which streams, contribute sediment. In the context of this study, these tools are used to trace the source of placer samples found in the streams, and determine the area that is potentially contributing sediment (eroded gold grains) to the placer pits. A potential weakness in this approach is the contribution of gold from the gold bearing Tantalus Formation, the sedimentary cover rocks found in the northern part of the Black

Hills Creek watershed. Any gold that has been re-worked from this unit could have originated from a bedrock source much further away.

CHAPTER 3: RESULTS

INTRODUCTION

The following chapter presents the results of morphological characterization and geochemical analyses for each of the six sample sites, from north to south (sites 1 to 6; Fig. 3.1). Each site is described in terms of its location, catchment area, grain morphology, and geochemical analysis of the individual sub-groups. Stratigraphic descriptions, provided by Jackson et al. (2009), were available for sites 4 and 5, and are summarized in this chapter.

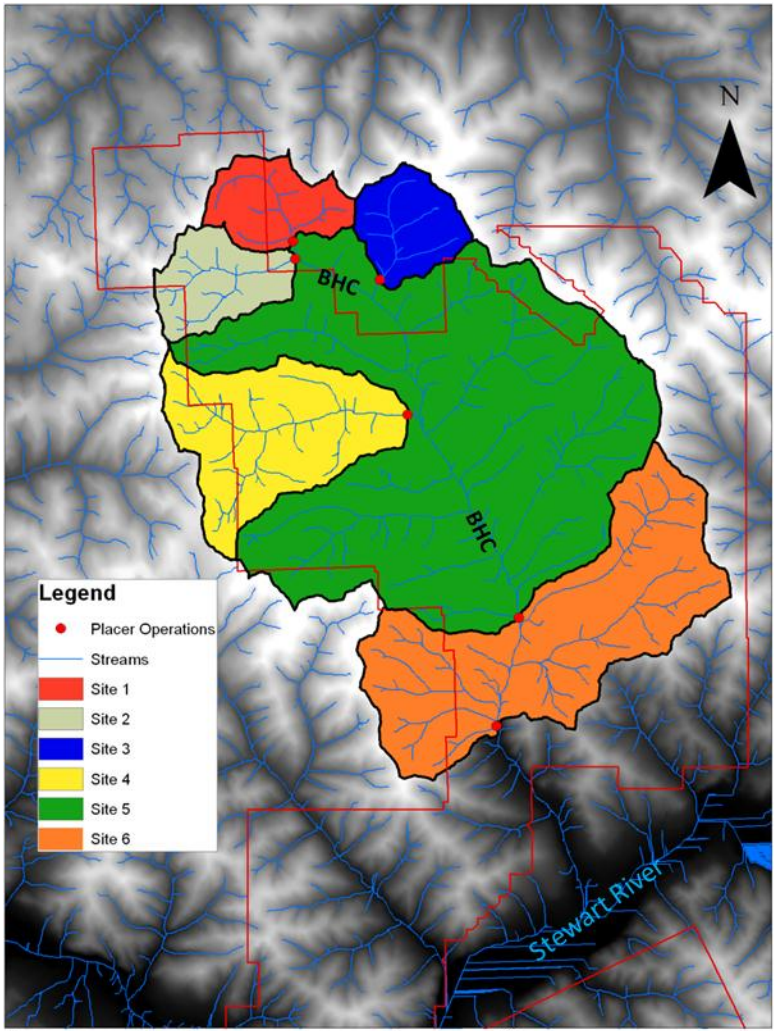

Figure 3.1 Map of the Black Hills Creek (BHC) Watershed, outlining the catchment areas (colour coded) of each placer operation. Note that for sites 5 and 6 include the catchment includes those of sites 1-4. Property boundary is highlighted in red.

3.1 Site 1

Eighty-five gold grains were obtained from site 1, which drains several small tributary valleys in the headwaters of the BHC (Fig 3.1). The contributing area was calculated to be 17 km^2. Grains were divided into the three subgroups with morphological results summarized in Figure 3.2. Thirteen A type grains range in size from 1 to 3 mm, with complex shapes, and pitted surface textures. Edges are angular to slightly rounded (Fig 3.3 A and B). Flatness measurements range from 2.6 to 4.4 (Table 3.1). A total of 55 B type grains make up the bulk of the sample, and range from 1 to 3 mm, and have complex to equant outlines (Fig 3.3 C and D). Most are pebble-like in appearance, and the edges are slightly rounded. Ten C type grain make up a third small sub group, and consist of large grains ranging from 2 to 6 mm (Fig 3.3, E and F). They are mostly equant in grain shape, with the exception of two elongated and rounded, needle shaped grains. These C type grains were too large to make inferences about flatness, and were left out of the histogram.

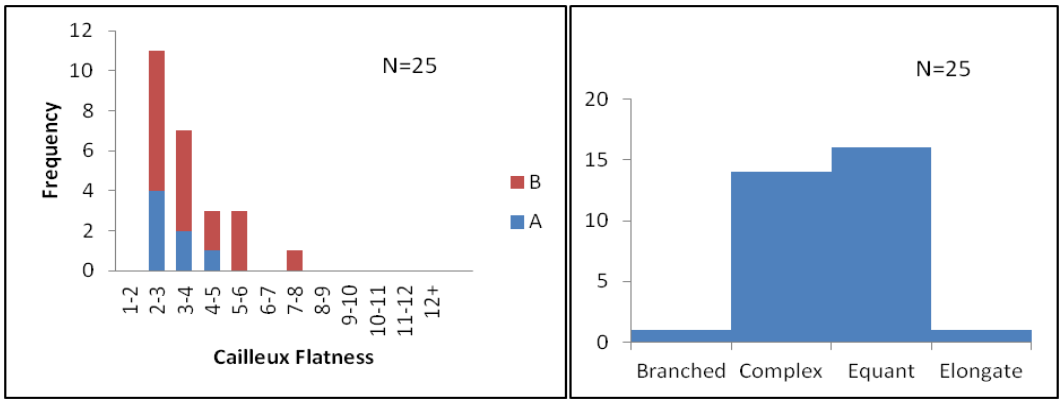

Figure 3.2 A set of histograms summarizing the distribution of flatness (left) and outline (right) from a representative site 1 grains. Note the single peak in the Flatness histogram.

Sample	# grains	Notes	Max size (mm)	a-axis (mm)	b-axis (mm)	Max flatness	Mean flatness
A	13	Irregular, angular	4.2	1.7-4.2	0.8-3.0	4.3	3.1
B	55	Rounded, pebble	2.9	0.7-2.9	0.6-2.2	7.6	3.7
C	10	Large, rounded	6.1	2.4-6.1	0.8-2.3	4.5	3.9

Table 3.1 Statistical summary of morphological results from site 1 grains, including outline and roundness observations, grain size, and maximum and mean flatness values.

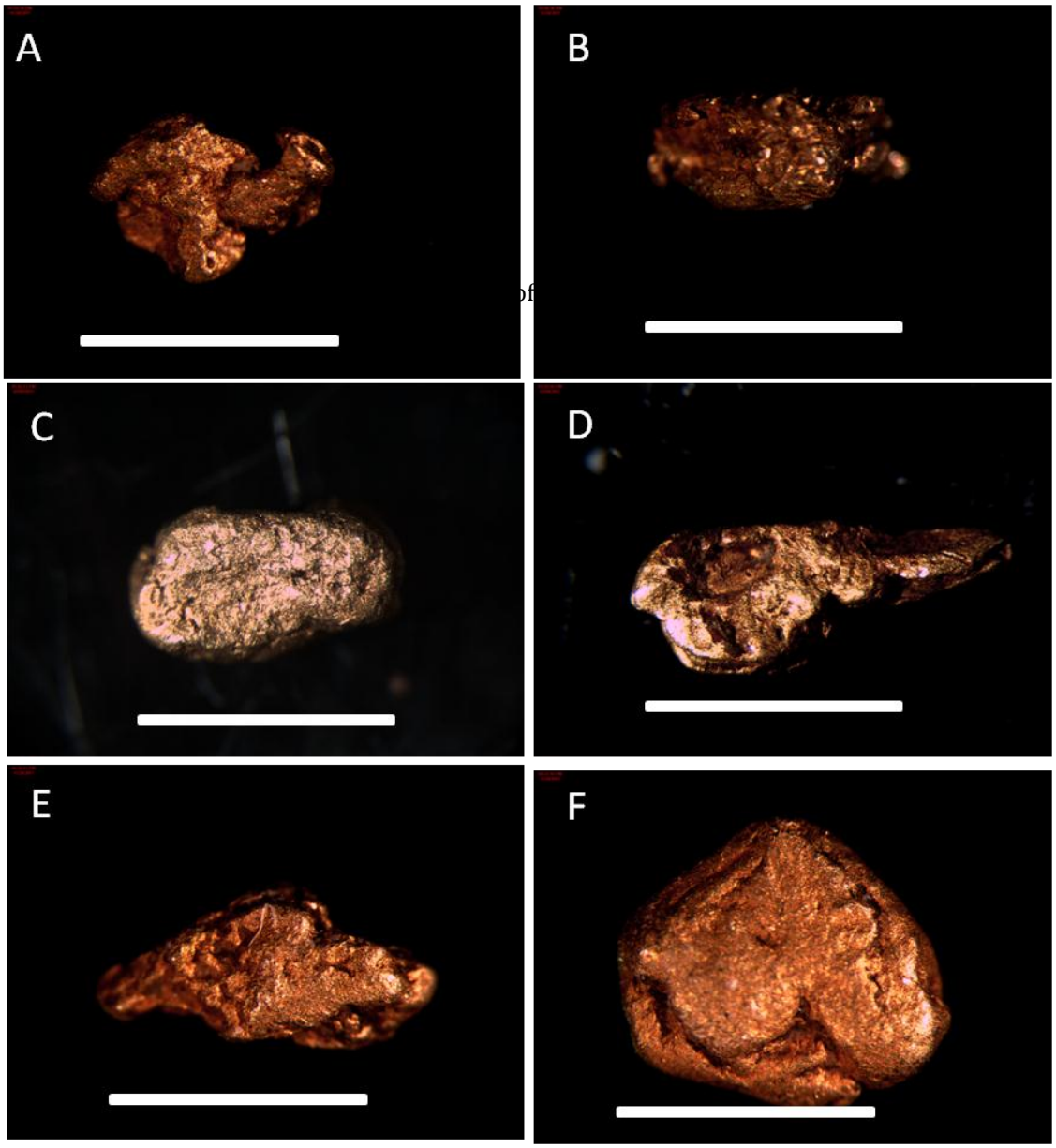

Figure 3.3 Incident light images of gold grains from site 1. Two examples of A type grains (A, B), displaying complex outlines, and slightly rounded edges which define the sub-group. B type grains (C,D,E) comprise the majority of the sample, displaying equant (C), and complex (D,E) outlines, with well rounded edges. C type grains are large with equant outlines and well rounded edges (F), and in some cases high flatness indices: 7.6 in (F). White scale bar is 2mm in all photos.

Geochemical results from site 1 show high silver content, with fineness values ranging from 490 to 750 (Table 3.2), with an average fineness in grain cores of 650. Several B and C type grains contained fineness values as low as 500, and mercury levels from 0.8 to 1.0 wt%. BSE images revealed some colour variation within grains (Fig 3.4), but when dark and light areas were analyzed, the alloy composition changed only slightly. Silver leached rims were absent in the majority of the grains, and only very narrow rims were seen in some of the C type grains.

	Au	Hg	Ni	Pb	Ag	Cu	Total	Spot	Fineness
248	64.987	0.084	0	0.049	30.331	0	95.455	A-core	681.7915
249	72.748	0.355	0.012	0.185	22.452	0	95.764	A-core	764.1597
250	71.508	0.132	0	0.081	24.033	0.008	95.762	B-core	748.4535
253	69.748	1.401	0.026	0.092	25.384	0	96.662	B-core	733.1708
254	45.639	1.072	0	0.123	46.87	0	93.736	B-core	493.3466
256	51.475	0.924	0.027	0.253	43.351	0	96.065	B-core	542.8364
258	73.433	0.084	0.006	0.04	22.94	0	96.52	B-core	761.9665
266	48.754	0.815	0	0.02	45.702	0.01	95.33	C-core	516.1557

Table 3.2 Results from WDS microprobe spot analyses from gold grains from site 1, element concentration are reported in wt %.

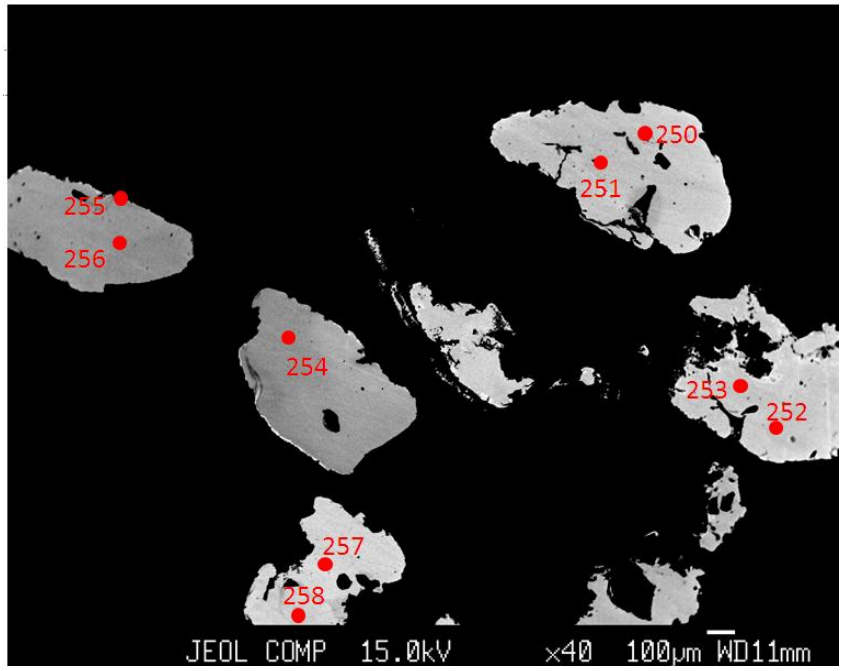

Figure 3.4 Back Scattered Electron Image displaying spot analyses 250-258. Two points were taken from each grain to check for compositional variation and

3.2 Site 2

Site 2 is located in a tributary valley in the north east part of the BHC watershed and has a contributing area of 16 km^2 (Fig. 3.1). Morphological results are displayed in Figure 3.5. The population of 72 grains was well sorted, and the long axis for most grains is between 0.7 and 1.7 mm. 17 A type grains ranged in size from 0.8 to 1.5 mm (Table 3.3), have complex to elongate outlines , and commonly contain pitted surfaces (Fig. 3.6B). Grain edges are angular to sub rounded. Flatness measurements range from 2.3 to 7.6. B type grains range from 0.6 to 2 mm, exhibit complex to equant outlines, contain slightly polished grain surfaces, and have weakly rounded edges. Flatness indices range from 1.6 to 7.4 for B type grains.

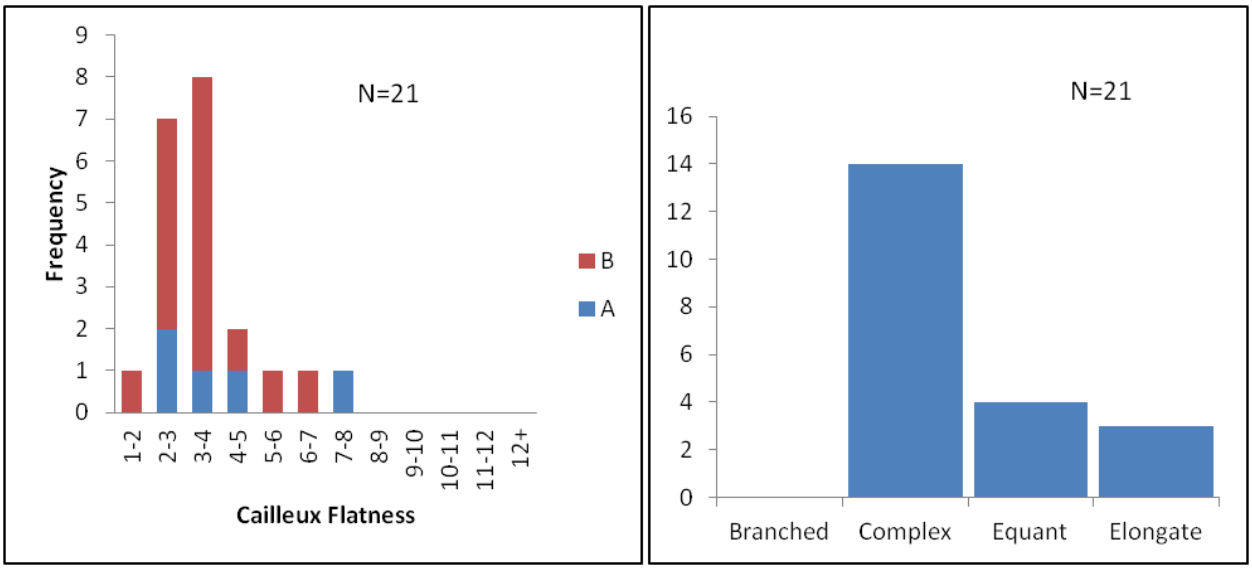

Figure 3.5 Morphological histogram from site 2 summarizing the distribution of flatness (left) and outline (right) from a representative sample of site 2 gains. Note the similar shape to the flatness histogram from site 1. Grain shapes are colour coded for flatness histogram.

Type	#	Notes	Max size (mm)	a-axis	b-axis	Max flatness	Mean
A	17	Complex, angular	1.2	0.7-1.2	0.4-0.6	7.6	4.0
B	55	Rounded, pebble	2.2	0.7-2.2	0.3-1.6	7.7	3.5

Table 3.3 Statistical summary of the morphological results from site 2

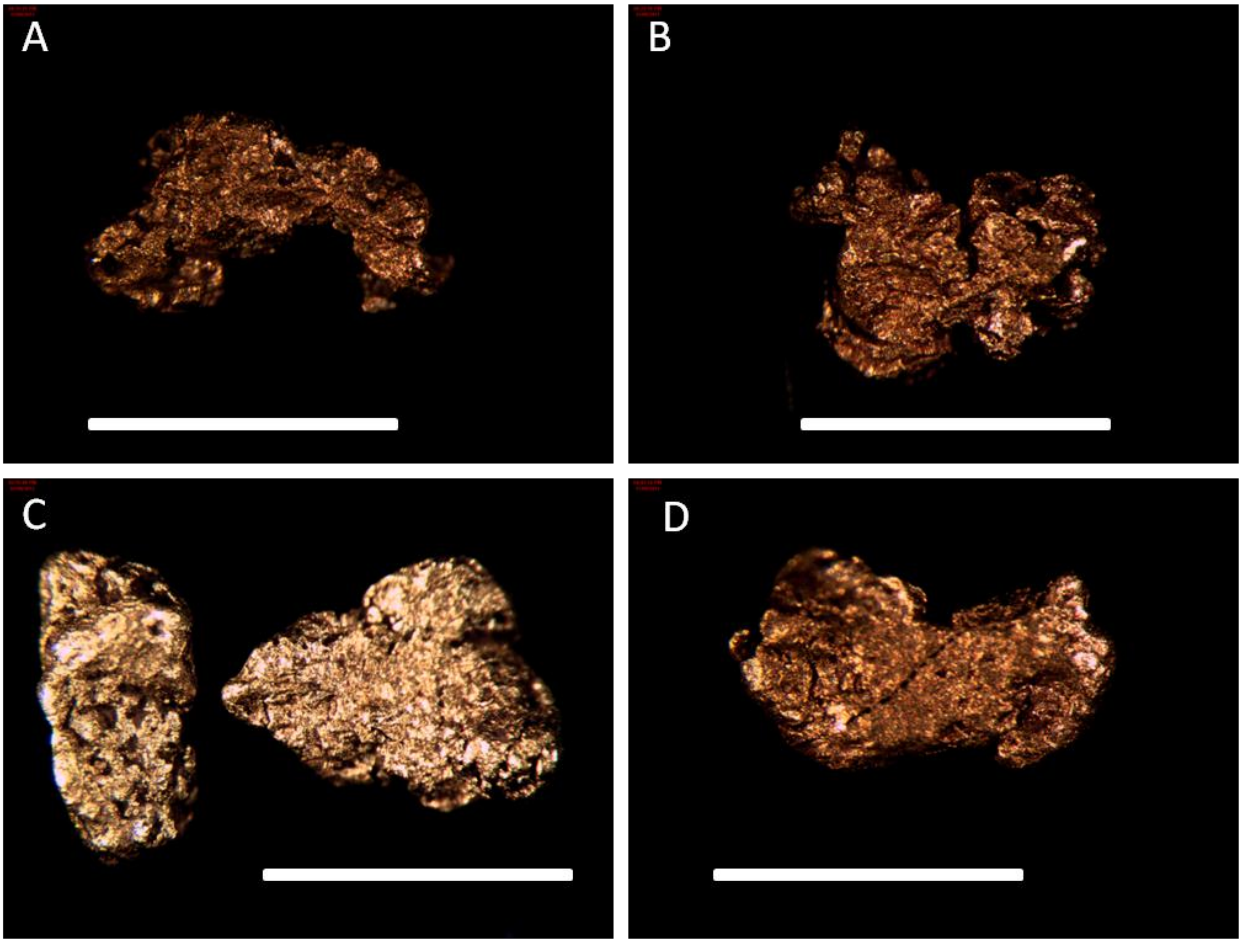

Figure 3.6 Incident light images of grains from site 2, displaying the range of morphologies observed in the sample. Only A (A,B) and B (C,D) type grains were observed. Complex outlines are common in all grains display sub rounded to rounded edges(A to D). Significant flattening was not observed where most grains have flatness indicies clustered between 2 and 4. White scale bar is 2 mm in each photo.

Geochemical results from site 2 two are limited to only five grains, and have fineness values strongly clustered between 660 and 720. Compositional variation among grains was seen with dark regions (lower gold concentrations) and light regions (Fig. 3.7). Mercury content was above detection limit for 4 of 5 quality analyses, ranging up to 1.2 wt%.

No.	Au	Hg	Ni	Pb	Ag	Cu	Total	Spot	Fineness
69	68.293	0.243	0	0	26.823	0.006	95.385	B-core	717.997
71	67.216	0.082	0.006	0.01	26.545	0	93.859	B-core	716.8866
72	65.54	0.987	0.012	0	28.569	0	95.119	B-core	696.4265
167	65.5935	1.2612	0	0.0539	33.0789	0	99.597	A-core	664.7604
224	69.48	0.18	0	0	26.49	0.035	96.185	B-core	723.9762

Table 3.4 Microprobe results from spot analyses from site 2, reported in wt%.

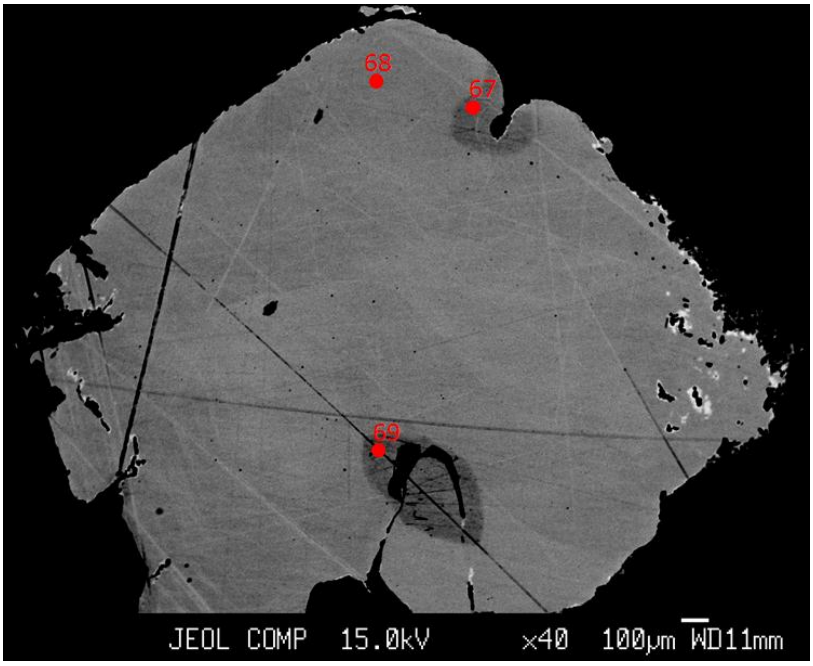

Figure 3.7 BSE image **of a** large gold grain from site 2. Note: scale bar of 100 microns in the bottom right corner.

3.3 Site 3

Site 3 is located in a NW tributary valley to the BHC, and has a contributing watershed of 18 km^2 (Fig.3.1). A small moderately sorted sample population contains mostly large gold grains (>3 mm). Morphological results are displayed in Figure 3.8. Fifteen A type grains, ranging in size from 0.8 to 1.7 mm display complex grain shapes with angular edges (Fig. 3.9A, B). Grain surfaces are pitted and crystalline. Several grains are still attached to quartz inclusions (Fig 3.9A). Flatness indices range from 2.5 to 6.2, with an average of 3.9 (Table 3.5). Twenty-four B type grains, ranging in size from 0.6 to 4 mm, make up the majority of the sample. Grain outlines are equant to elongate, contain rounded edges, but some irregular surfaces, display pitting (Fig. 3.9C) and gangue mineral aggregates. Flatness indices range from 2.5 to 9.7. Ten C type grains range in size from 2 to 4 mm. Grain shapes are consistently elongated, with well rounded edges and smooth surfaces. Flatness indices range from 3 to 20. Due to limited availability of ideal sized grains (0.5 to 2 mm), morphological results include those from larger (> 3 mm) grains.

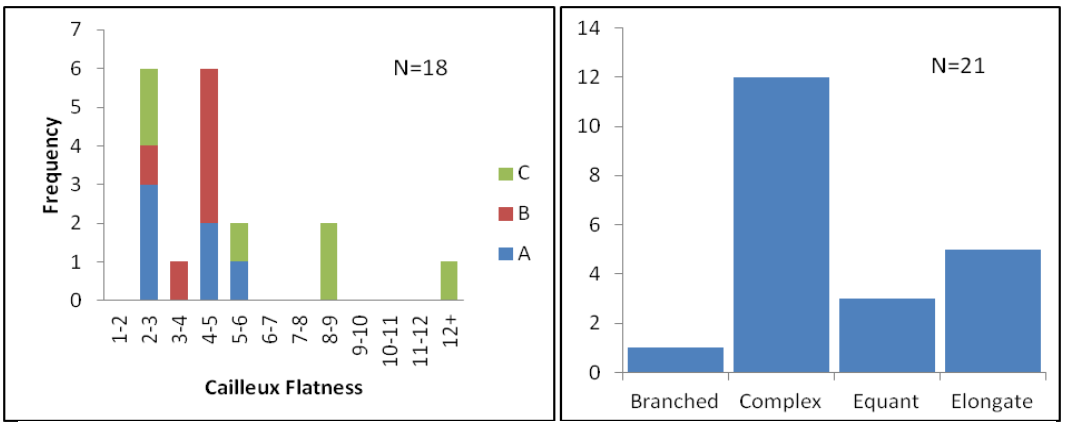

Figure 3.8 Morphological histogram from site 3. Outliers in flatness (values of 8 and 12+) and outline (Elongate) were produced from grains longer than 3 mm.

Type	#	Notes	Max size (mm)	a-axis	b-axis	Max flatness	Mean
A	15	Crystalline, Quartz	1.7	0.8-1.7	0.4-0.8	6.2	3.8
B	24	Irregular, rounded	4.0	1.2-4.0	0.9-2.1	9.8	5.4
C	10	Smooth, rounded	4.1	2.0-4.1	0.9-2.4	20.8	8.6

Table 3.5 Statistical summary of morphological results from site 3

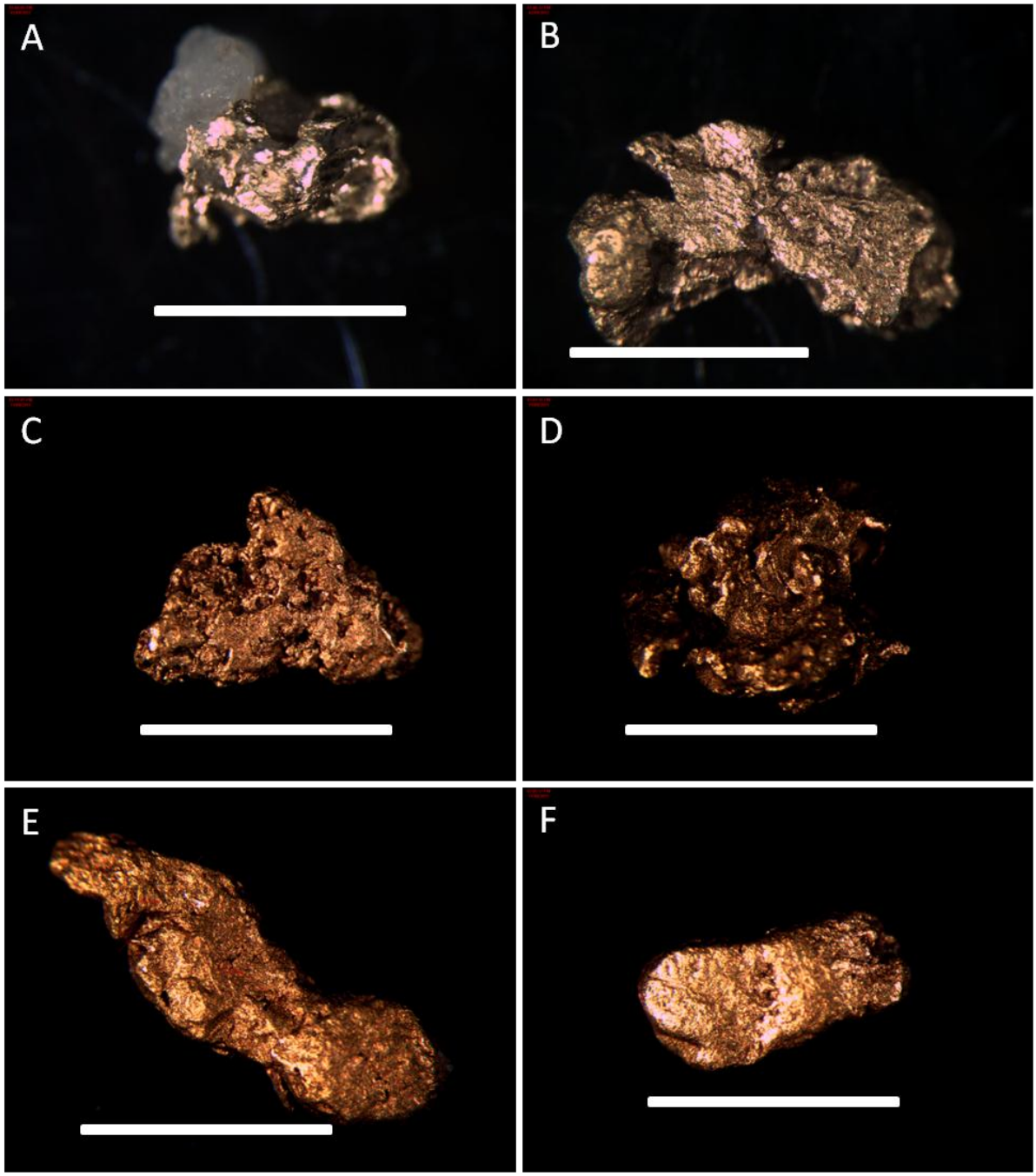

Figure 3.9 Incident light images of grains from site 3. A wide range of grain morphologies are evident. The photos are organized from those least morphologically evolved in (A) and the most evolved in (F). In some cases grains still remain attached to quartz aggregates. Branched outlines are seen in (A,B), while the majority display complex shapes and surface textures (C,D). C type grains (E,F) are typically large, well rounded and with polished surfaces.

Microprobe results from site 3 show the gold fineness ranging from 660 to 812 (Table 3.6). Mercury content was generally low, and above detection limit (2.2 wt %) for only 1 of 8 analyses. Very narrow (approx. 10 microns) silver leached rims were seen in B and C type grains (Fig. 3.10), but spot analysis showed that the silver leaching did not extend significantly into the grains.

No.	Au	Hg	Ni	Pb	Ag	Cu	Total	Spot	Fineness
64	71.843	0	0	0.072	24.541	0.01	96.469	A-core	696.9365
299	72.624	0.048	0	0	24.045	0	96.744	A- core	751.2646
301	63.332	0	0	0.205	32.299	0	95.836	A- core	662.2539
302	76.75	0.023	0.005	0.445	19.485	0.043	96.751	A- core	797.5269
307	56.499	0.003	0.014	0.52	39.357	0.004	96.407	B-core	589.4154
309	76.527	2.162	0	0.093	17.657	0	96.441	B-core	812.5265
314	74.155	0	0	0.097	22.568	0	96.82	B-core	766.6739
317	71.968	0.03	0	0.127	23.412	0.009	95.546	C-core	754.5397

Table 3.6 Microprobe spot analyses results from site 3, reported in wt%

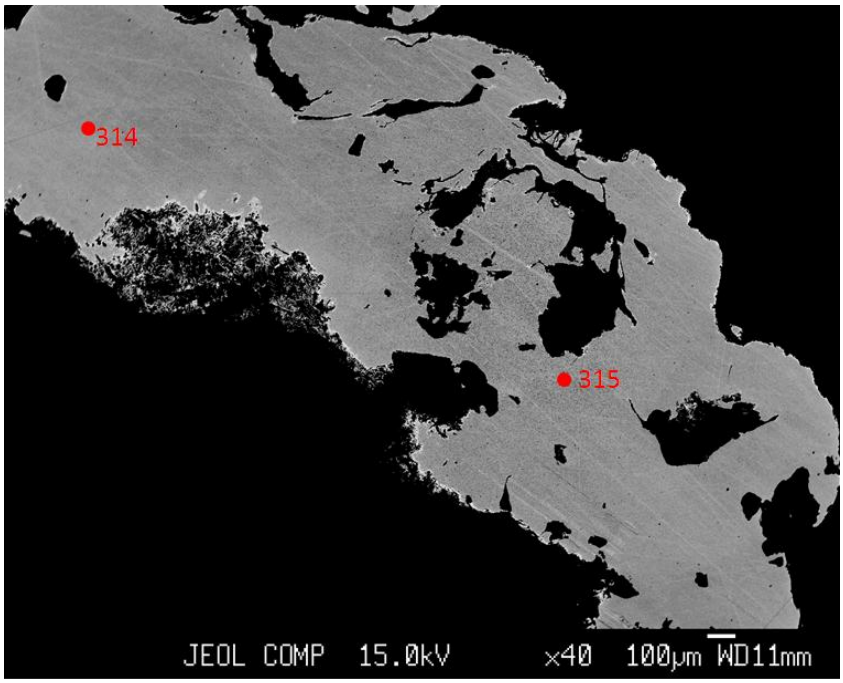

Figure 3.10 BSE of a large gold grain, with a very thin silver leached rim, seen as the light zone on the grain perimeter. Note scale bar of 0.1 mm in bottom right corner.

3.4 Site 4

Jackson et al. (2009) described an excavated trench near site 4 (Fig 3.11), partly based on unpublished work by the Yukon Geological Survey in 1993. In a trench located near the placer operation, a clast-supported colluvium and gravel layer is approximately 1.5 m thick. Clasts are angular to sub angular, up to 18 cm in diameter, and mainly quartzite and schist compositions, both of local provenance (Fig 3.11). Also noted were two reddish brown soil horizons. The entire Quaternary succession overlies a biotite-muscovite quartzo-feldspathic basement rock.

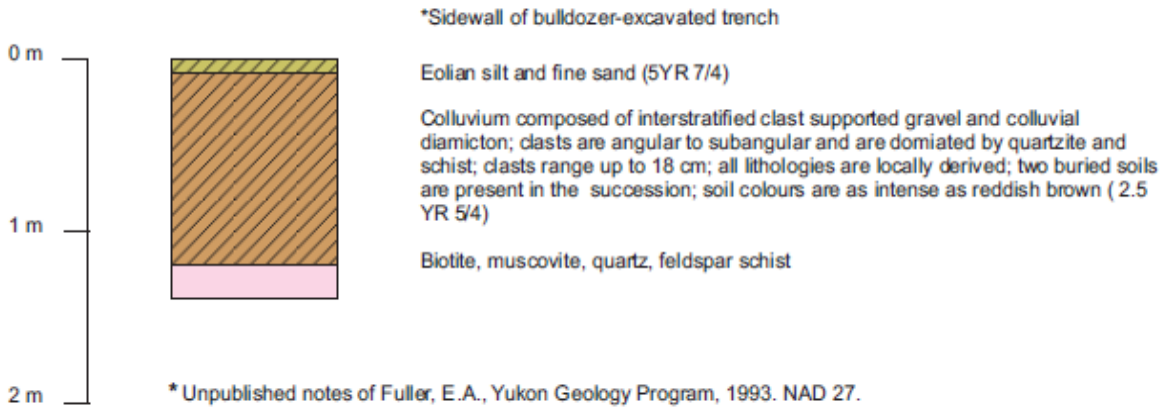

Figure 3.11 Stratigraphic column of an excavated trench from site 4, from Jackson et al. (2009)

The site 4 sample contains more than 150 grains and is located in a western tributary to the BHC with a contributing area of 48 km^2 (Fig. 3.1). Morphological results are summarized in Fig 3.12 and Table 3.7. This sample is well sorted and comprised mainly of fine grains of complex shapes (Fig. 3.13 A,B). Site 4 was divided into three subgroups on the basis of edge roundness and surface texture. A total of 23 A type grains range in size from 1 to 2.5 mm. Grain shapes are branched and highly irregular (Fig 3.13 A, B). Angular grain edges are common along with crystalline surfaces. A type grains are consistently bright

yellow, in contrast to a dull tarnish common in other samples. Grains tend to be angular with very little rounding and have flatness values of 2.6 to 7.1 (Table 3.7). B type grains make up the majority of the sample and range in size from 1.2 to 1.9 mm. Grain shapes are generally complex to equant, with edges significantly more rounded than A type grains. Flatness indices range from 3.7 to 7.1 (Fig. 3.12). The topography and surfaces of these grains is irregular, with little evidence of hammering. Sixteen C type grains were identified, ranging in size from 1.1 to 1.5 mm. Grain shapes are equant to slightly elongate, with rounded edges and polished surfaces. Minor folding of edges is evident in a few C type grains. Flatness indices range from 4.7 to 7.7 (Fig 3.12 and Table 3.7).

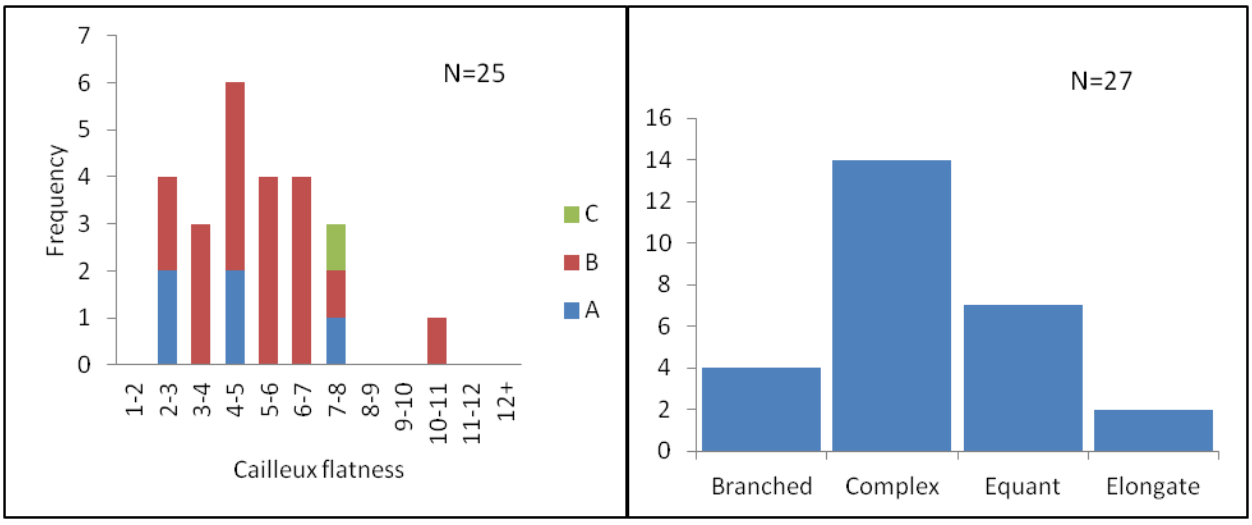

Figure 3.12 Morphological histograms from site 4. The peak in the flatness distribution curve, left, is wider than for sites 1 to 3. Grain outline for site 4 is mostly complex. Grain types (A,B,C) are colour coded for flatness histogram.

Sample	#	Notes	Max size (mm)	a-axis	b-axis	Max flatness	Mean
A	23	Complex, angular	2.4	1.4-2.4	0.7-1.3	7.1	3.9
B	12	Complex, rounded	1.9	1.0-1.9	0.5-1.2	11.5	5.3
C	16	Polished, rounded	1.6	1.0-1.6	0.9-1.3	7.7	3.1

Table 3.7 Statistical summary of morphological characteristics of grains from site 4.

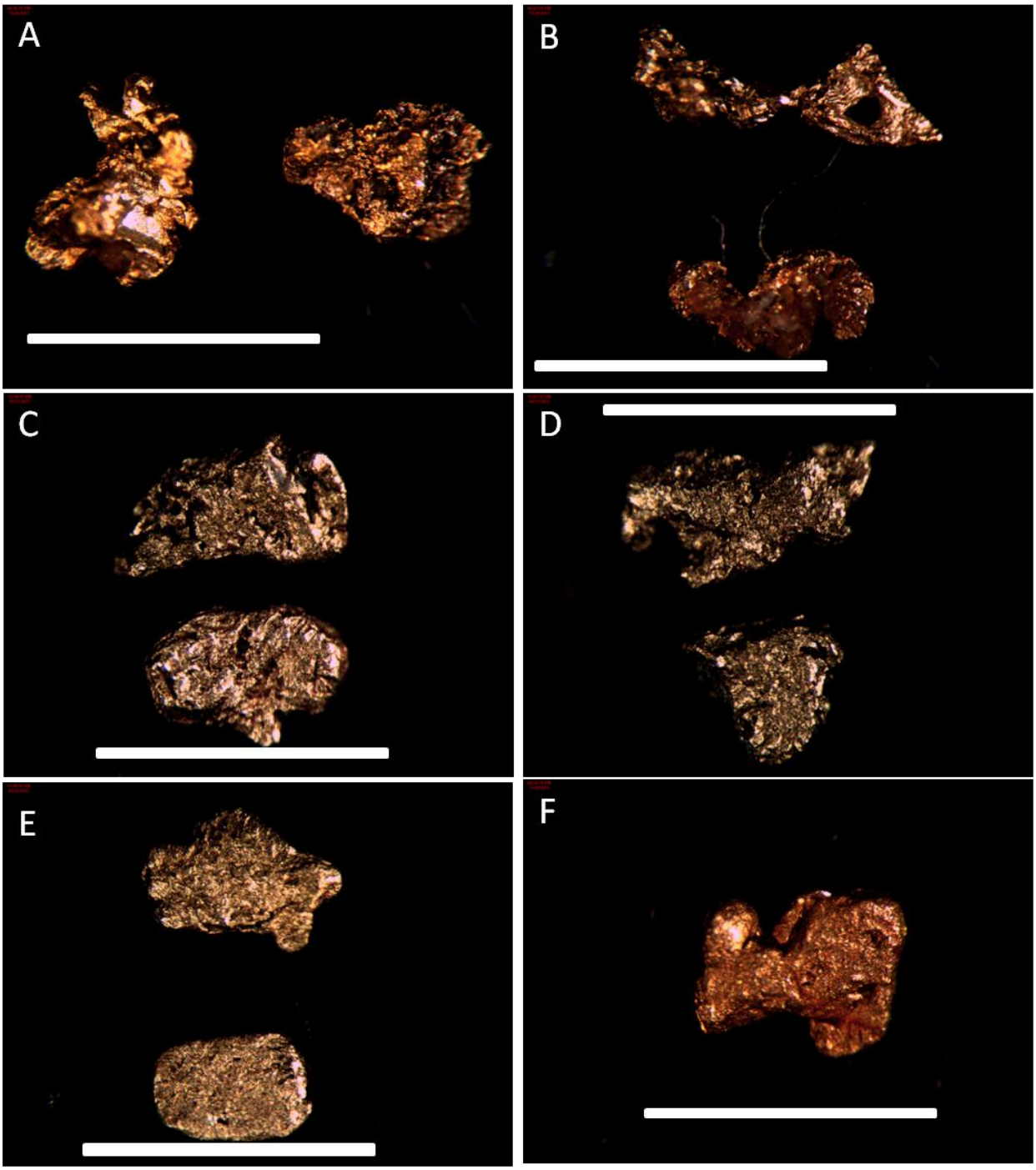

Figure 3. 13 Incident light images of grains from site 4. A wide range of grain morphologies are present. The A type grains are characterized by quartz inclusions (B, lower), crystalline surface textures (A, B), and branched and complex outlines with angular grain edges. B type grains (C, D) are characterized by complex to equant outlines and sub rounded edges. The C type grains (E ,F) display the most evolved morphology having well rounded edges (E, F) and equant outline (E, bottom). White scale bar is 2 mm in each photo.

Microprobe analyses show that core fineness of gold in the site 4 sample are tightly confined between 727 and 770. Mercury content was above detection limit for 2 of 9 analyses, but with two anomalously high values of 4 and 5 wt% (Table 3.8. Compositional variations are common in A type grains, where dark (gold poor) patches are visible near the edges of grains, possibly where sediments have attached to the grain surface, thereby modifying the alloy composition. These dark regions (Fig. 3. 14) are also seen in B and C type grains, though less common. Narrow silver leached rims are present in some of the C type grains.

No.	Au	Hg	Ni	Pb	Ag	Cu	Total	Spot	Fineness
16	73.736	0	0.008	0	22.079	0.002	95.825	A-core	769.5664
285	72.631	0.036	0	0	23.645	0	96.318	A-core	754.404
289	72.985	0	0	0	22.775	0	95.777	A-core	762.1658
290	72.156	0	0.013	0	22.553	0.003	94.729	A-core	761.8706
292	71.544	0	0.011	0.058	26.864	0	98.479	B-core	727.0141
294	66.922	5.806	0	0.186	23.516	0	96.456	B-core	739.9766
295	70.112	4.089	0	0.105	21.877	0	96.192	B-core	762.1781
297	70.511	0.104	0	0.095	25.091	0.025	95.842	C-core	737.5473
2	94.892	0.091	0	0.052	1.853	0	96.928	C-rim	980.8466

Table 3.8 Microprobe spot analyses results from site 4, reported in wt %.

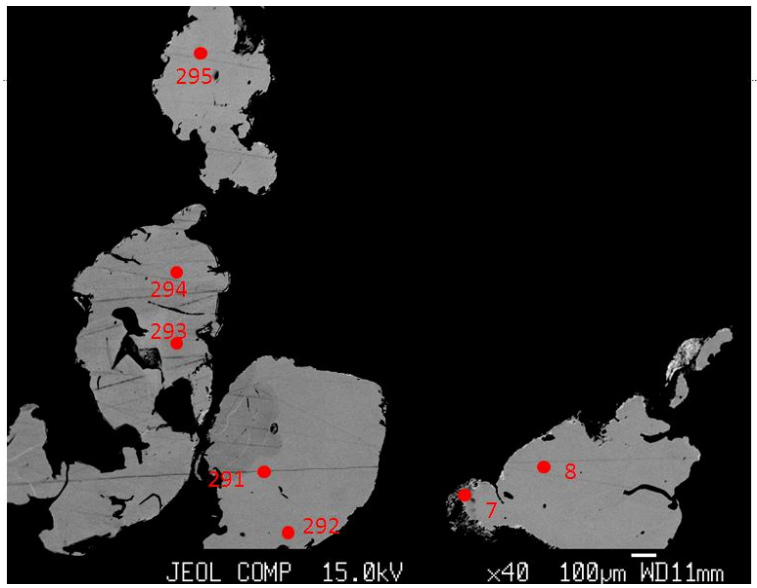

Figure 3.14 BSE image of B type grains from site 4.

3.5 Site 5

Jackson et al. (2009) described a fluvial terrace near the site 5 (Fig. 3.15) placer operation as a 3 m section of cobble (64 to 256 mm) clasts in a pebble (4 to 64 mm) sand (<2 mm) matrix. Clast lithologies are all locally derived and consist of mafic and felsic shists, with subordinate metaquartzite and gneiss. The 3 m section overlies poorly exposed schist basement rock.

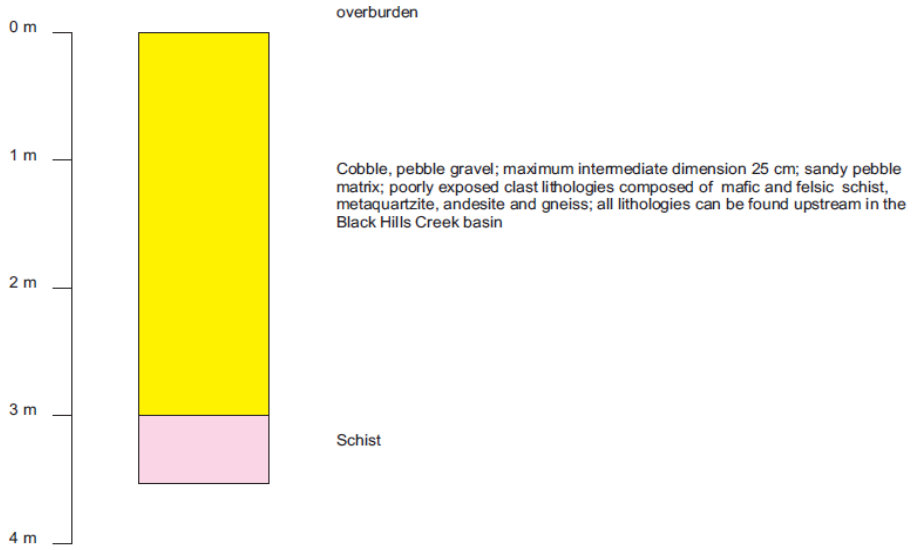

Figure 3.15 Stratigraphic column of an excavated fluvial terrace near site 5, from Jackson et al. (2009).

Ninety grains were sampled from site 5 in the southern BHC with a contributing area of 292 km^2 (Fig. 3.1). The sample is poorly sorted containing mostly medium to coarse grains, but with significant variation with respect to particle flatness and surface textures (summarized in Fig. 3.16). The population was divided into three subgroups (Table 3.9). A type grains are all bright yellow in colour, and exhibit branched to complex grain shapes (Fig 3.17 A, B). Edges show minor rounding with unpolished and sometimes pitted surfaces. There are 36 B type grains, ranging in size from 1.2 to 4 mm. Grain shapes vary

between slightly complex and elongated, irregular un-pitted surfaces. Flatness indices range from 3.7 to 10.2 (Table 3.9).

A total of 32 C type grains were identified, and are quite distinct from A and B type grains. These grains range in size from 1.5 to 2.7 mm and have equant to elongated grain shape. Edges are very well rounded and grain surfaces well polished (Fig 3.17 E, F). C type grains have a darker colour than A and B types (Fig 3.17 A to D). Minor folding is observed on the edges of two C type grain. Flatness indices range from 7 to greater than 20, and the short axis of extremely thin grains becomes more difficult to measure accurately. Histograms of the site 5 flatness indices reveal a strongly bimodal distribution, with clusters around 4 to 5, and greater than 12 (Fig 3.16)

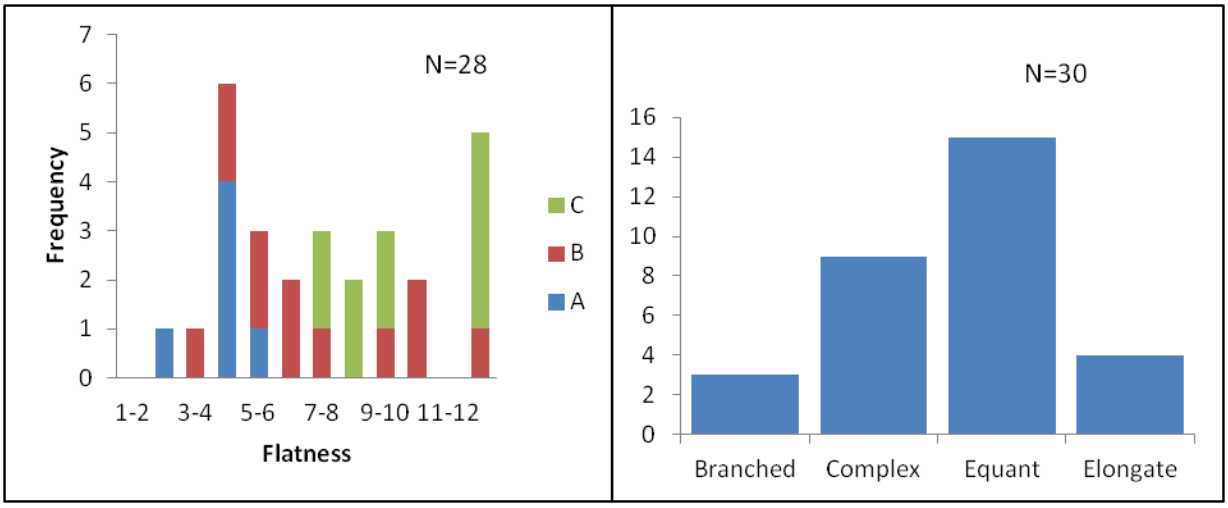

Figure 3.16 Histograms of morphological results from site 5 representative sample. Flatness histogram is strongly bimodal, and the outline histogram shows grains from each outline class.

Sample	#	Notes	Maximum	a-axis	b-axis range	Max flatness	Mean
A	25	Irregular, angular	3.0	1.6-3.0	1.0-2.2	4.5	4.0
B	36	Irregular, rounded	4.1	1.3-2.9	0.6-1.5	19	7.3
C	30	Polished, rounded	2.7	1.1-2.7	0.9-1.9	27	14

Table 3.9 Statistical summary of morphological analysis of a representative analyses from site 5.

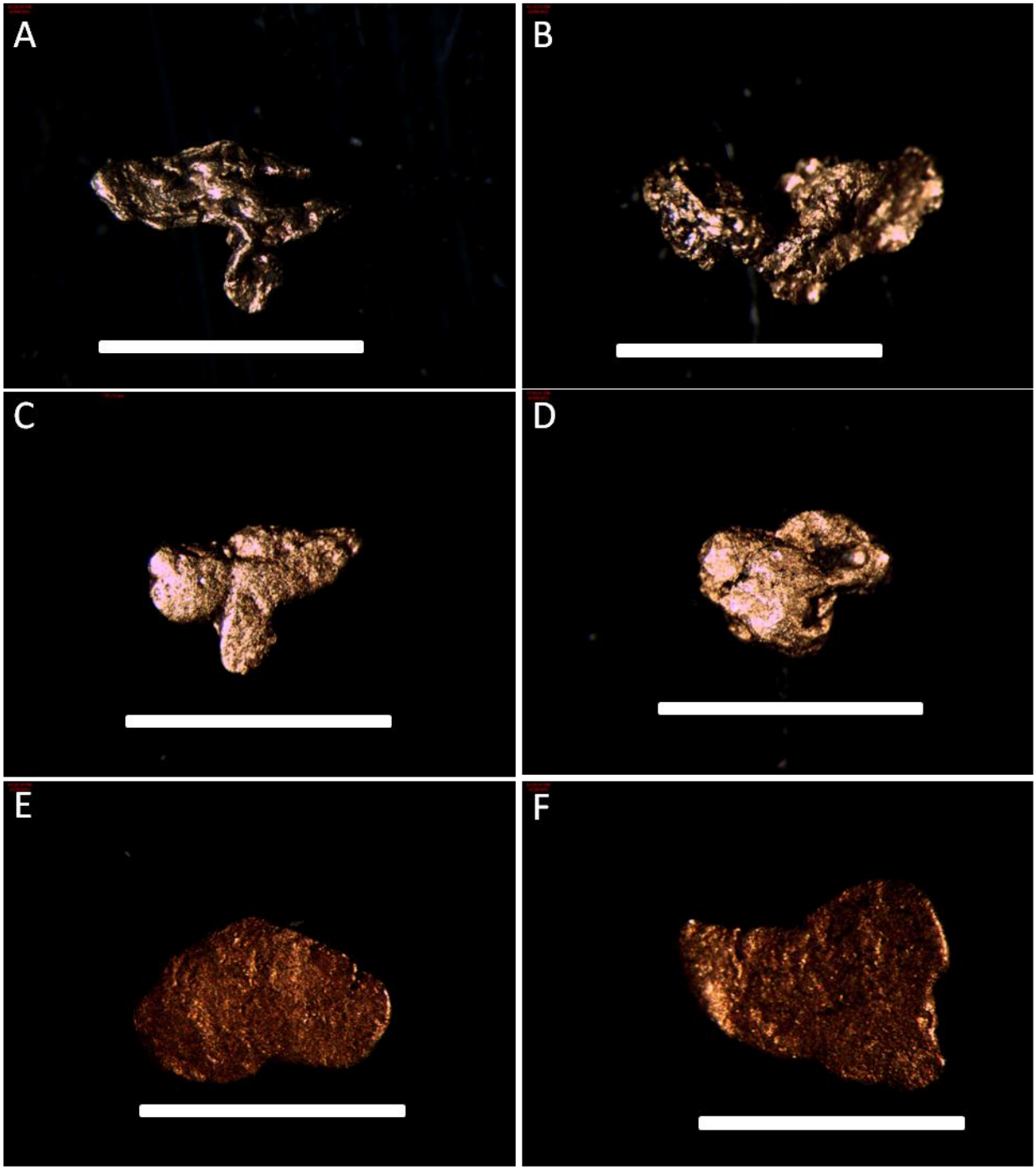

Figure 3.17 Incident light images of grains from site 5. A wide range of grain morphologies are present, including branched (A, B) complex (C, D, F) and equant outlines. Roundness also ranges from angular (A, B) to rounded (C, D) and well rounded (E, F). White scale bar is 2 mm in each photo.

Microprobe results from site 5 show gold fineness values ranging from 593 to 940. A wide range of silver concentrations is seen in B and C type grains, from 9 to 35 wt % (Table 3.10). Mercury values are above detection limits in both the B and C types. Narrow silver leached rims are well developed in C type grains (Fig 3. 18) and are consistent along the perimeter of the surface. Fineness values in the rims are as high as 980 (Table 3.10).

No.	Au	Hg	Ni	Pb	Ag	Cu	Total	Spot	Fineness
235	89.866	0.332	0	0	7.179	0.048	97.427	A-core	926.024
240	89.369	0.272	0	0	5.684	0.011	95.354	A-core	940.2018
232	82.021	0.032	0	0	18.339	0	100.396	A-core	817.2678
273	74.444	1.383	0	0	19.63	0.004	95.461	B-core	791.3345
275	85.807	0.183	0	0.16	11.893	0.011	98.057	B-core	878.2702
277	82.505	0.208	0.007	0	14.491	0	97.239	C-core	850.6021
24	58.924	0.338	0.052	0.078	35.566	0	94.993	C-core	623.6004
281	66.102	0.276	0	0.223	28.86	0.004	95.476	C-core	696.089
283	81.022	0.203	0	0.005	13.181	0.006	94.417	C-core	860.0788
23	80.966	0.042	0	0.133	14.351	0	95.499	C-rim	849.4392
26	93.507	0	0.003	0	1.5	0	95.057	C-rim	984.046

Table 3.10 Representative microprobe analyses from site 5, reported in wt %. Additional analyses in Appendix II.

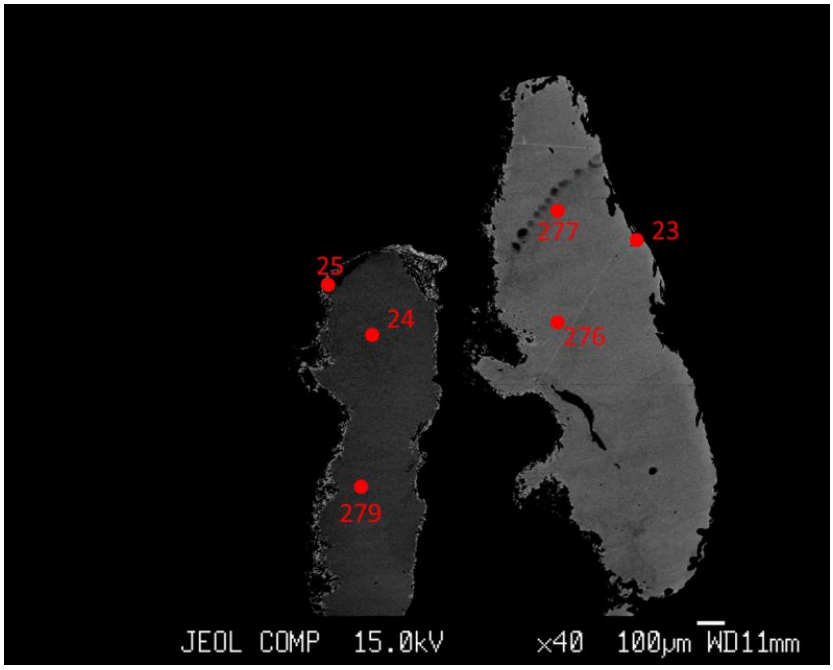

Figure 3.18 BSE image of two C type grains from site 5. Colour variation is a result of alloy composition, where brighter colours, right, indicate higher gold concentration. Note the thin silver leached rim present in the grain on the left.

3.6 Site 6

Site 6, the southernmost placer operation in the BHC watershed, has a contributing area of 378 km^2 (Fig. 3.1). The site 6 sample contained only B and C type grains, distinguished based on grain morphology and summarized in Figure 3.19. B type grains range in size from 1.6 to 2.5 mm and all grains display some degree of rounding. Grain surfaces are pitted and unpolished, while grain outlines are complex to equant. B type grains exhibit varying degree of flattening with indices ranging from 3.2 to 12.5. C type grains are primarily equant to elongate in outline and range in size from 1.4 to 3.7 mm in the a-axis. Most C type grains have polished surfaces and well rounded edges (Fig 3.20 E, F) Several C type grains were seen to have been folded (Fig 3.20F). Flatness indices for C type grains are consistently high, ranging from 10.4 to 22 (Table 3.11).

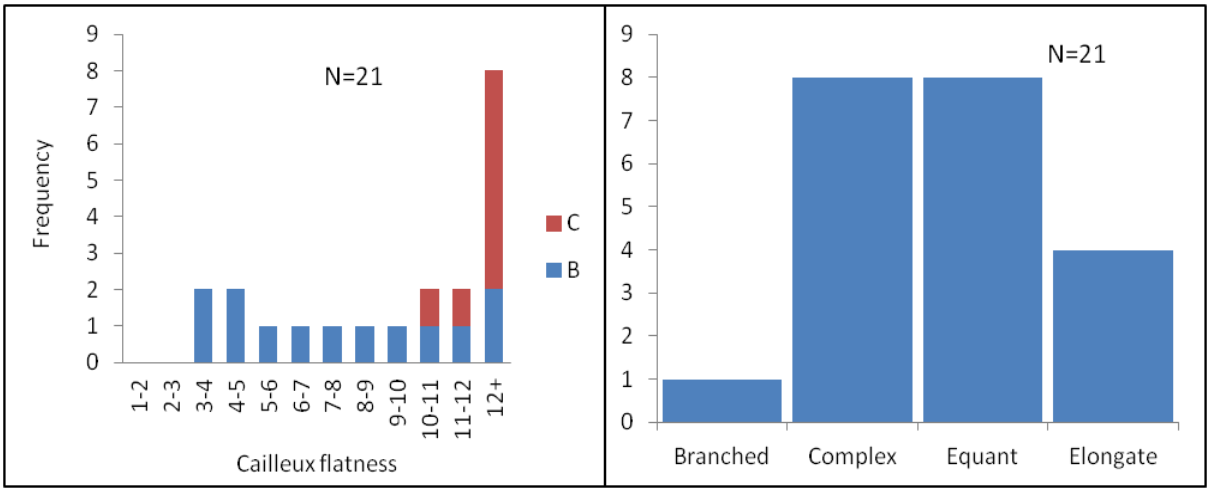

Figure 3.19 Morphological histograms of representative grains from site 5.

Sample	#	Notes	Max size(mm)	a-axis	b-axis	flatness index	Mean
B	87	Irregular, rounded	1.2	1.6-2.5	0.8-1.7	3.2-12.5	5.8
C	40	Polished, equant	3.7	1.4-3.7	0.6-2.1	10.4-22	15

Table 3.11 Statistical summary of grain morphology analysis of a representative sample from site 6.

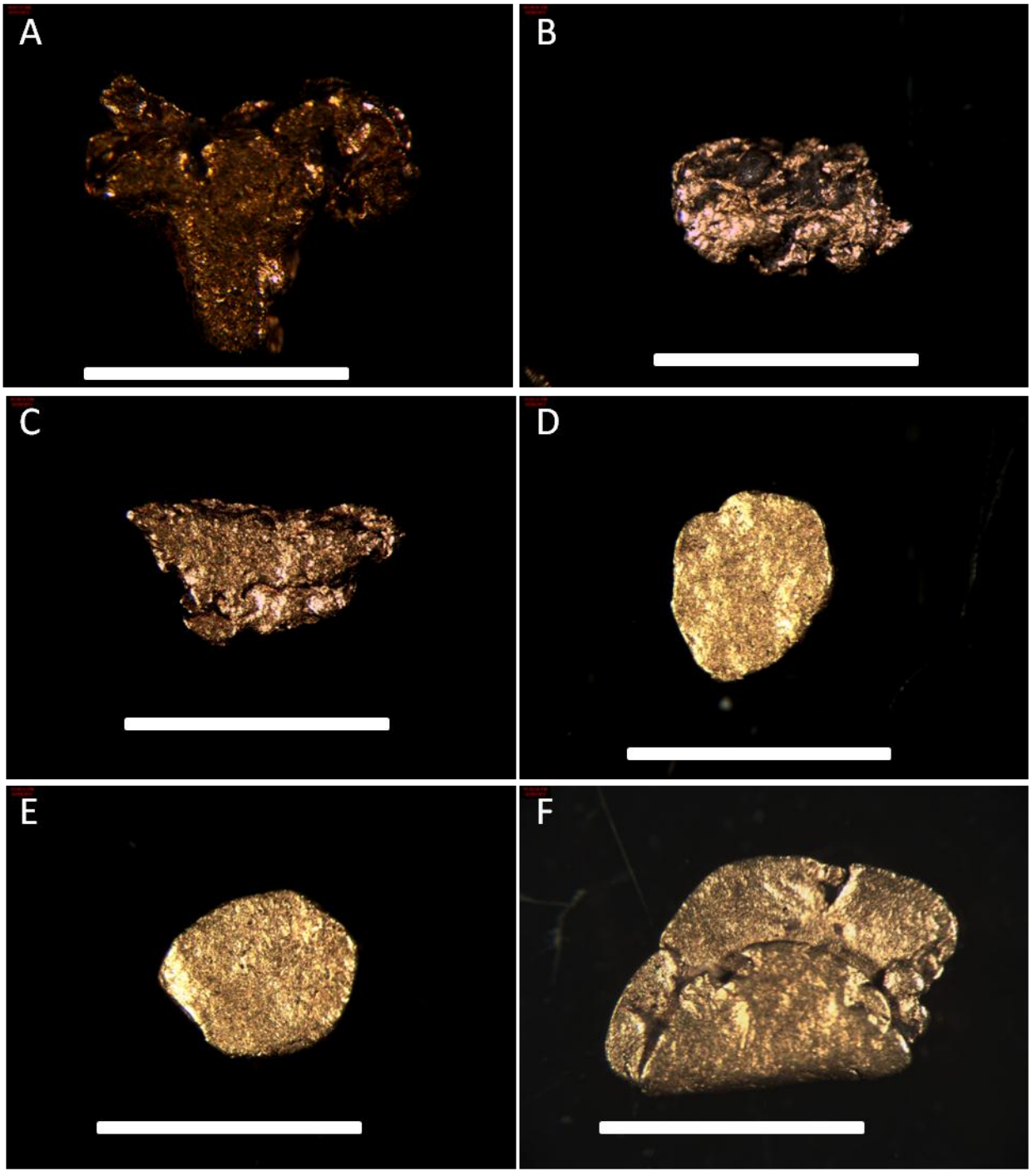

Figure 3.20 Incident light images of grains from site 6. Grains from site 6 display a wide range of morphology. B type grain (A,B,C,) show significantly less surface polishing, and flattening that C type grains (D,E and F)White scale bar is 2 mm in each photo.

Microprobe results from site 6 (Table 3.12) show consistent fineness values, between 795 and 895. This fineness value is characteristic of both B and C type grains. Both grain types also share similar mercury content, with most grains above detection limits, up 0.4 wt%. Interpretations for site 6 are limited by the low number of quality analyses from site 6

No.	Au	Hg	Ni	Pb	Ag	Cu	Total	Spot	Fineness
154	76.755	0.42	0	0	19.239	0	96.421	B-core	799.5812
155	76.532	0.373	0.03	0.13	19.667	0	96.764	B-core	795.5592
207	80.989	0.192	0.041	0	15.152	0	96.379	B-core	842.3981
210	89.825	0	0	0	9.481	0.043	99.376	B-core	904.5274
157	84.092	0.251	0.006	0	12.162	0	96.514	C-core	873.6468
162	86.527	0	0	0	11.624	0	98.151	C-core	881.5702

Table 3. 11 Microprobe spot analyses from site 6 grains, reported in wt%.

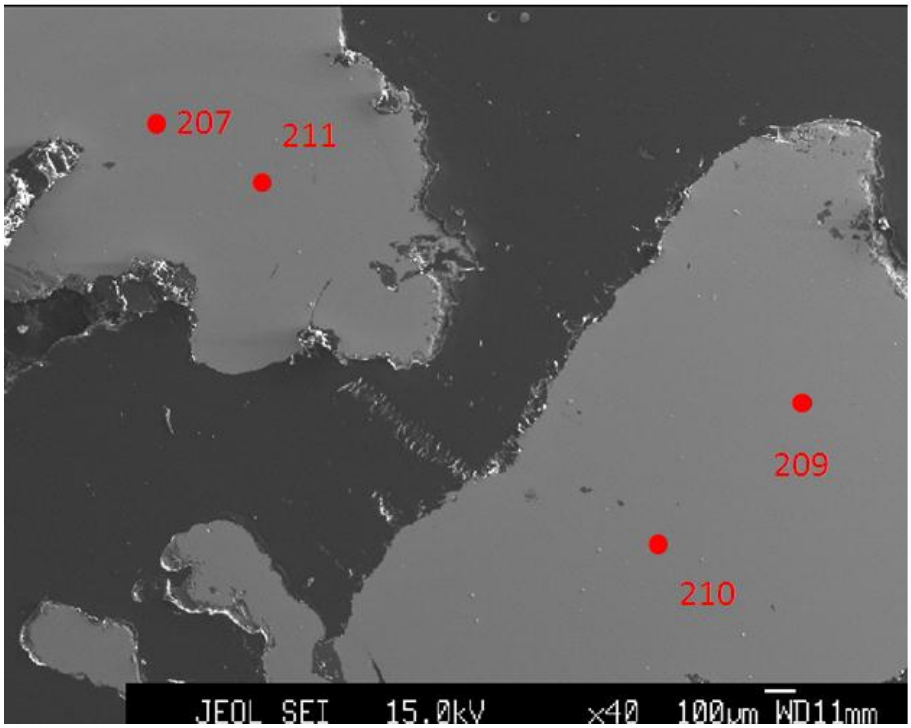

Figure 3.21 BSE image from two B type grains from site 6.

CHAPTER 4: DISCUSSION

4.1 Introduction

The extent to which the flatness indices of a gold grain can be used as distance to source indicator has been determined with varying degrees of certainty. For example, in the Klondike, Knight et al. (1999a) suggested that flatness is a sensitive measure of transport distance within the first 5 km. However, based on measurements in the Otago region of New Zealand, a goldfield analogous the western Yukon, Youngson and Craw (1999) concluded that rounding of particles is active within the first 10 km, without significant flattening (indices greater than 7). Townley et al. (2003), in a study of gold grains from the Andes, proposed extremely refined distance-to-source indicators capable of identifying fluvial transport distances as low as 100m, but the resolution of their methods seems too high. Taking into account the maximum stream distances within the BHC watershed (sites 1 to 3: 5 to 7 km, site 4: 10 km, site 5: 20 km and site 6: 25 km; Fig. 4.1), the results of this study provide insight into the morphological evolution of gold particles during the early stages (0 to 25 km) of fluvial transport.

In this study, each placer sites have been characterized as either primitive or trunk placers according to the definitions provided by Youngson and Craw (1999). Primitive placers are defined as first cycle placers that collect gold particles from proximal sources (<10 km), and are located in moderate to high gradient and deeply incised tributary valleys. Grain morphology in primitive placers is typically characterized by rounding, moderate flattening, and the absence of folded particles.

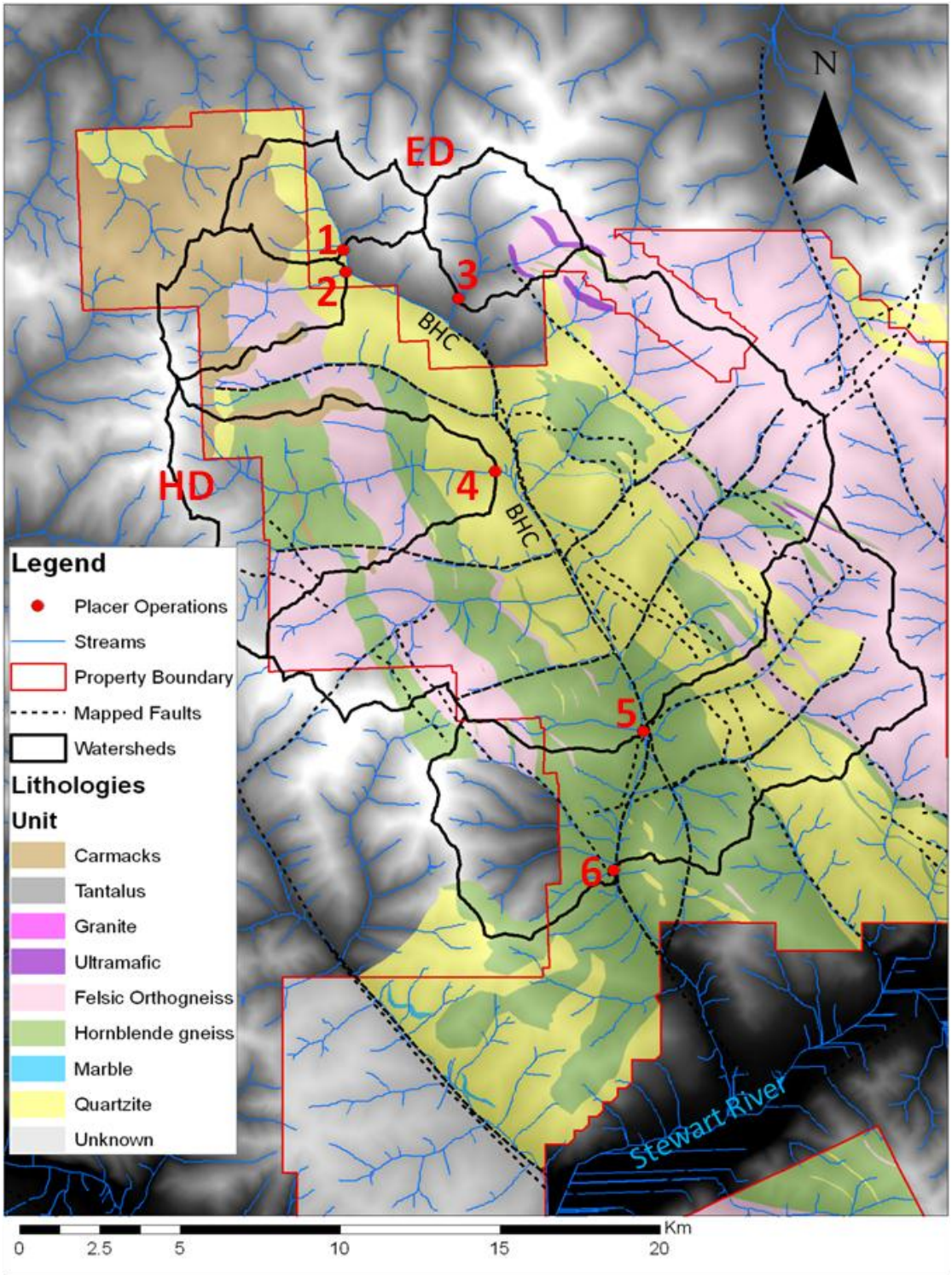

Figure 4.1 Geologic Map of the Black Hills Creek (BHC) overlain by catchment areas of each placer site, indicated in red, with their catchments areas in black. Catchments from sites 1 to 4 are limited to tributary valleys of the Black Hills Creek, while catchments for site 5 and 6 include encompass the entire watershed. Eureka Dome (**ED**) and Henderson Dome (**HD**) are highlighted in red.

Trunk, or transitional placers, are typically bigger than primitive placers and commonly have lower gold concentration deposits. They are typically found downstream from primitive placers where tributaries emerge into wide major trunk valleys and stream gradients rapidly drop. Grain morphology is characterized by broad ranges in particle roundness and flatness indicative of multiple bedrock gold sources (Youngson and Craw, 1999). Thus, modal occurrences of flatness, rather than the sire average are used to estimate the distance of fluvial transport.

Alloy compositions (Au-Ag-Hg-Cu) for gold grains from each site were determined by microprobe spot analysis on the unaltered core and only these core values were plotted, and interpreted in this chapter. Previous studies (Knight et al., 1999b; Dumula and Mortensen 2002; Mortensen et al., 2004; and Chapman et al., 2010) have shown this method to be an accurate reflection of the composition of the bedrock source, and can provide insight into the mineralization style. Previous studies in the region have produced geochemical signatures that were compared with the results of this study (Table 4.1). Chapman et al. (2010) identified two grain types of orogenic gold from the Klondike (Fig. 4.2). Orogenic, a subtype of mesothermal gold, is associated with precipitation of gold from metamorphic fluids during orogenic events. These fluids form epigenetic gold occurrences typically associated with greenchist facies metamorphism during collisional tectonic events. The lithostatic pressure associated with crustal thickening drives fluid migration, which then precipitates gold at depths of 1.5 to 4.5 km, and temperatures of around 300°C. In the Klondike, these are associated with major deformation in the Jurassic (refer to Fig. 1.5). Type 1 Klondike grains are characterized fineness values of 700 to 850, without any mercury. Type 2 Klondike grains have a lower fineness value (550 to 700), and have

mercury present as high as 5 wt%. Dumula and Mortensen (2002) characterized epithermal type gold grains in the Eureka Creek and White River areas (Fig. 4.2). Epithermal deposits form in shallow hydrothermal systems (50m to 1 km depth) in proximity to volcanic and plutonic arcs, which act as heat sources that drive metal leaching and fluid migration. They form at lower temperatures, more conducive to the precipitation of mercury. In our study area, epithermal gold is attributed to the Late Cretaceous volcanic units (Carmacks group, Fig. 4.1) Eureka grains were found to have low fineness values (500 to 700) and mercury content in the range of 0.3 to 0.7 wt%. Grains from the White River area, sourced by late Cretaceous Golden Saddle deposit, are characterized by high fineness (800 to 920) and mercury content between 0.2 and 0.5 wt%. Considerable overlap between these signatures is evident, and is a challenge when making interpretations.

Gold Occurrence	Placer Grain Geochemical Signature	Mineralization Style	Age	References
Klondike	Type 1: Fineness: ~700 to 850, Hg absent Type 2: fineness: ~550to 700, Hg up to 5 wt%	Orogenic style, formed during tectonic stacking, peak metamorphism.	Jurassic	Knight et al. (1999), Chapman et al. (2010;2011)
Eureka Dome	20-50 wt% Silver, low fineness: ~500 to 700 High Hg content ~0.3 to 0.7 wt%,	Epithermal veins, related to Carmacks Volcanic group	Late Cretaceous-Early Cenozoic	Dumula and Mortensen (2002) Chapman et al.(2011)
White River Area (Golden Saddle, Coffee Deposit)	8-20 wt% Silver, high fineness: 800 to 900 Moderate Hg content: ~ 0.2 to 0.5 wt%	Hydrothermal	Late Cretaceous-Early Cenozoic	Placer signature: Dumula and Mortensen (2002); Style and timing: Mackenzie and Craw (2009)
Henderson Dome	20-50% wt%, 0.3 - 3% Hg	Epithermal veins related to Carmacks Volcanic group (inferred from placer studies)	Late Cretaceous-Early Cenozoic	Bond and Chapman (2007)

Table 4.1 Summary of known gold occurrences located near the BHC watershed. It includes their geochemical fingerprint, mineralization style and age. See Figure 4.2 for locations.

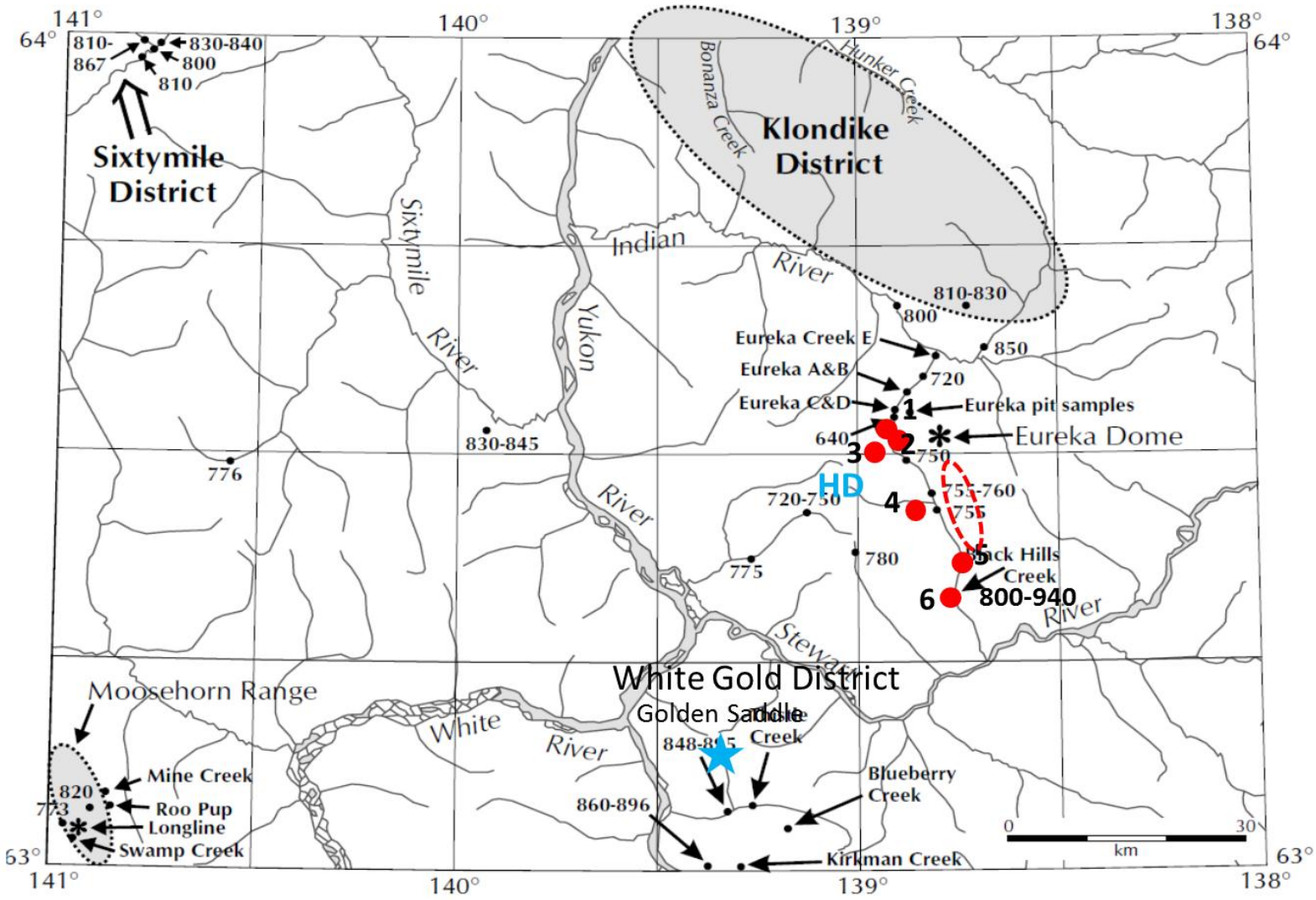

Figure 4.2 Regional map of the western Yukon area, highlighting both the Klondike and White Gold District. The BHC is situated between known orogenic gold sources to the north, and epithermal occurrences in of the Eureka Dome , Henderson Dome (**HD**) and White Gold District. Blue star indicates the location of the Golden Saddle deposit (>1Moz) Approximate placer locations are highlighted with red dots, while the red oval indicates the location of epithermal style targets in the eastern flank of the BHC. Geochemical signatures of placer gold grains are given for each of these occurrences. Modified from Dumula and Mortensen (2002)

4.2 Discussion of Sites 1 to 3

4.2.1 Distance-to-source indicators: Sites 1 to 3

Results from the GIS watershed analysis are similar for sites 1 to 3. Each placer has a contributing area between 16 and 18 km^2 and a maximum fluvial transport distance from the headwaters to the placer sites of approximately 5 to 7 km (Fig. 4.1). Morphological characteristics of grains from these three sites are also comparable and are summarized in Figure 4.3. Flatness indices are strongly clustered between 2 and 5 suggesting that all three of these sites are primitive, single source placers (Table 4.1). Considering the maximum transport distances are between 5 and 6 km for each site, the effectiveness of flatness as a distance to source indicator is limited, leaving outline and roundness as the best indicator of fluvial transport. Grain outlines from each of these three sites are commonly complex and edges of most grains show a low degree of rounding. Both of these trends suggest at least some morphological evolution in the fluvial environment and suggest estimates of fluvial transport between 2 and 5 km (Table 4.2). Sites 1 to 3 contain small populations of large (>3 mm) C type grains which have flatness values greater than 7, and well rounded and elongate outlines, characteristics of far travelled particles. Given that maximum transport in the modern fluvial system in all three sites is 5 to 6 km, their evolved morphological features could be explained two ways. Large grains are less easily suspended and transported than small grains, spending more time in the stream bed, or caught in the small crevices of bedrock and gravel bars (Youngson and Craw, 1999). This means that these grains sit stationary, while bypassing particles continue to hammer and abrade the surface. The result is that compared to other grains in the same sample these well rounded grains are more morphologically evolved due to a longer period of physical

weathering, but no additional fluvial transport. Alternatively, these coarse grains may have been sourced from the reworked, gold-bearing Cretaceous Tantalus Formation inheriting pale-placer morphological characteristics from previous cycles of erosion, transport and deposition.

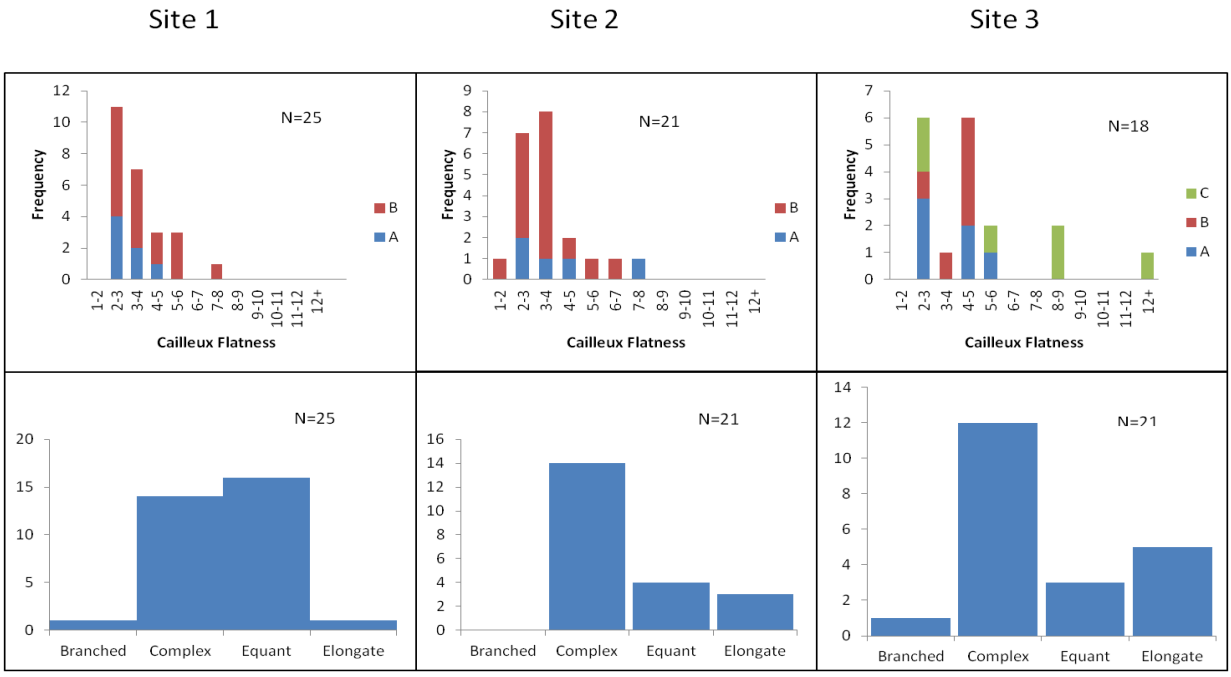

Figure 4.3 Summary of morphological results from Sites 1-3. These histograms highlight the predominance of low flatness grains(seen on top) with complex outlines.

Site	Type (%)	Notes	Flatness Range	Site Avg.	Type Avg.	Est. Transport
1	A -17%	Branches, sub rounded	2.5-4.3	3.8	3.1	1-5 km
	B -71%	Rounded, complex outline	2.3-7.6		3.7	1-5 km
	C-12%	Coarse (3-6 mm), rounded	3.3-4.5		3.9	1-5 km
2	A - 25%	Complex	2.3-7.6	3.6	4.0	1-5 km
	B - 75%	Rounded, pitted surface	1.6-7.7		3.5	1-5 km
3	A - 30%	Crystalline, complex	2.0-4.8	5.7	3.8	1-5 km
	B - 50%	Irregular, rounded	2.7-8.9		5.4	1-5 km
	C - 20%	Large(2-4 mm), polished,	3.4-20		8.6	>10 km,

Table 4.2 Statistical summary of morphological results from sites 1 to 3 including estimates of transport distances.

4.2.2 Geochemical signatures: Sites 1 to 3

Alloy compositions for all grains from sites 1 to 3 are plotted in Figure 4.4 and show considerable variability, with silver contents ranging from 15 to 45 wt%. In general, silver composition is high (>25 wt. %). Fineness values were low (500 to 700) for short travelled A and B type grains. These values are consistent with similarly low fineness values and high mercury contents associated with epithermal style gold mineralization in the Eureka Dome area (Fig. 4.5; Table 4.1). High fineness values (700 to 800) grains are also present in many C type grains, particularly from site 3. These more gold rich grains are generally found with mercury below detection limits. Their geochemical signature (gold-rich, mercury-poor) best matches type 1 Klondike signature, defined by Chapman et al. (2010). While it is possible that this mineralization style reaches as far south as the BHC, these far travelled C type grains may not be local to the BHC. There is potential that they are re-worked, Klondike style grains, from the gold bearing conglomerates of the Tantalus Formation.

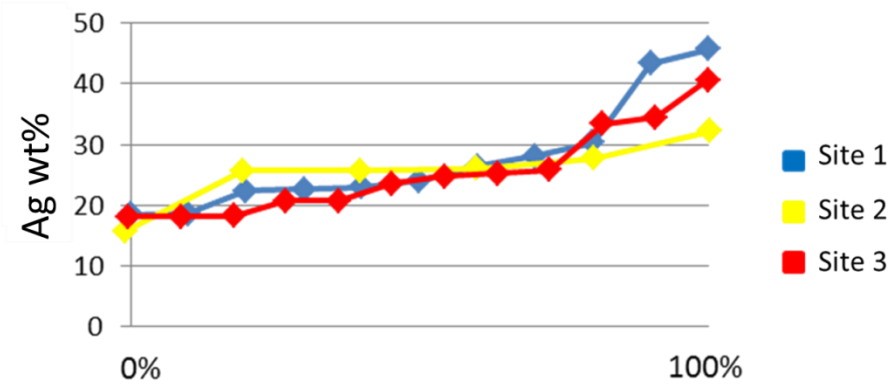

Figure 4.4 Cumulative percentile plot for silver content from the cores of all grains analyzed from sites 1-3. Grains with the lowest silver content start on the left. The slope of the line is an indication of the alloy variation, and in turn fineness, present at each site. Note that most grains from sites 1-3 contained between 20-30 wt% silver, but several grains were found with high silver contents of between 30 and 50 wt%. In general, the geochemical signature of sites 1 to 3 was defined by low fineness values (i.e. high silver content).

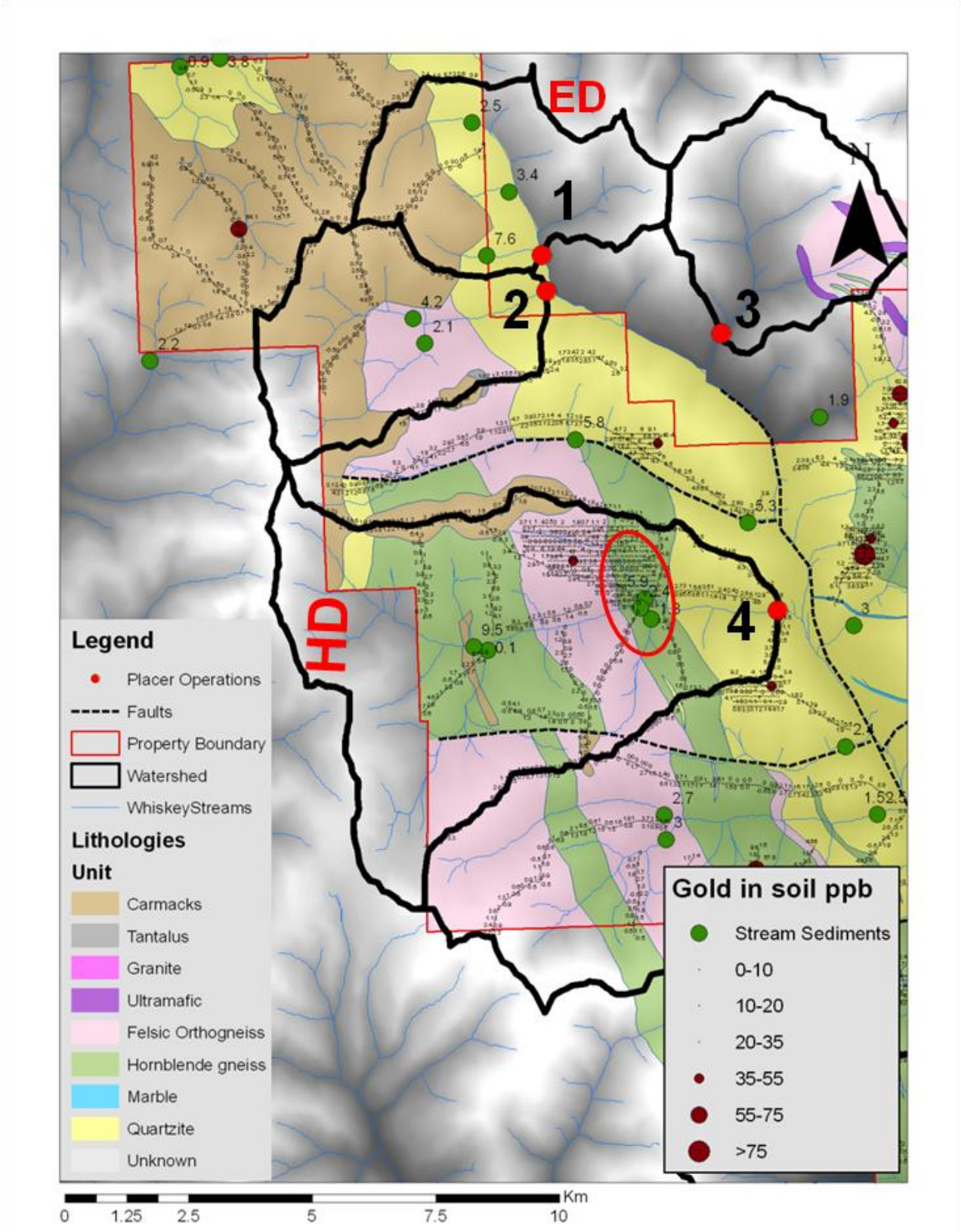

Figure 4.5 Map of the northern BHC watershed, outlining the watersheds of sites 1-4. Known gold occurrences of the Eureka Dome (ED), and Henderson Dome (HD) are indicated in red. Stream sediment samples are listed in ppm.

4.3 Discussion of Site 4

4.3.1 Distance-to-source indicators: Site 4

Results from site 4 grains reveal a wide range of morphologies. A small portion of the sample (~15%) consists of A type grains which display original crystal habit, complex surface textures, and branched outlines. Flatness indices range from 2.6 to 7.0 (excluding those that displayed primary crystal structure) and grain edges are typically very angular, suggesting short transport distance of less than 3 km (Table 4.3). B type grains are the predominant population (~75%) at site 4 and are characterized by complex to equant outlines and rounded edges. Flatness indices are clustered between 3 and 7 (Fig. 4.6), and as high as 11. Estimated fluvial transport distances range from 2 to 5 km (Table 4.3). Finally, a small number of C type grains were identified and display polished surfaces and flatness indices as high as 11, suggesting significant transport. The distribution of the flatness indices shown in the histogram in Figure 4.5 is distinct from those of sites 1 to 3.

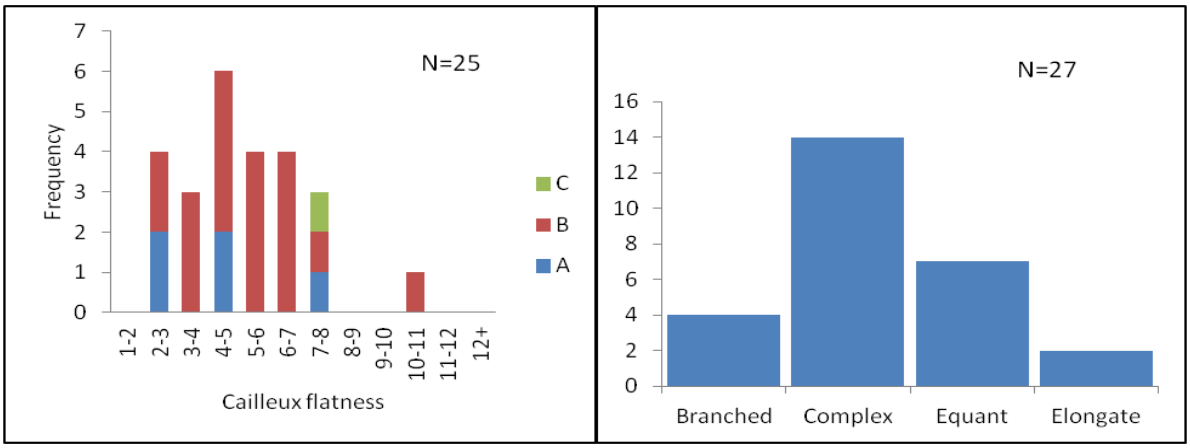

Figure 4.6 Summary of morphological results from site 4.

Site	Type (%)	Notes	Flatness Range	Site Avg.	Type Avg.	Est. Transport
4	A-20% -	crystalline habit, angular edges	2.6-7.0	5.1	3.9	< 3 km
	B-70%	irregular outline, rounded edges	3.0-7.7		5.3	2-5 km
	C-10%	Polished surfaces, equant outline	7.8-10.5		3.1	~10 km

Table 4.3 Statistical summary of morphological results from site 4, including estimates of transport distances.

Flatness indices seem to cluster evenly between 2 and 8. The generally low flatness indices of A and some B type grains suggest a proximal source, while the presence of more evolved C type grains suggests input from a more distal source.

The stream valley which contributed sediment to the site 5 placer also runs parallel to a set of E-W trending faults (Fig 4.5). Considering that there are no significant gold in soil targets, but that stream sediment samples returned values of up 9ppm gold (Fig 4.5), the rocks mantling the stream itself could potentially be a source of mineralization. Perhaps the stream itself is occupying a mineralized fault zone. Alternatively, the gold could be derived from the Henderson dome area (Fig 4.5), although this would make it difficult to explain the predominance of less evolved, nearly crystalline A and B type grains.

4.3.2 Geochemical signature: Site 4

The silver composition plot shown in Figure 4.7 shows a narrow range of alloy composition for site 4. Mercury content is anomalously high (4 and 6 wt %) for two of the grains analyzed, but in general was below detection. Considering the range of morphologies present at site 4, consistent silver concentration suggest a single source, and supports the idea of linear alteration zone within the creek bed or parallel to the stream itself.

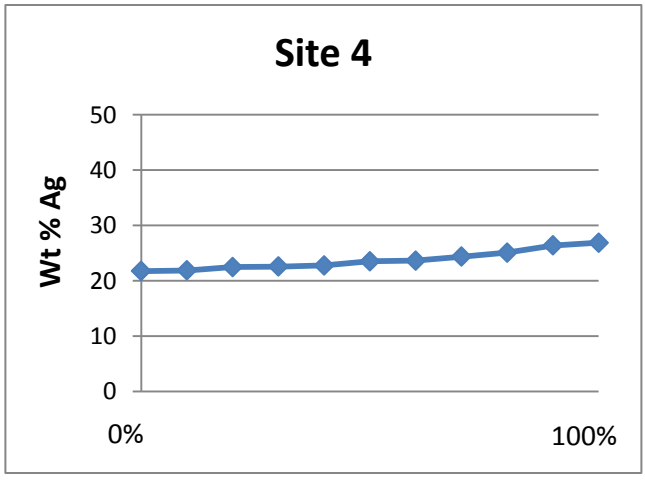

Figure 4.7 Cumulative percentile plot for silver content from the cores of all grains analyzed from site 4. The alloy composition is very consistent across all grain types

4.4 Discussion of Site 5

4.4.1 Distance-to-source indicators

From the DEM model, a maximum transport distance of approximately 20 km to the source can be inferred from the headwaters of the BHC, to the site 5 placer. The catchment area includes the drainages of sites 1 to 4, which need to be considered as potential sources for site 5. Morphological results show a strong bimodal distribution of flatness indices (Fig 4.8). The two populations consist of A and B type grains with flatness indices between 4 and 5 and predominantly C type grains with flatness indices greater than 10. This bimodal distribution is also evident in the variations of outlines from site 5, where numerous A type grain display branched and complex outlines having experienced little rounding, and all C and some B type grains with equant outlines and well rounded edges (Fig 4.8). This wide range of morphological characteristics are typical of a transitional, or trunk placer, and suggest that multiple sources are contributing placer gold to site 5.

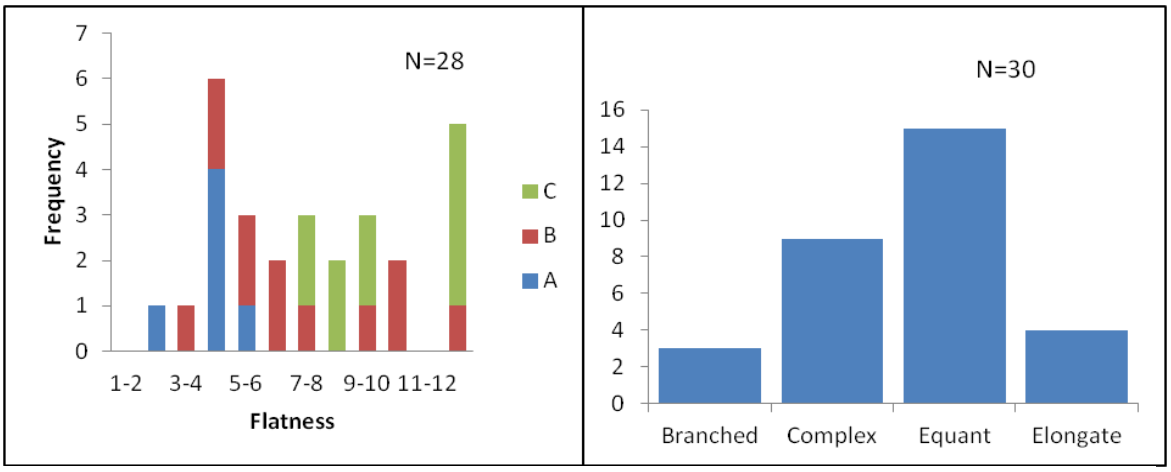

4

Figure 4.8 Morphological results from site 5. The bimodal flatness suggests multiple sources

Site	Type (%)	Notes	Flatness Range	Site Avg.	Type Avg.	Est. Transport
5	A - 27%	Irregular outline, sub rounded edges	2.7-5.2	8.9	4.0	4-6 km
	B - 40%	Irregular outline, rounded edges	4.3-19		7.3	4-15 km
	C - 33%	Equant outline, v. rounded edges	7.2-27		14	>10 km

Table 4.4 Statistical summary of site 5 morphology, including transport estimates from multiple sources.

Proximal sources (between 4 and 6 km) are inferred for A and some B type grains, while a more distal (likely greater than 15 km) sources are contributing grains with more evolved morphologies. When considered with gold in soil anomalies, 2 target zones with up to 271 ppb gold are highlighted as the likely origin of A and B type grains (Fig 4.9). These targets have been trenched and mapped in 2011 and consist of vuggy quartz veins with sericite, jarosite and hematite alteration halos. These target zones are interpreted to be related to an epithermal-style hydrothermal alteration system associated with Cretaceous brittle faulting (Smerchanski and Arne, 2011). In addition, grab samples from the trenching program yielded sample with up to 6.6 g/t gold.

4.4.2 Geochemical Fingerprint: Site 5

Silver compositions (Fig 4.10) show the largest variation in alloy composition of any site. A type, short-traveled grains, and have a consistent high fineness (800 to 940), also present in several B and C types grains. However, C type grains display a wide range in fineness (620 to 850), strengthening the interpretation that site 5 is multiple source deposit. Mercury was consistently above detection limits for A, B and C grains, with most values between 0.2 and 0.4 wt %. The high fineness and moderate mercury content, when compared with other regional gold occurrences (Table 4.1), best resemble that of placer grains from the White Gold District to the southwest (Fig 4.2; Table 4.1). The proposed proximal source of A and B type grains and their geochemical signature (gold rich, with mercury above detection limit) suggests these grains are sourced from a nearby mineralization zone, defined as epithermal style by Smerchanski and Arne (2011) (Fig. 4.9).

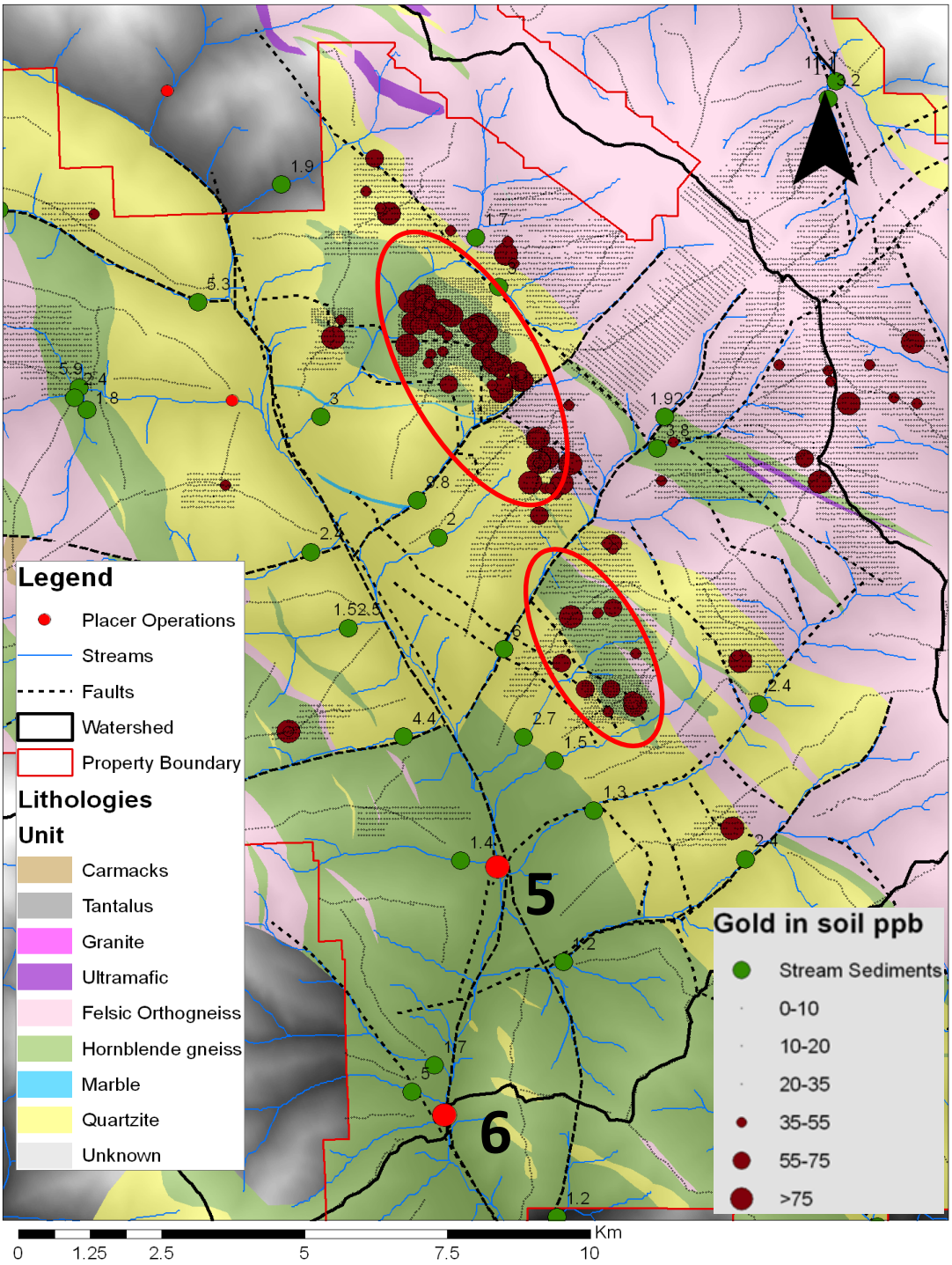

Figure 4.9 Geologic map of the area close to sites 5 and 6. Highlighted in red ovals are the inferred proximal sources of A and B type grains. Maroon dots are gold-in-soil anomalies, with their corresponding values listed in the legend. Green dots are gold anomalies in stream sediments, with their values listed in ppm.

The geochemical signature of these short travelled grains however, does not fit well to the epithermal signature of the Eureka Dome (Table 4.1). Lower fineness (i.e. higher silver content), and moderate to high mercury content of further travelled B and C type grains are likely sourced from epithermal occurrences in the northern watersheds of the BHC .

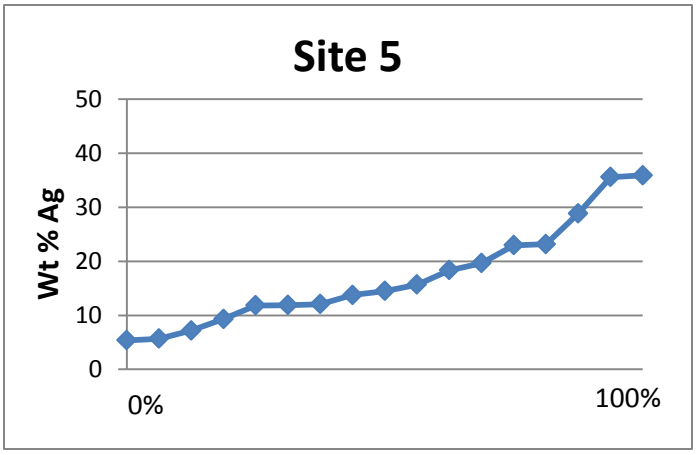

Figure 4.10 Cumulative percentile plot for silver content from the cores of all grains analyzed from site 5. The variation in alloy composition suggests multiple sources.

4.5 Site 6

4.5.1 Distance-source-indicators: Site 6

Site 6 is also a trunk placer located in the main valley of the BHC and has a catchment area that contains those of sites 1 to 5. It is important to consider the sources of all previous placer sites when interpreting potential sources of this type of multi-source placer. A type grains were not found at site 6, and while some complex outlines, and sub-rounded edges were observed, the sample was predominantly morphologically evolved B and C type grains. Flatness indices range from 3 to 22, but as seen in Figure 4.11 the flatness histogram is strongly skewed towards grain with flatness indices greater 12. The first appearance of well folded gold particles is also at site 6 (refer to Fig 3.20 F). The lack of A type grains suggests no proximal source exists downstream from site 5, with the observed difference in morphologies attributed to the additional fluvial transport (approximately 5 to 6 km) required to move a grain from site 5 to site 6. Significant re-working of grain outline and flatness has evidently taken place in those additional 5 km.

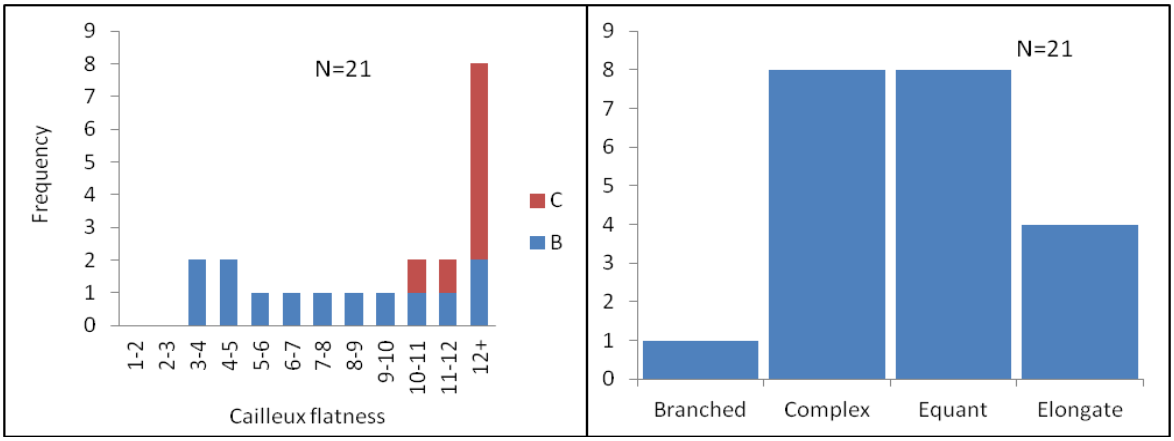

Figure 4.11 Morphological results from site 6 that display morphology more evolved than site 5

Site	Type (%)	Notes	Flatness Range	Site Avg.	Type Avg.	Est. Transport
6	B-70%	Irregular outline, sub-rounded edges	3.2-13	11.3	5.8	~5-10 km
	C-30%	Polished surface, v. rounded edges	10-22		15	10-20 km

Table 4.5 Statistical summary of site 6 grains, including estimates of transport distances.

4.2.4 Geochemical Fingerprint: Site 6

Interpretation of mineralization is limited by the number of grains (6) that yielded good quality spot analysis. Alloy composition is gold rich (80 to 90 wt%; Fig. 4.12), and shows mercury well above detection limits for 3 of 6 grains. The geochemical signature is similar to A type grains from site 5, with no grains that display the low fineness signature of sources from the northern tributaries. This may suggests that the majority of grains in these trunk placer systems are sourced from the identified trend of epithermal style targets in the eastern flank of the BHC watershed (Fig. 4.9), however additional samples would be required to confirm the different proportions of these types of multiple source placers.

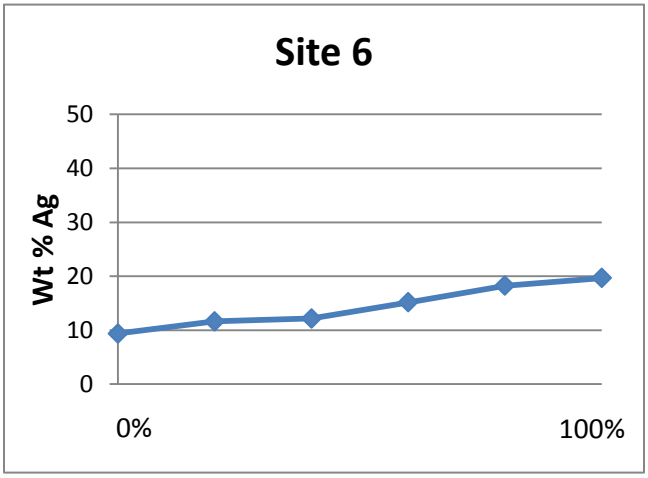

Figure 4.12 Cumulative percentile plot for silver content from the cores of all grains analyzed from site 4. The alloy composition is very consistent across all grain types

4.3 Comparisons with Regional Signatures

4.3.1 Northern Sites (1 to 4)

Numerous studies of placer gold from the Stewart River area have produced a good geochemical database from which to compare microprobe results from the study area. As seen in Figure 4.2 and Table 4.1, geochemical fingerprints have been defined for the orogenic, Klondike style mineralization (Knight et al., 1999b; Chapman et al., 2008; 2010), as well epithermal occurrences in the White Gold District, and the Eureka Dome area (Dumula and Mortensen , 2002). Additionally, the input of re-worked gold from the Tantalus Formation is likely. The BHC is close to all three and consists of a wide range of geochemical results. Within northern placers (sites 1 to 3), morphological analysis suggests most grains are sourced from bedrock within the BHC watershed, while a small proportion display evolved morphological characteristics likely inherited from previous cycles of transport and deposition (e.g. re-worked gold from the Tantalus Formation). Geochemical signatures of site 1 to 3 are predominantly restricted to fineness values of less than 800, but mercury contents range from 0 to 1.5%. The most likely sources contributing to the northern sites are by direct input from *in situ* epithermal mineralization related to that of the Eureka Dome (outside the claim block) with additional input from the Tantalus Formation (re-concentrated, Klondike grains). Results from site 4 are interesting. Geochemical signatures from site 4 are well constrained and indicate a single style of mineralization. Microprobe results previously reported by Bond and Chapman (2007) and Dumula and Mortensen (2002) for epithermal style mineralization in the Henderson Dome area (Fig.4.2) are consistent with the results of this study

4.3.2 Site 5 and 6

Sites 5 and 6 are the only two placers which source sediment from the eastern flanks of the BHC (Fig 4.1), where current exploration is focused, and potential for gold mineralization is thought to be the highest (Smerchanski and Arne 2011). Morphology of gold grains from site 5 indicate multiple sources, which is supported by wide range of alloy composition seen in site 5 (Figure 4.10). These sources likely include significant contribution of A and B type grains from the identified targets in the eastern BHC (Fig. 4.9). The geochemical signature of these proximal sources is defined by high fineness (800 to 940) and low to moderate mercury concentrations. These data do not fit well with the orogenic Klondike signature as proposed by Chapman et al. (2011) or the epithermal fingerprint of the Eureka Dome (Table 4.1). The predominant geochemical signature of these sites best matches established geochemical signatures for placer gold from Kirkman, Blueberry and Thistle Creek placers in the White Gold District (Fig 4.2). Dumula and Mortensen (2002) characterized these placers by high fineness (800 to 900) and low moderate mercury content (0 to 1%, commonly above detection limit) The authors proposed that these placers were likely sourced from intrusion related sources, but this hypothesis pre-dates the recent discovery of the Late Cretaceous epithermal-related Golden Saddle deposit (Fig 4.2). Given its proximity and tonnage, it is the likely source of placer gold in the Kirkman, Blueberry and Thistle Creeks. The structural setting and timing of gold occurrences in the eastern BHC is also a better match with the mineralization style in the White Gold District (Mackenzie and Craw 2011). In both cases brittle normal faulting, associated with late Cretaceous extension are observed to host gold bearing

hydrothermal mineralization (Mackenzie and Craw 2009; 2011, Smerchanski and Arne, 2011).

Ideally, short travelled grains from epithermal-style targets would display the same geochemical signature as the Eureka Dome, but the results of this study, and data from BHC gold grains in Chapman et al. (2011) do not suggest an association between the mineralization in the eastern BHC and the Eureka dome. If interpretations of mineralization are to be based solely on the geochemistry of placer gold, including characterizations which rely heavily on inclusion suites (Chapman et al., 2011), no association can be made between the epithermal occurrence in the Eureka Dome. His study concluded that since they did not share the characteristics of the Eureka Dome (High silver and mercury content), the Jurassic aged orogenic mineralization in the Klondike must extend as far south as the BHC. These inclusions are found in only a small proportion of placer gold grains, and are easily removed during physical weathering. Thus, it is difficult to assess the effectiveness of this type of characterization.

Results from this study show that the fineness values (800 to 940) and mercury content (0 to 0.5 wt %) of site 5 and 6 grains sourced from epithermal style targets are most comparable with placer grains from the White Gold District, where a second phase of Late Cretaceous mineralization is known to be pervasive. The similarities also extend to structural similarities based on extensive field mapping. Perhaps these hydrothermal systems are re-mobilizing Klondike style orogenic gold, concentrating them into shallower hydrothermal deposits, and inheriting their gold-rich alloy composition. This may explain the non-association with the Late Cretaceous Eureka Dome signature.

CHAPTER 5: CONCLUSIONS AND RECOMMENDATIONS

5.1 Conclusions

1. The majority of gold grains from the BHC placer operations have anomalously low flatness indices that are less than 7. Grains from sites 1 to 4 strongly indicate transport distances of less than 5 km, and geochemical signatures most compatible with the Eureka Dome. Downstream in the trunk placers with multiple sources higher, morphological results suggest significant input from both proximal and distal sources, with significant contribution from exploration targets in the eastern flank of the BHC. flatness indices indicate significant transport distances (sites 5 and 6), estimates of 10 to 20 km transport are reasonable if sourced from the headwaters of the BHC. This suggests that placer gold grains in the BHC are derived from bedrock occurrences within the BHC watershed, with the exception of a small proportion of potential inputs from re-worked Tantalus Formation

2. The effectiveness of grain flatness as a distance to source indicator has been shown with varying degrees of certainty and scale. The morphological results of this study suggest that flatness is a good indicator of moderate transport distances, within 5 to 15 km. With very short distances, initial grain shapes predominate and average or modal flatness is difficult to interpret. Long distances can are also difficult because once a grain has become sufficiently flat (i.e. the surface area to volume ratio has become very large) grains are more easily suspended and transported. Based on the results from site 5, the characterization of placer grain populations based on flatness seems most effective for distinguishing between single and multiple source placers. However, results from site 6 suggest that this distinction becomes less obvious as the distance from the most proximal

source increases. Additional fluvial transport, where sub-types become more difficult to identify

3. While recent exploration in the White Gold District has focused primarily on ridges and spurs, significantly less time and resources have been devoted to exploration in the valley bottoms and streams themselves. Mapped faults in the BHC (Fig 4.7, 4.10) suggest that the spatial distribution of streams is controlled by the structural history of the area. Bedrock offset is observed in parallel fault zones now occupied by modern streams. These faults are seen parallel to stream that feeds site 4, where the alloy compositions suggest a single mineralization event. Morphological results indicate that grains from site 4 have experienced a variety of transportation histories, including extremely short travel distances, inferred from near crystalline grains. Offset in the stream has not been identified during mapping, but a linear mineralization zone parallel to or within the stream itself is inferred from the combined geochemical and morphological results. Considering the lack of gold-in-soil anomalies on the ridges which surround the drainage, the stream itself may be worth increased exploration focus.

4. The short travelled grains from site 5 show are likely sourced from identified epithermal style targets in the eastern part of the BHC watershed (Fig 4.10). Fluvial transport distances of approximately with When analyzed with the microprobe, site 5 grains show a geochemical fingerprint distinct from sites 1 to 4, but similar to grains from site 6. The majority of placer gold in the trunk placers (sites 5 to 6) is interpreted as sharing this geochemical fingerprint. When compared with other studies in the Stewart River area, this signature best matches placer samples from the White Gold District (Fig. 4.4). Additionally,

the structural controls on these targets also match that of known deposits in the White Gold District, namely the Golden Saddle and Coffee. The preferred interpretation of the mineralization style of these targets is interpreted as low sulphidation epithermal style. Considering everything mentioned above and the high gold grades in grab samples from this target (up to 6 g/ton), this undrilled target should be a priority for the upcoming 2012 field season.

5. Exploration in covered areas requires the use of unconventional techniques. This study combined grain morphology, geochemistry and DEM analysis to determine the provenance of placer gold within the BHC. This multidisciplinary approach proved successful and has added to the understanding of gold mineralization in the BHC. Morphology allows us to physically characterize each placer sample based on the number and proximity of potential sources. Geochemistry, when considered with previous work in the region, allows for interpretation of the style of mineralization. These interpretations were greatly improved by the extensive database provided by the sponsoring company. An enormous amount of geochemical data and field observations allowed for correlation between morphology and mineralization style.

5.2 Recommendations:

1. With respect to the geochemical analyses, this study highlighted some of the challenges involved. Several steps could be taken to improve the geochemical fingerprinting of gold from the BHC. Preparation of additional samples would allow for improved characterization of the alloy composition and inclusion suites present in the different sources contributing to placers in the BHC. The results of our microprobe analysis were

limited by both time and the efficiency of sample preparation, both limiting size of the database. Ideally, to more confidently characterize the geochemical fingerprints, additional samples would be prepared and extensive time spent on microprobe analysis. Large databases are particularly important to the characterization of placers which are thought to contain multiple sources. Continuing with this study, priority should be focused on short travelled grains from sites 5 and 6.

2. Additionally, Laser ablation ICP-MS (LA-ICP-MS) analysis of placer gold grains reveals concentrations of trace elements not detectable by microprobe analysis. Nickel, iron and other pathfinder elements such as molybdenum, tellurium, bismuth, are known to exist in variable amounts in bedrock-hosted gold showings and could be used to assign much more accurate geochemical fingerprints to placer gold grains. ICP-MS applied to gold grains is a relatively new analytical approach, but with significant ongoing placer gold research in the Western Yukon, comparable databases are growing.

REFERENCES

Bond, D. P., and Chapman, R. (2006). Evaluation of the origins of gold hosted by the conglomerates of the Indian River formation, using combined sedimentological and mineralogical approach. Yukon Exploration Geology , 93-103.

Chapman,R. J. M. (2010). Microgeochemical studies of Placer and Lode Gold in the Klondike District, Yukon, Canada:1. Evidence for a Small, Gold-Rich, Orogenic Hydrothermal System in the Bonanza and Eldorado Creek Area. Economic Geology v. 105 , 1369-1392.

Chapman, R.J., Mortensen, J.K. and Lebarge, W.P. (2011). Styles of lode gold mineralization contributing to the placers of the Indian River and Black Hills Creek, Yukon Territory, Canada as deduced from microchemical characterization of placer gold grains. Miner Deposita , 881-903.

Dumula, M., and Mortensen, J. (2001). Composition of placer and lode gold as an exploration tool in the Stewart River map area, Western Yukon. Yukon Exploration and Geology , 87-102.

Duk-Rodkin, A., Barendregt, R.W., Froese, D.G., Weber, F., Enkin, R., Smith, I.R., Zazula, G.D., Waters, P and Klassen, R. (2004) Timing and extent of Plio-Pleistocene glactiations in north-western Canada and east-central Alaska. Quaternary glaciations-Extent and Chronology , Part II pp 131-345.

Dusfrene, M., Morison, S., and Nesbitt, B. (1986). Evidence of hydrothermal alteration in the White Channel sediments and bedrock of the Klondike area,west-central Yukon. Yukon Geology Volume 1.Exploration and Geological Services Division, Yukon Region, Indian and Northern Affairs Canada , 44-49.

Ryan, J., and Gordey, S. 2002. Bedrock geology of Yukon-Tanana terrane in southern Stewart River map area, Yukon Territory. Geological Survey of Canada, Current Research, no. 2002-A1, 11 pages.

Hallbauer, D., & Utter, T. (1977). Geochemical and Morphological Characteristics of Gold Particles from Recent River Deposits and the Fossil Placers of the Witwatersand. Mineralium Deposita Vol.12 , 293-306.

Jackson, L., Froese, D., Huscroft, C., F.E.Nelson, Westgate, J., Telka, A., (2009). Surficial Geology and Late Cenozoic History of the Stewart River and Northern Stevenson Ridge Map Areas, West-Central Yukon Territory. Ottawa: Geological Survey of Canada, Open File 6059.

Jenson, S., and Domingue, J. (1988). Extracting Topographic Structure from Digital Elevation Data for Geographic Information System Analysis. Photogrammetric Engineering and Remote Sensing Vol. 54, No. 11 , 1593-1600.

Knight, J., Morison, S., and Mortensen, J. (1999a). The relationship between Placer Gold Particle Shape, Rimming and Distance of Fluvial Transport as Exemplified by Gold from the Klondike District, Yukon Territory, Canada. Economic Geology Vol. 94 , 635-648.

Knight, J., Mortensen, J., & and Morison, S. (1999b). Lode and Placer Gold Composition in the Klondike District, Yukon Territory, Canada: Implications for the Nature and Genesis of Klondike Placer and Lode Gold Deposits. Economic Geology Vol. 94 , 649-664.

Lowey, G. W. (2006). The origin and evolution of the Klondike goldfiends, Yukon, Canada. Ore Geology Reviews Vol. 28 , 431450.

Mackenzie, D., and Craw, D. (2009). Structural controls on hydrothermal gold mineralization in the White river area, Yukon. Yukon Exploration and Geology , 253-263.

Mackenzie, D., and Craw, D., (2011). The structural setting of the Smash Minerals Claim Geoup in the Stewart River area, Yukon Canada. Vancouver: Smash Minerals Corporation.

Mair, J., Goldfarb, R., Johnson, C., Hart, C., and Marsh, E. (2006). Geochemical Constraints on the Genesis of the Scheelite Dome Intrusion-Related Gold Deposit, Tombstone Gold Belt, Yukon, Canada. Economic Geology Vol. 101 no.3 pp 523-553.

Mortensen, J., R.Chapman, LeBarge, W., and L.Jackson. (2005). Application of placer and lode gold geochemistry to gold exploration in western Yukon. Yukon Exploration and Geology 2004. pp 205-212

Nelson, J., and Colron, M. (2007). Tectonics and Mettalogeny of the British Columbia, Yukon and Alaskan Cordillera, 1.8 Ga to the Present. Exploration Methods: Geological Association of Canada , 755-791.

Smechanski, P., and Arne, D. (2011). Technical Report on the Whiskey Property, Yukon Territory, Canada For Smash Minerals. Vancouver: Revelation Geoscience Ltd.

Tarboton, D.G., Bras, R.L., and Rodrigues-Iturbe, I.,(1991). On the Extraction of Channel Networks From Digital Elevation data. Hydrological Processes, Vol. 5 , 81-100.

Tempelman-Kluit, D. (1982). White Channel Gravel of the Klondike. Yukon Exploration Geology 1981, Exploration and Geologic Services Division, Yukon Region, Indian and Northern Affairs Canada. , 74-79.

Townley, B.K., Herail, G., Maksaev, V., Palacios, C.,de Parseval, P., Sepuldeva, F., Orellana, R., Rivas, P. and Ulloa, C. (2003). Gold grain morphology and composition as an exploration tool: application to gold
exploration in covered areas. Geochemistry, Exploration, Environment, Analysis, 3, p. 29-38.

Wainwright, A., Simmonds, A., C.Finnigan, T. S., and R.Carpenter. (2010). Geology of new gold discoveries in the Coffee Creek area, White Gold District, west-central Yukon. Yukon Exploration and Geology , 233-247.

Youngson, J., and Craw, D. (1999). Variation in Placer Style, Gold Morphology, and Gold Particle Behavious Down Gravel Bed-Load Rivers: An Example from the Shotover/Arrow-Kawarau-Clutha River System, Otago, New Zealand. Economic Geology Vol. 94 , 615-634.

APPENDIX A: GRAIN MEASUREMENTS

Images containing measurements are listed in column 1, and can be found on the CD Appendix 1.

SITE 1

	Site 1: Smith (PG4)					
Type	Photo	A(μm)	B(μm)	C(μm)	Flatness	Outline
A	PG4A (2)	4196	3045	827	4.377872	complex
A	PG4A3	4199.77	2885.7	1236	2.86629	equant
A	PG4A(7,8)	3007.73	1660	936	2.493446	complex
A	PG4A(12,14)	1830	862.65	513	2.624415	complex
A	PG4A(	2032	1894	579	3.390328	complex
A	PG4A(17,18)	1985	1559	525	3.375238	equant
A	PG4A(21,20)	1730	1208	496	2.961694	complex
B	PG4B(1,2)	2048	1210	683	5.540678	equant
B	PG4B(29,30)	1848	988	591	2.399323	equant
B	PG4B(32,33)	1163	760	328	2.931402	complex
B	PG4B(35,36)	1158	1012	273	3.974359	equant
B	PG4B(38,39)	919	634	102	7.612745	complex
B	PG4B(38,39)	767	586	121	5.590909	equant
B	PG4B(4,5)	1124	755	242	3.882231	complex
B	PG4B(7,8)	1628	810	416	2.930288	complex
B	PG4B(10,11)	2934.05	1201.1	359	5.759262	complex
B	PG4B(13,14)	1427.5	780	413	2.672518	equant
B	PG4B(16,17)	1325	693	325	3.104615	complex
B	PG4B(19,20)	1271	1234	472	2.653602	Equant
B	PG4B(22,24)	1687	1108	618	2.261327	Complex
B	PG4B(26,27)	1266	1070	286	4.083916	Equant
B	PG4B(41,42)	1988	1619	886	2.035553	Equant
B	PG4B(52,54)	2579	2258	522	4.633142	Equant
B	PG4B(44,45)	2082	1310	335	5.062687	Complex
B	PG4B(46,47)	2082	1304	558	3.03405	Complex
B	PG4B(48,49)	2150	1555	469	3.949893	equant?
C	PG4C	6040	3922	633	7.868878	Equant
C	PG4C4	4407	720	220	11.65227	Elongate
C	PG4C7	4528	3825	450	9.281111	Equant
C	PG4C10	3617	3743	890	4.134831	Equant
C	PG4C13	4054	2075	818	3.746333	Complex
C	PG4C16	2415	868	486	3.377572	Complex
C	PG4C19	3092	2357	600	4.540833	Equant

SITE 2

	Site 2: Nixdorff (PG3)					
Type	Photo	A(µm)	B(µm)	C(µm)	Flatness	Outline
A	PG3A(1,2)	908	614	244	3.118852	complex
A	PG3A(4,5)	1066	645	368	2.324728	complex
A	PG3A(7,8)	1217	395	279	2.888889	complex
A	PG3A(9,11)	699	518	80	7.60625	complex
A	PG3A(14,15)	736	523	144	4.371528	complex
B	PG3B1	821	336	155	3.732258	complex
B	PG3B(26,28)	782	292	155	3.464516	complex
B	PG3B(30,31)	682	450	162	3.493827	complex
B	PG3B(33,34)	932	527	94	7.760638	complex
B	PG3B(4,2)	1261	857	334	3.170659	equant
B	PG3B(4,2)	1809	944	266	5.174812	complex
B	PG3B(6,7)	1682	736	546	2.214286	complex
B	PG3B(8,10)	1204	791	617	1.616694	equant
B	PG3B(8,10)	1163	1288	365	3.357534	complex
B		1207	790	301	3.317276	complex
B	PG3B(12,13)	1966	1046	514	2.929961	elongate
B	PG3B(12,13)	2205	1623	400	4.785	equant
B	PG3B(14,16)	1100	733	329	2.785714	complex
B	PG3B(14,16)	1085	679	404	2.183168	equant
B	PG3B(18,19)	1951	895	494	2.880567	elongate
B	PG3B(18,19)	1741	843	412	3.135922	elongate

Site 3

	Site 3 :Klippert (PG-2)					
Type	Photo	A(µm)	B(µm)	C(µm)	Flatness	Outline
A	PG2A1	1234	580	347	2.613833	complex
A	PG2A(57),	1344.22	777	404.67	2.620926	complex
A	PG2A(30,31)	3022	1394	678	3.256637	complex
A	PG2A(16,17)	1716	841	207	6.176329	equant
A	PG2A(18,20)	769	482	305.33	2.048603	complex
A	PG2A(57,58)	1379	1259	317	4.160883	complex
A	PG2A(22,23)	1038	787	190	4.802632	branched
B	PG2B(23,24)	2019	1704	384	4.847656	equant
B	PG2B(26,27)	1212	992	406	2.714286	equant
B	PG2B(29,30)	1833	1293	370	4.224324	complex
B	PG2B(1,2)	2309	1255	284	6.274648	complex
B	PG2B(4,6)	2035	1528	392	4.544643	equant
B	PG2B(10,12)	3491	2126	288	9.751736	complex
B	PG2B(13,15)	4033	1019	305	8.281967	elongate
B	PG2B (16,18)	2230	1405	532	3.416353	complex
B	PG2B(7,9)	2142	1872	430	4.667442	complex
C	PG2C(1,2)	2010	927	421	3.488124	elongate
C	PG2C(3,4)	3529	1171	286	8.216783	elongate
C	PG2C(5,6)	4095.8	1529	134	20.98806	elongate
C	PG2C(7,8)	3113.96	1589	612	3.842288	elongate
C	PG2C(9,11)	2559	2363.4	393	6.262595	complex
C	PG2C(15,18)	2998	2045	286	8.816434	branched
C		2341	1385			complex

Site 4

	Site 4: Armstrong (PG1)					
Type	Photo	A(μm)	B(μm)	C(μm)	Flatness	Outline
A	PG1A (0L, 4L)	1628	1224.5	490	2.910714	branched
A	PG1A(0R,4R)	1527	1012.3	481	2.639605	complex
A	PG1A(3,6)	2419.9	743.2	N/A		CRYSTALLINE
A	PG1A(3,6)	1543.97	739.65	260	4.391577	complex
A	PG1A(8,9)	1728	937.3	188	7.088564	branched
A	PG1A(11,12)	2445	1307	461	4.069414	complex
B	PG1B(27,29)	1084.8	1261.8	366	3.205738	branched
B	PG1B(28,30)	1129	755	122	7.721311	complex
B	PG1B(32,33)	1795	992	273	5.104396	complex
B	PG1B(32,34)	1564	1055	191	6.856021	complex
B	PG1B(36,37)	1902.4	1104	227	6.622026	complex
B	PG1B(36,38)	1296	1138.5	370	3.289865	equant
B	PG1B(40,41)	1550	939	261	4.768199	complex
B	PG1B(40,42)	1164	813	167	5.919162	equant
B	PG1B(6,7)	1799	963	339	4.073746	complex
B	PG1B(9,10)	1374	857	160	6.971875	elongate
B	PG1B9,11)	992	959	161	6.059006	equant
B	PG1B(1314)	1662	779	261	4.676245	complex
B	PG1B(15,17)	1618.6	663.7	227	5.027093	complex
B	PG1B(19,20)	1218	722	324	2.993827	complex
B	PG1B(22,23)	1491	450	182	5.332418	elongate
B	PG1B(25,26)	1154	750	83	11.46988	equant
B	PG1B(25,26)	1247	804.25	218	4.704702	equant
B	PG1B(1,4)	1261	1084	397	2.953401	branched
B	PG1B(1,3)	1129	755	276	3.413043	complex
C	PG1C(2)	1525	1239	178	7.764045	complex
C	PG1C3	1680	1318			equant
C	PG1C(5,6)	1017	854	359	2.60585	equant

SITE 5

	Site 5: Stuart (PG5)					
Type	Photo	A(μm)	B(μm)	C(μm)	Flatness	Outline
A	PG5A (8,9)	1691	992	330	4.065152	equant
A	PG5A(26,27)	2357	1113	636	2.727987	branched
A	PG5A (8,10)	2127	1317	409	4.210269	branched
A	PG5A(12,13)	2772	2209	188	13.24734	complex
A	PG5A(15,16)	2078	1559	402	4.523632	complex
A	PG5A (1,3)	1990	1448	389	4.419023	equant
A	PG5A(5,6)	2992.8	2043.9	587	4.290204	equant
B	PG5B(1,2)	1281	847	223	4.7713	equant
B	PG5B(4,5)	1565	1003	174	7.37931	complex
B	PG5B(6,8)	1770	634	233	5.158798	complex
B	PG5B(14,15)	1511	711	204	5.446078	equant
B	PG5B(17,18)	1520	1152	358	3.731844	complex
B	PG5B(20,21)	1902	1472	165	10.22424	equant
B	PG5(B11,12)	1207	624	135	6.781481	complex
B	PG5B(3,5)	4171	1549	315	9.079365	elongate
B	PG5B(27,28	1320	830	216	4.976852	complex
B	PG5B(7,8)	2973	1158	106	19.48585	elongate
B	PG5B(23,25)	1711	1149	142	10.07042	branched
B	PG5B(10,11)	1564	1065	340	3.866176	complex
B	PG5B(12,2)	2290	1496	311	6.086817	complex
C	PG5C(2,3)	1969	1572	74	23.92568	equant
C	PG5C(7,5)	2746	1525	215	9.932558	elongate
C	PG5C(9,10)	1922	1104	56	27.01786	equant
C	PG5C(13,12)	2222	1370	116	15.48276	equant
C	PG5C(18,17)	1249	1890	93.63	16.76279	equant
C	PG5C(23,24)	1647	1162	181	7.759669	equant
C	PG5C(25,26)	1193	862	115	8.934783	equant
C	PG5C(28,29)	1300	930	117	9.529915	equant
C	PG5C(32,33)	2308	1573	222	8.740991	equant
C	PG5C(35,36)	1095	862	135	7.248148	equant

SITE 6

	Site 6: Hambrook (NB2)					
Type	Photo	A(μm)	B(μm)	C(μm)	Flatness	Outline
B	NB2B(20,21)	2557.6	2101.72	516	4.514845	branched
B	NB2B(23,24)	1555	1699	243	6.695473	complex
B	NB2B(25,26)	1809.7	1157	208	7.13149	equant
B	NB2B(3,4)	2020	849	447	3.209172	elongate
B	NB2B(7,8)	1863	1070	323	4.540248	complex
B	NB2B(10,11)	1858	1457	305	5.434426	complex
B	NB2B(12,13)	1266	804	303	3.415842	complex
B	NB2B(18,19)	2118	988	193	8.046632	complex
B	NB2B(15,16)	2100	1157	175	9.305714	complex
C	NB2C(37,38)	3271	799	162	12.56173	elongate
C	NB2C(40,41)	3276	2136	145	18.66207	equant
C	NB2C(43,44)	3677	1578.7	204.9	12.82504	elongate
C	NB2C(45,47)	2435	1467	164.5	11.86018	complex
C	NB2C(4,8)	1882	992	100	14.37	elongate
C	NB2C(10,11)	1487	1261	84	16.35714	equant
C	NB2C(12,14)	1535	1312	136	10.46691	equant
C	NB2C(20,17)	2777	1767	122	18.62295	equant
C	NB2C(22,23)	1663	1448	150	10.37	complex
C	NB2C(25,26)	1428	644	50	20.72	elongate
C	NB2C(15,16,17)	3667	2247	132	22.40152	folded
C	NB2C(34,35)	3476	2056.4	174	15.8977	equant
C	NB2C(31,32)	1623	1404	136	11.12868	equant

APPENDIX 2: BSE IMAGES AND MICROPOBE POINT ANALYSES

Site 1

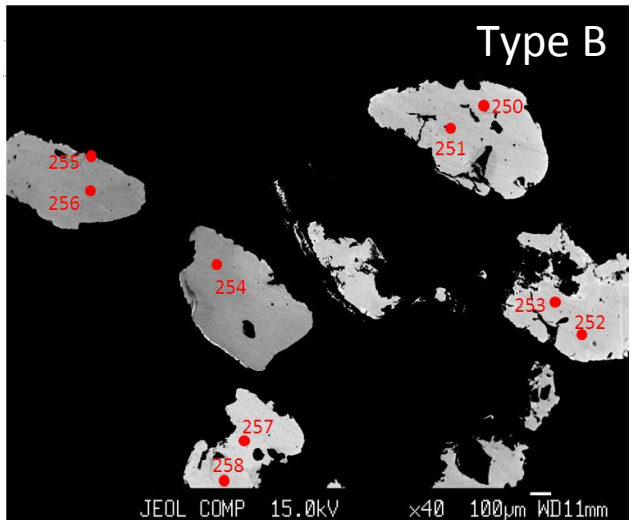

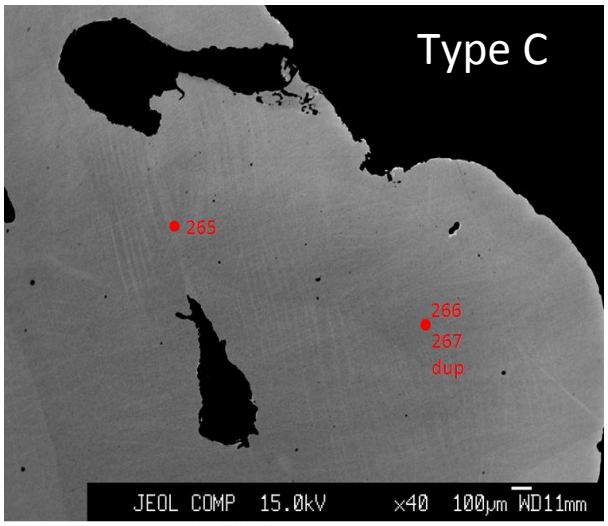

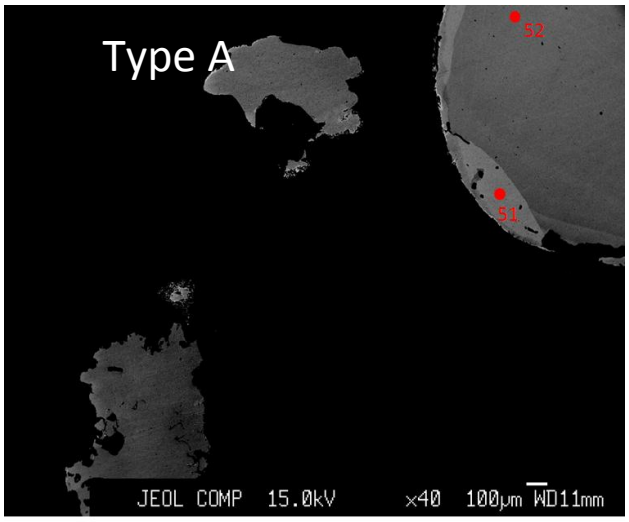

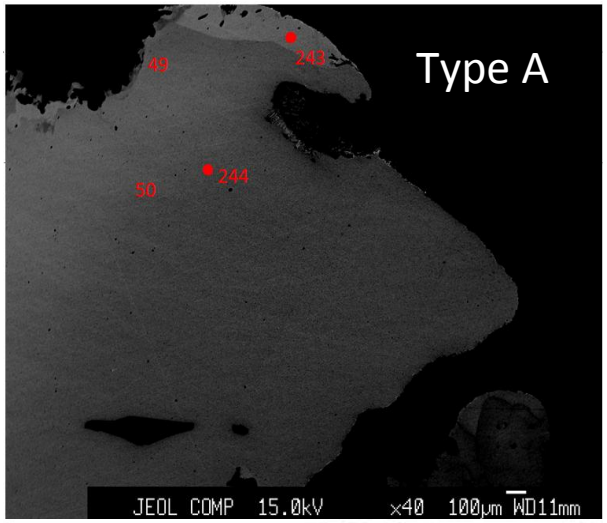

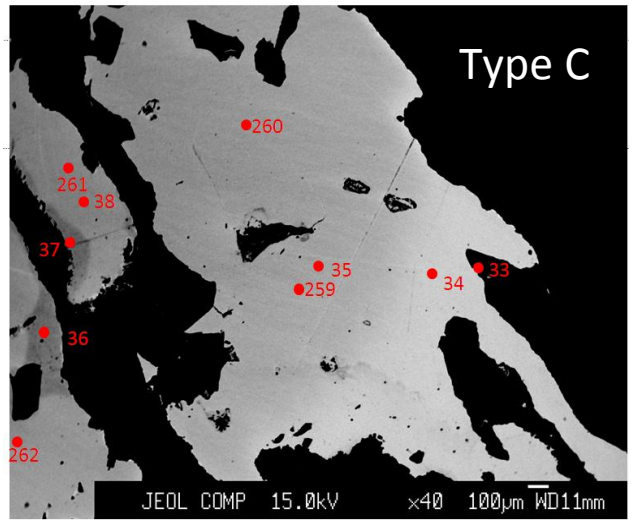

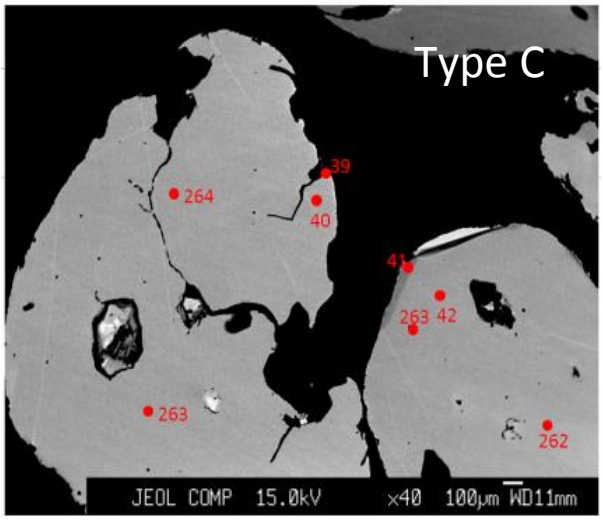

Site 1													
No.	Au	S	As	Fe	Hg	Sb	Ni	Pb	Ag	Cu	Total	Spot	Fineness
33	76.171	0	0.001	0.034	0.014	0	0.008	0.179	17.624	0	94.031	C-rim	812.1009
34	75.774	0	0	0.026	0.045	0	0.047	0	18.362	0	94.254	C-core	804.9418
35	75.861	0	0	0	0	0	0	0	18.077	0	93.938	C-core	807.5646
36	69.891	0.007	0.015	0	0.038	0	0.018	0.118	23.487	0	93.574	C-rim	748.4739
37	66.399	0.003	0	0.01	0.133	0	0	0	26.124	0	92.669	C-rim	717.6486
38	66.938	0	0	0	0	0	0	0	26.101	0.027	93.066	C-core	719.4617
40	75.012	0.004	0	0	0.096	0	0	0	18.596	0	93.708	C-core	801.3418
41	67.992	0	0.002	0	0.146	0	0	0	23.158	0.011	91.309	C-rim	745.9353
42	69.986	0	0	0	0.124	0	0	0.031	22.519	0	92.66	C-core	756.5645
49	66.308	0.015	0.001	0	0.509	0	0	0	25.178	0.037	92.048	A-core	724.7885
50	66.352	0	0	0	0.063	0	0	0.062	27.637	0.013	94.127	C-Rim	705.955
51	67.881	0	0	0	0.31	0	0	0.056	25.565	0	93.812	A-rim	726.4195
52	64.21	0	0.001	0.007	0.09	0	0	0.054	29.017	0	93.379	A-core	688.749
243	65.618	0.01	0.037	0.012	0.21	0	0.02	0.113	27.882	0.011	93.913	A-core	701.7968
244	63.897	0.018	0.012	0	0.412	0	0.004	0.016	27.459	0.036	91.854	A-core	699.4286
245	50.618	0.008	0	0	1.325	0	0	0	41.13	0.01	93.091	A-core	551.7068
246	49.123	0.009	0	0	0.606	0	0	0.226	43.114	0.012	93.09	A-core	532.5737
247	63.144	0.155	0	0	0.2	0	0	0	30.212	0.014	93.725	A-core	676.3786
248	64.987	0.004	0	0	0.084	0	0	0.049	30.331	0	95.455	A-core	681.7915
249	72.748	0.006	0	0.006	0.355	0	0.012	0.185	22.452	0	95.764	A-core	764.1597
250	71.508	0	0	0	0.132	0	0	0.081	24.033	0.008	95.762	A-core	748.4535
251	71.9	0	0.009	0	0	0	0	0	24.581	0.002	96.492	B-core	745.2244
252	65.531	0.01	0	0	1.36	0	0	0	28.132	0	95.033	B-core	699.6466
253	69.748	0	0	0.011	1.401	0	0.026	0.092	25.384	0	96.662	B-core	733.1708
254	45.639	0.011	0	0.021	1.072	0	0	0.123	46.87	0	93.736	B-core	493.3466
255	48.633	0.023	0.012	0.034	1.032	0	0.019	0.145	45.121	0.012	95.031	B-core	518.7299
256	51.475	0.013	0.013	0.009	0.924	0	0.027	0.253	43.351	0	96.065	B-core	542.8364
257	71.965	0	0	0.039	0	0	0	0.188	22.881	0	95.073	B-core	758.7563
258	73.433	0.007	0.01	0	0.084	0	0.006	0.04	22.94	0	96.52	B-core	761.9665

259	78.325	0	0	0.01	0	0	0	0.026	18.383	0	96.744	C-core	809.9123
260	79.699	0	0	0.016	0	0	0.003	0.096	18.492	0	98.306	C-core	811.6732
261	68.439	0	0	0	0.116	0	0	0.152	26.433	0.008	95.148	C-core	721.3825
262	73.045	0	0	0	0.141	0	0.049	0.023	22.605	0.021	95.884	C-core	763.6696
263	77.518	0	0	0	0	0	0	0.117	18.664	0	96.299	C-core	805.9512
264	75.558	0.003	0	0.005	0.019	0	0.003	0.096	18.343	0.022	94.049	C-core	804.656
265	47.877	0	0	0	0.975	0	0.009	0	45.41	0	94.271	C-core	513.2226
266	48.754	0	0.02	0.009	0.815	0	0	0.02	45.702	0.01	95.33	C-core	516.1557
267	47.713	0.003	0	0	1.013	0	0.011	0	45.285	0	94.025	C-core	513.054

Site 2

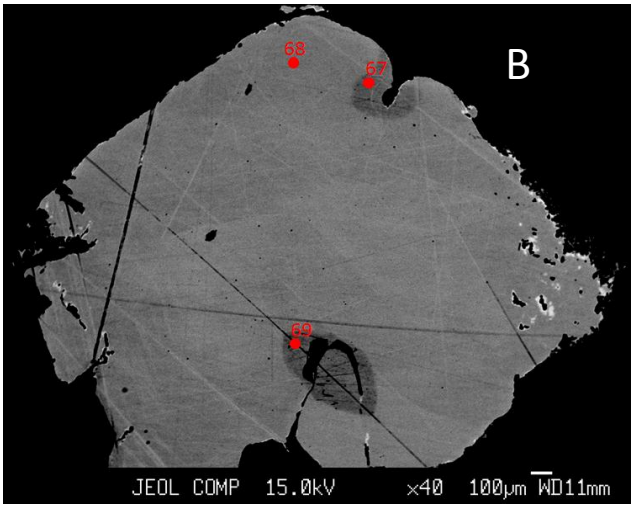
B
68
67
69
JEOL COMP 15.0kV ×40 100µm WD11mm

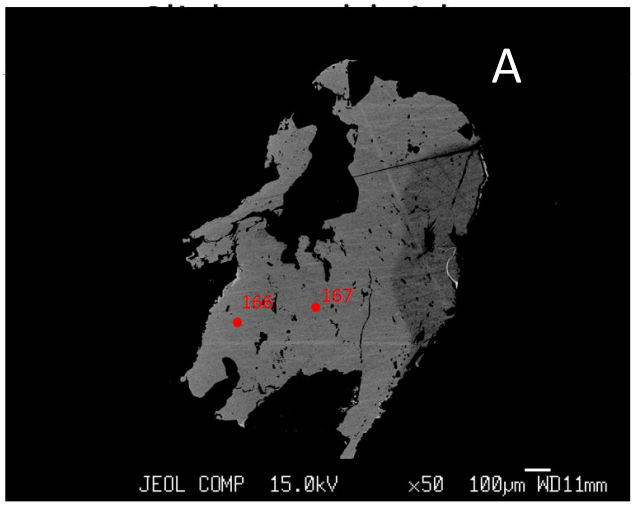
A
166
167
JEOL COMP 15.0kV ×50 100µm WD11mm

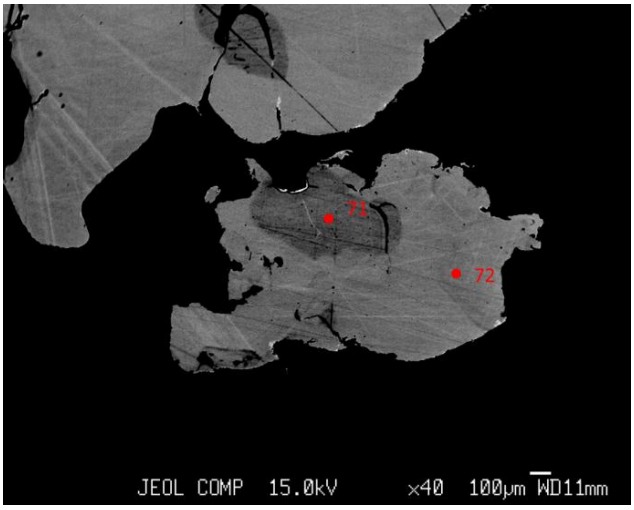
71
72
JEOL COMP 15.0kV ×40 100µm WD11mm

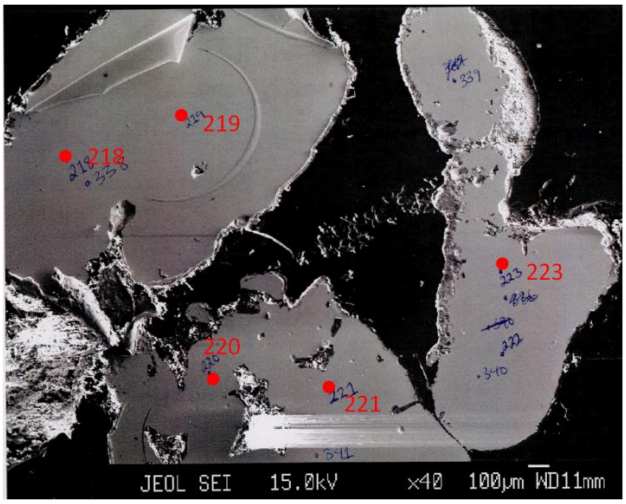
219
218
223
220
221
JEOL SEI 15.0kV ×40 100µm WD11mm

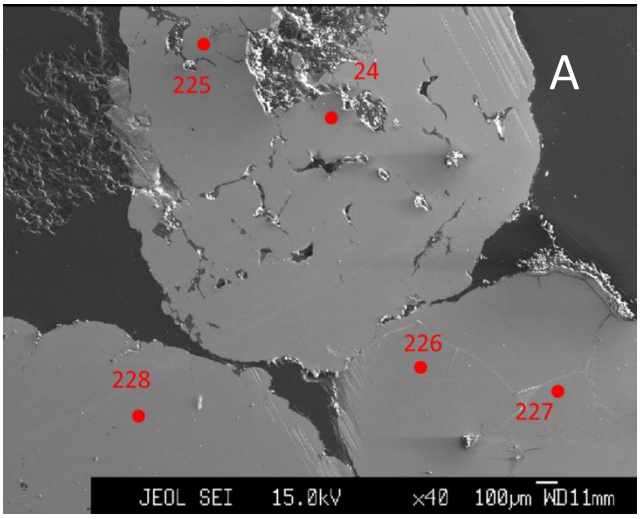
A
225
24
226
228
227
JEOL SEI 15.0kV ×40 100µm WD11mm

SITE 2	Wt%	Wt%	Wt%	Wt%	Wt%	Wt%							
No.	Au	S	As	Fe	Hg	Sb	Ni	Pb	Ag	Cu	Total	Spot	Fineness
67	69.891	0.01	0.02	0	0.038	0	0.	0.118	23.487	0	93.574	B -Core	748.4739
68	66.399	0.00	0	0.01	0.133	0	0	0	26.124	0	92.669	B-core	717.6486
69	68.293	0	0.02	0	0.243	0	0	0	26.823	0.006	95.385	B-core	717.997
70	69.48	0	0	0	0.18	0	0	0	26.49	0.035	96.185	B-core	723.9762
71	67.216	0	0	0	0.082	0	0.0	0.01	26.545	0	93.859	B-core	716.8866
72	65.54	0	0.01	0	0.987	0	0.01	0	28.569	0	95.119	B-core	696.4265
165	83.538	0	0	0	0	0	0	0.003	16.420	0.037	100		835.7291
166	65.593	0	0	0.012	1.261	0	0	0.053	33.078	0	99.999	A-core	664.7604
216	68.195	0	0	0	0.223	0	0	0.011	22.454	0	90.883	B-core	752.2973
217	68.746	0	0	0.026	0.158	0	0.0	0	21.627	0	90.571	B-core	760.6918
218	69.935	0	0	0	0.076	0	0	0.049	22.659	0	92.719	B-core	755.2865
219	67.931	0	0	0.018	0.283	0	0.00	0	20.587	0.065	88.885	B-core	767.4258
220	77.288	0	0	0	0	0	0.	0.19	15.289	0	92.785	B-core	834.851
221	76.615	0	0.01	0	0	0	0	0.132	15.776	0	92.533	B-core	829.2474
222	67.221	0	0.01	0	0.057	0	0.02	0.043	25.652	0.002	93.002	B-core	723.7949
223	66.384	0	0	0.002	0.306	0	0.01	0.024	26.061	0.035	92.818	B-core	718.0918
224	69.517	0	0	0.016	0.199	0	0.02	0.227	21.844	0.014	91.838	A-core	760.9045
225	68.601	0	0	0	0.021	0	0	0.095	21.905	0.007	90.629	A-core	757.9718
226	70.31	0	0	0	0.358	0	0	0.479	21.23	0.009	92.386	A-core	768.0795
227	70.746	0	0	0	0.584	0	0	0.263	21.5	0	93.093	A-core	766.9276
228	66.729	0	0	0	0.206	0	0.017	0.281	23.715	0.013	90.961	A-core	737.7936

Site 3

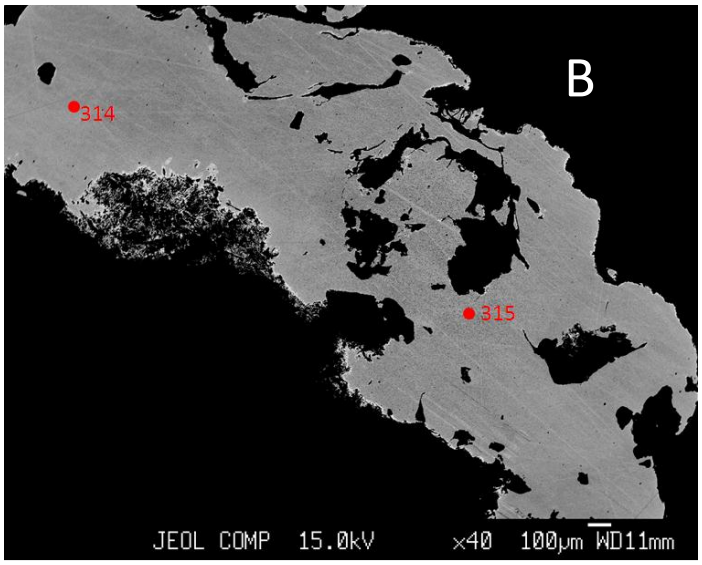
B
314
315
JEOL COMP 15.0kV ×40 100µm WD11mm

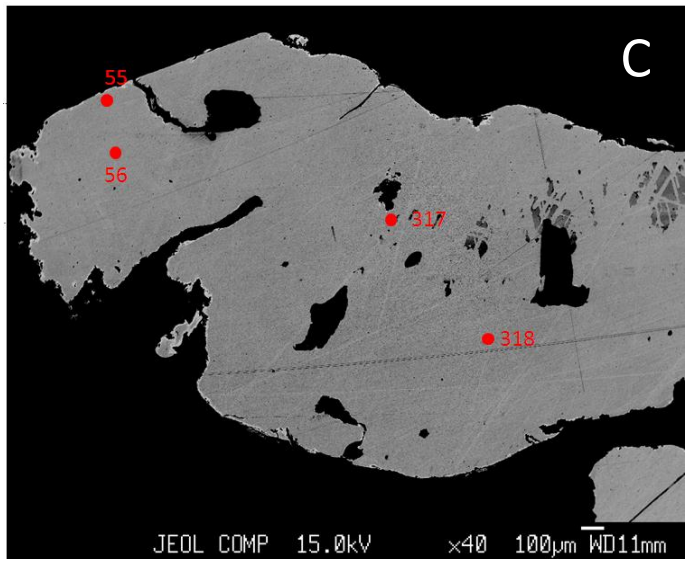
C
55
56
317
318
JEOL COMP 15.0kV ×40 100µm WD11mm

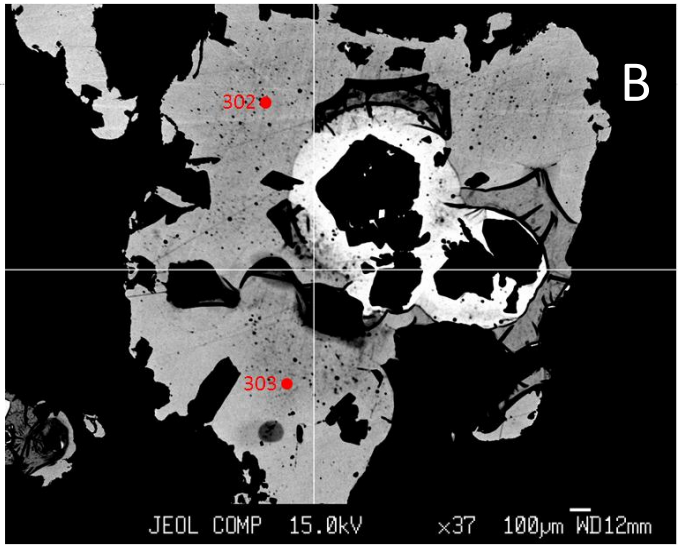
B
302
303
JEOL COMP 15.0kV ×37 100µm WD12mm

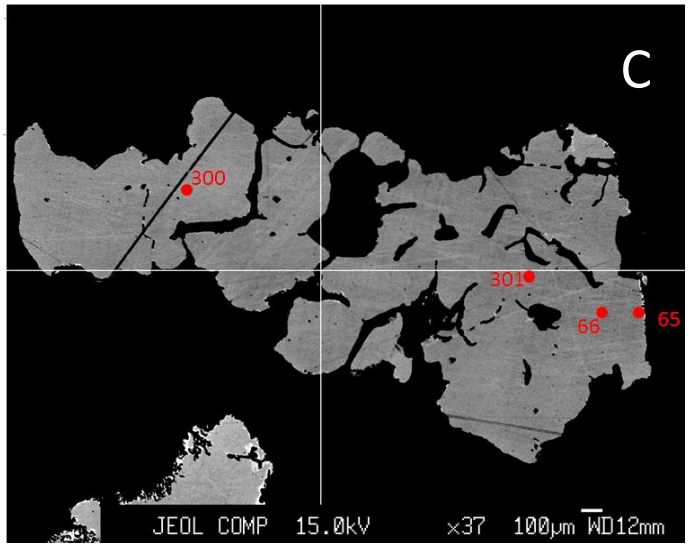
C
300
301
66
65
JEOL COMP 15.0kV ×37 100µm WD12mm

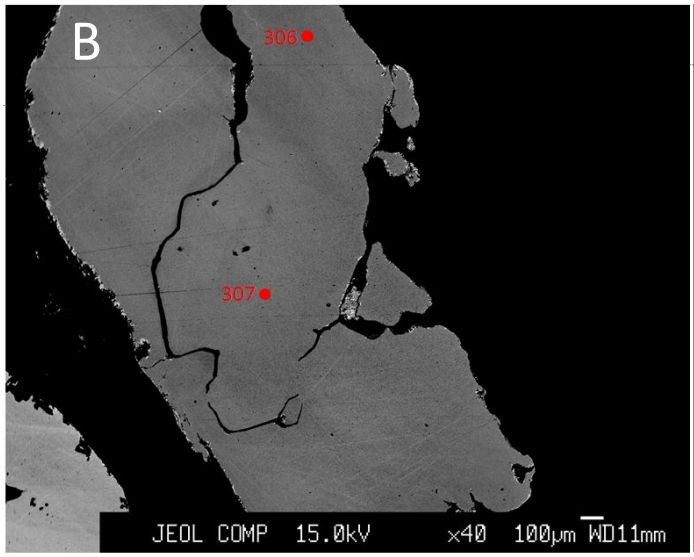
B
306
307
JEOL COMP 15.0kV ×40 100µm WD11mm

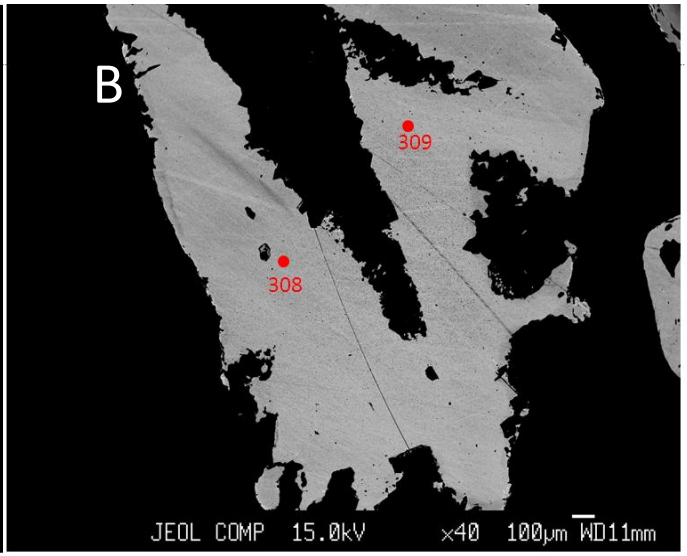
B
309
308
JEOL COMP 15.0kV ×40 100µm WD11mm

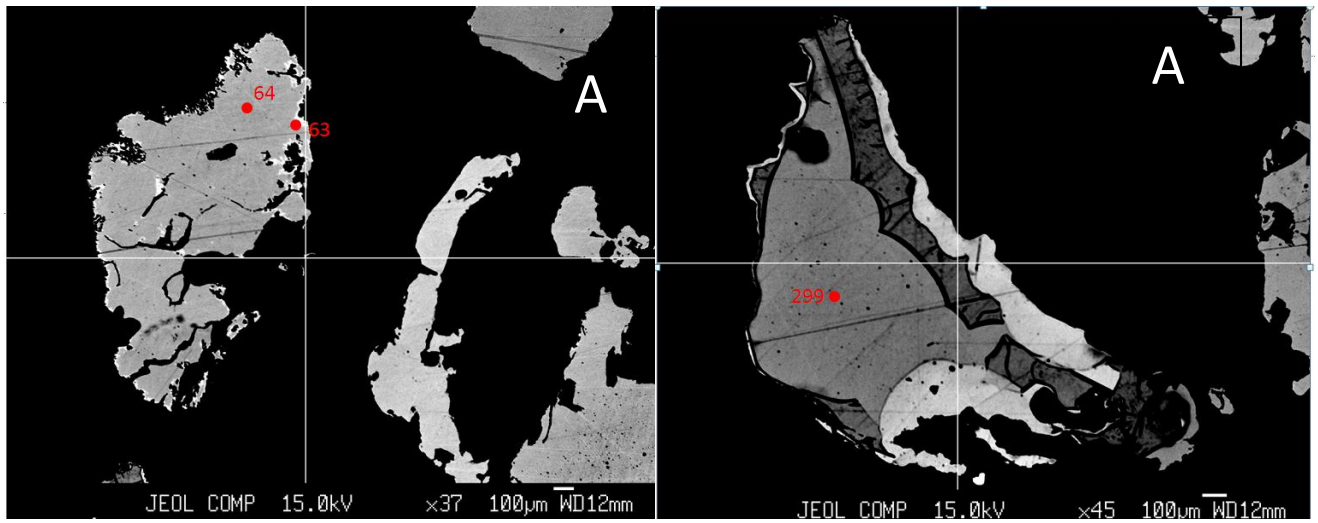

PG2	Wt%	Wt%	Wt%	Wt%	Wt%	Wt%	Wt%	Wt%	Wt%	Wt%	Wt%		
No.	Au	S	As	Fe	Hg	Sb	Ni	Pb	Ag	Cu	Total	Comment	
55	70.999	0	0	0	0.084	0	0	0.03	23.07	0	94.183	C-rim	756.0163
56	71.095	0	0	0	0.074	0	0.027	0.037	22.913	0.042	94.188	C-core	800.0878
63	76.784	0	0	0.02	0	0	0	0.09	18.14	0	95.034	A-rim	757.7992
64	71.843	0	0	0.003	0	0	0	0.072	24.541	0.01	96.469	A-core	696.9365
65	64.565	0	0	0.013	0.096	0	0	0.051	31.241	0	95.966	A-core	672.272
66	62.583	0	0	0	0.154	0	0.037	0.047	31.475	0.065	94.361	A-core	722.4339
299	72.624	0	0	0.027	0.048	0	0	0	24.045	0	96.744	A- core	751.2646
300	64.842	0	0	0.006	0	0	0	0	32.171	0.017	97.036	A- core	668.3846
301	63.332	0	0	0	0	0	0	0.205	32.299	0	95.836	A- core	662.2539
302	76.75	0	0	0	0.023	0	0.005	0.445	19.485	0.043	96.751	A- core	797.5269
303	76.344	0	0	0	0.068	0	0	0.273	20.075	0	96.76	A- core	791.7941
304	74.577	0	0.013	0	1.082	0	0	0.193	19.416	0	95.281	B-core	793.4314
305	71.882	0	0	0	3.24	0	0	0	20.146	0	95.268	B-core	781.0884
306	57.966	0	0	0	0.064	0	0.004	1.013	37.544	0	96.591	B-core	606.9103
307	56.499	0	0	0.01	0.003	0	0.014	0.52	39.357	0.004	96.407	B-core	589.4154
308	78.026	0	0	0	0.994	0	0	0	17.822	0.038	96.88	B-core	814.0598
309	76.527	0	0.002	0	2.162	0	0	0.093	17.657	0	96.441	B-core	812.5265
310	77.8	0	0	0	0	0	0	0.483	18.146	0.042	96.471	B-core	810.8728
311	79.048	0	0	0.026	0	0	0	0.869	17.941	0	97.884	B-core	815.0203
312	76.95	0	0	0.007	0.15	0	0.02	0.267	17.86	0	95.254	B-core	811.6232
313	78.514	0	0	0	0.012	0.007	0	0	17.826	0	96.359	B-core	814.9678
314	74.155	0	0	0	0	0	0	0.097	22.568	0	96.82	B-core	766.6739
315	72.966	0	0	0.017	0.019	0	0	0.008	22.324	0	95.334	B-core	765.7257
316	66.476	0	0	0	0.519	0	0	0.219	20.847	0	88.061	C-core	761.2656
317	71.968	0	0	0	0.03	0	0	0.127	23.412	0.009	95.546	C-core	754.5397
318	73.036	0	0	0	0	0	0	0	23.637	0.029	96.702	C-core	755.4953

Site 4

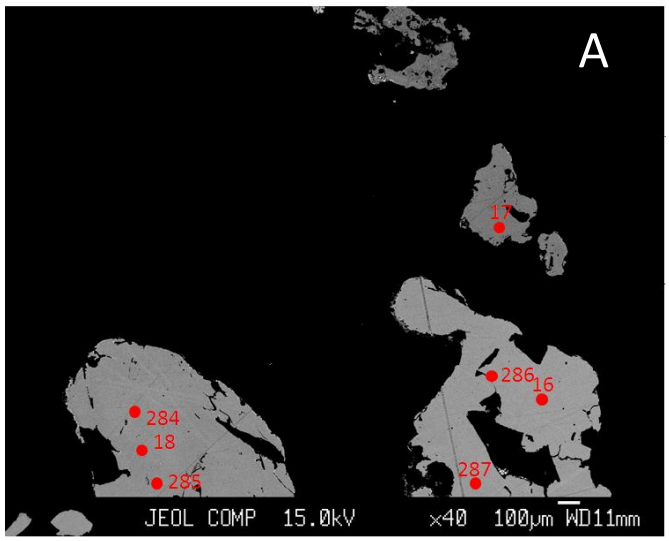
A
17
286
16
284
18
285
287
JEOL COMP 15.0kV ×40 100µm WD11mm

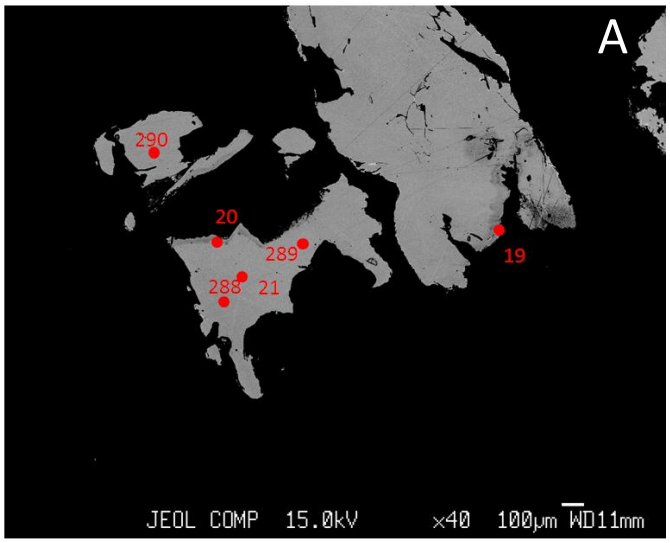
A
290
20
289
19
288
21
JEOL COMP 15.0kV ×40 100µm WD11mm

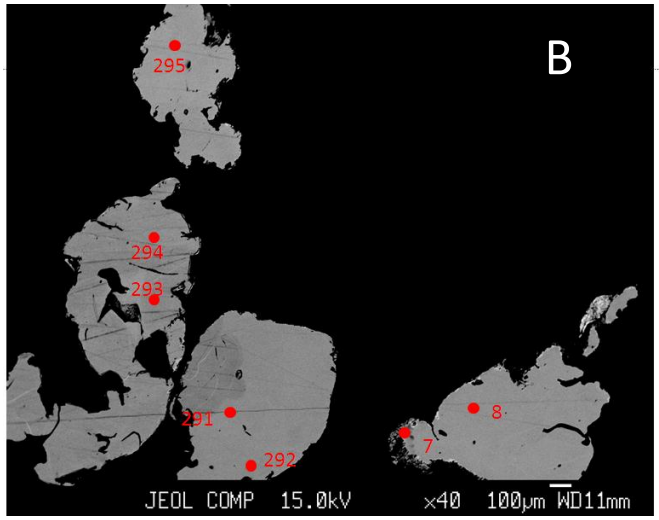
B
295
294
293
291
8
7
292
JEOL COMP 15.0kV ×40 100µm WD11mm

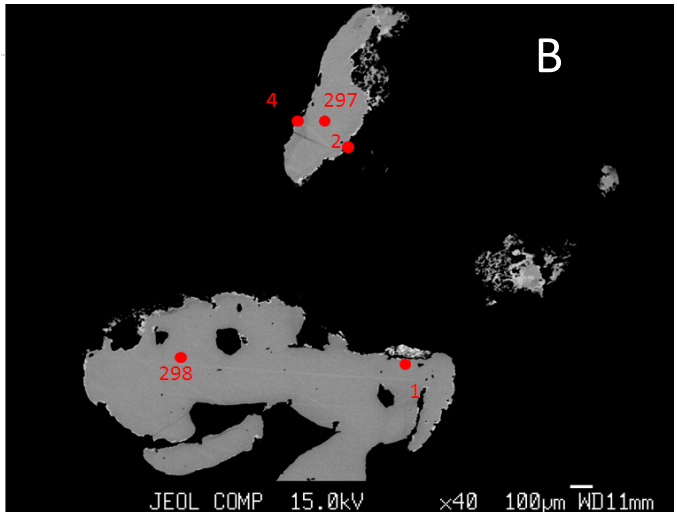
B
4
297
298
1
JEOL COMP 15.0kV ×40 100µm WD11mm

Site 4	Wt%	Wt%	Wt%	Wt%	Wt%	Wt%	Wt%	Wt%	Wt%	Wt%	Wt%		
No.	Au	S	As	Fe	Hg	Sb	Ni	Pb	Ag	Cu	Total	Comment	
2	94.892	0	0.01	0	0.091	0.03	0	0.052	1.853	0	96.928	C-rim	980.8466
3	69.399	0	0	0.002	0	0	0	0.078	24.29	0.005	93.774	C-core	740.738
4	69.457	0	0.026	0	0	0	0	0.035	24.462	0	93.98	C-core	739.5415
5	67.028	0	0	0	0	0	0.03	0.02	26.234	0	93.312	B-rim	718.7064
6	67.708	0	0	0.007	0.061	0	0	0.005	26.22	0	94.001	B-core	720.85
7	68.372	0	0	0	0.207	0	0	0	25.675	0	94.254	B-rim	726.9982
8	67.486	0	0	0	0	0	0	0	24.721	0.034	92.241	B-core	731.8967
9	72.138	0.006	0	0	0.054	0	0	0	21.535	0.013	93.746	B-core	770.1045
10	77.11	0	0	0	0.05	0	0.01	0.081	16.476	0.005	93.732	B-rim	823.948
11	77.462	0	0.013	0.018	0	0	0	0	16.374	0	93.867	B-rim	825.5041
12	78.121	0	0	0	0.013	0	0.082	0	16.623	0.042	94.881	B-core	824.5483
13	64.554	0	0	0	5.63	0	0	0	22.261	0	92.445	B-core	743.5812
14	68.739	0	0.006	0	0	0.003	0	0	26.395	0.035	95.178	B-core/dark area	722.5492
15	67.864	0	0	0	0	0	0.024	0	25.908	0.037	93.833	B-core	723.7128
16	73.736	0	0	0	0	0	0.008	0	22.079	0.002	95.825	A-core	769.5664
17	61.927	0	0	0.022	0	0	0.023	0	32.683	0	94.655	A-core	654.5503
18	71.417	0	0.011	0.006	0	0.026	0.019	0.019	23.538	0	95.036	A-core	752.1142
19	70.171	0.006	0	0	0.165	0	0	0	24.218	0	94.56	A-rim	743.4235
20	71.163	0	0	0.016	0	0	0	0	22.373	0.011	93.563	A-rim	760.8087
21	71.078	0	0	0	0.094	0	0	0	22.447	0.012	93.631	A-core	759.9893
284	70.722	0	0	0	0	0	0	0.068	24.354	0	95.144	A-core	743.847
285	72.631	0.006	0	0	0.036	0	0	0	23.645	0	96.318	A-core	754.404
286	72.953	0	0	0	0	0	0	0.069	22.482	0	95.504	A-core	764.426
287	71.678	0	0	0	0	0	0	0	22.105	0	93.783	A-core	764.2963
288	72.142	0	0.009	0.004	0.076	0	0.033	0	23.224	0.044	95.532	A-core	756.4751
289	72.985	0.017	0	0	0	0	0	0	22.775	0	95.777	A-core	762.1658
290	72.156	0	0	0.004	0	0	0.013	0	22.553	0.003	94.729	A-core	761.8706
291	69.982	0	0	0.004	0	0	0	0	27.125	0	97.111	B core	720.669
292	71.544	0.002	0	0	0	0	0.011	0.058	26.864	0	98.479	B core	727.0141
293	67.877	0	0	0	3.797	0	0	0.062	24.406	0	96.142	B core	735.5309
294	66.922	0	0	0.026	5.806	0	0	0.186	23.516	0	96.456	B core	739.9766
295	70.112	0	0	0.009	4.089	0	0	0.105	21.877	0	96.192	B core	762.1781
296	70.127	0	0	0	4.103	0	0	0.194	21.747	0	96.171	B core	763.2954
297	70.511	0	0	0.016	0.104	0	0	0.095	25.091	0.025	95.842	C-core	737.5473

Site 5

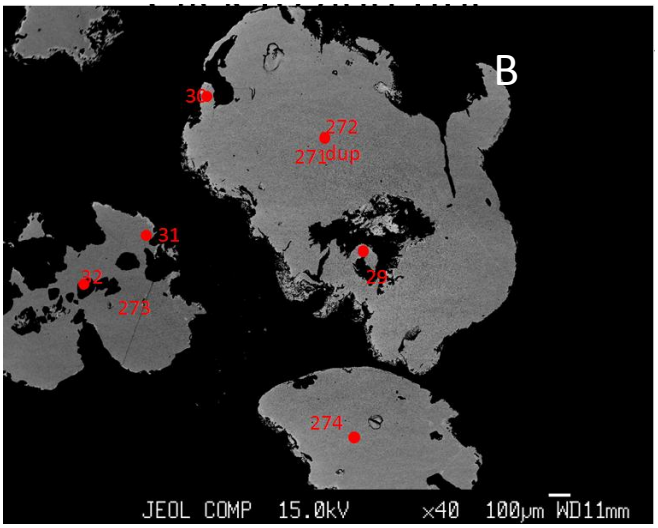
B
30
272
271dup
31
32
273
29
274
JEOL COMP 15.0kV ×40 100µm WD11mm

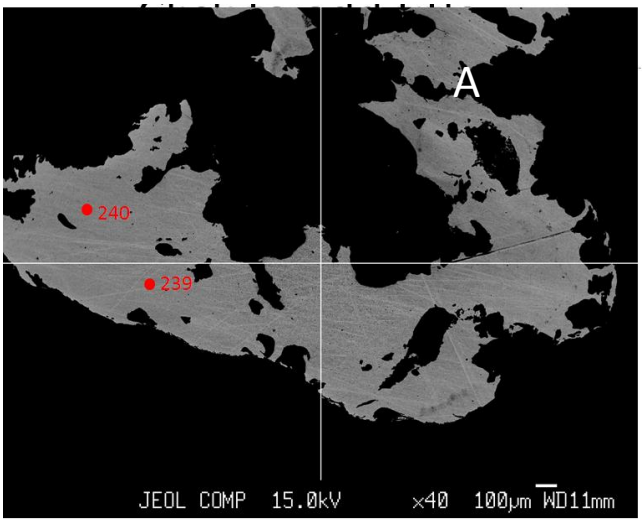
A
240
239
JEOL COMP 15.0kV ×40 100µm WD11mm

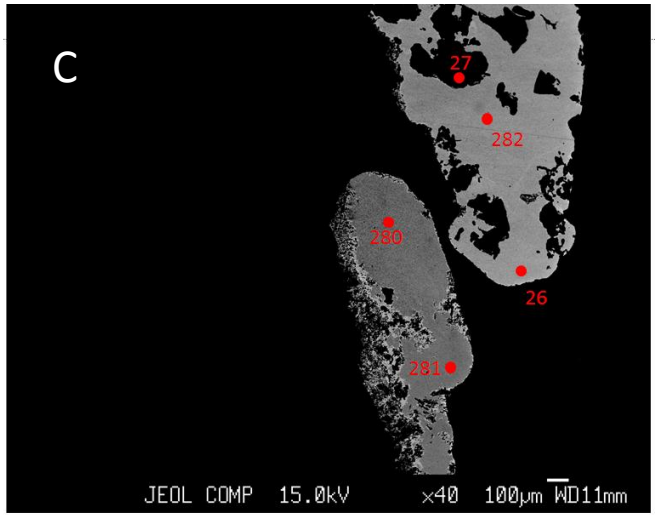
C
27
282
280
26
281
JEOL COMP 15.0kV ×40 100µm WD11mm

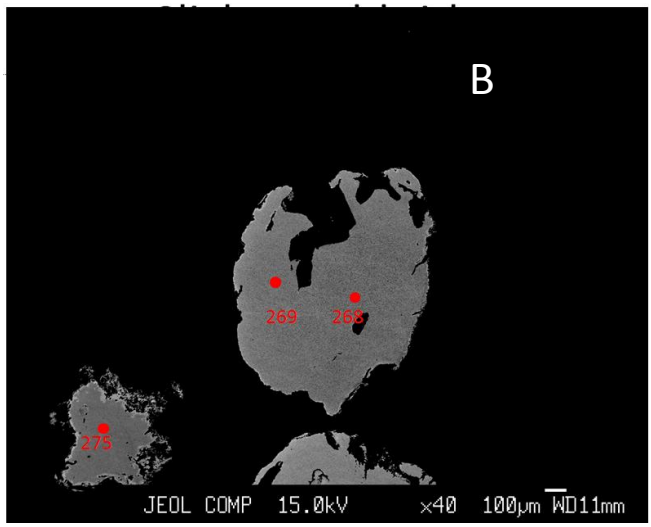
B
269
268
275
JEOL COMP 15.0kV ×40 100µm WD11mm

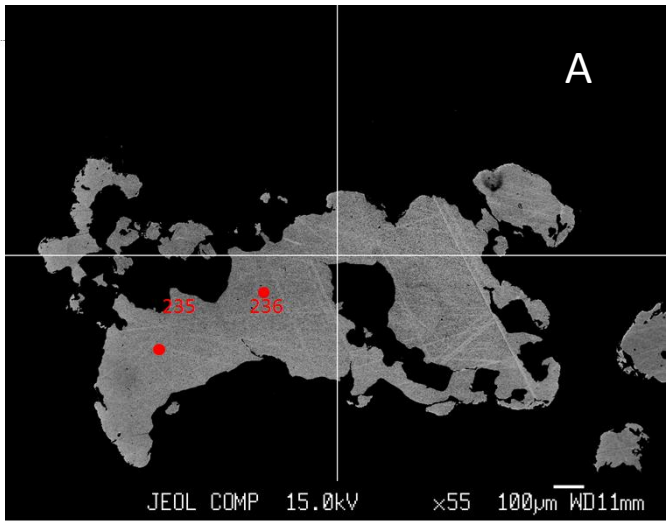
A
235
236
JEOL COMP 15.0kV ×55 100µm WD11mm

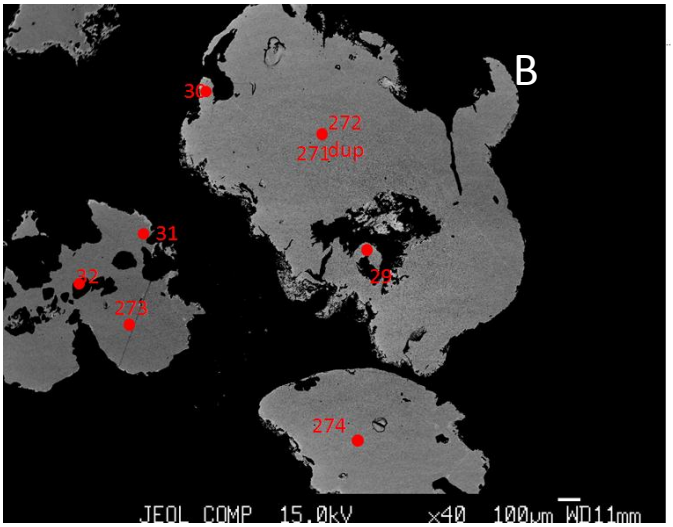
B
30
272
271dup
31
32
273
29
274
JEOL COMP 15.0kV ×40 100µm WD11mm

Site 5	Wt%	Wt%	Wt%	Wt%	Wt%	Wt%	Wt%	Wt%	Wt%	Wt%	Wt%		
No.	Au	Wt% S	As	Fe	Hg	Sb	Ni	Pb	Ag	Cu	Total	Spot	Fineness
22	78.133	0	0	0	0	0	0	0.084	14.145	0	92.362	C-core	846.7132
23	80.966	0	0	0.007	0.042	0	0	0.133	14.351	0	95.499	C-rim	849.4392
24	58.924	0.021	0.014	0	0.338	0	0.052	0.078	35.566	0	94.993	C-core	623.6004
25	55.414	0.044	0.018	0.016	0.09	0	0	0.074	37.92	0	93.576	C-rim	593.7172
26	93.507	0	0	0.031	0	0	0.003	0	1.516	0	95.057	C-rim	984.046
28	81.17	0	0	0	0.352	0	0.025	0	12.781	0	94.328	C-core	863.961
30	86.444	0	0	0	0	0	0	0.004	9.305	0.012	95.765	B-core	902.8188
269	80.801	0	0	0.02	0.166	0	0	0.023	15.679	0.003	96.692	B-core	837.4896
270	73.993	0	0.036	0	0.067	0	0.005	0.042	22.95	0	97.093	B-core	763.2629
271	86.469	0	0.014	0	0	0	0	0.04	9.196	0.018	95.737	B-core	903.8729
272	86.579	0	0	0	0.018	0	0.008	0	9.094	0	95.699	B-core	904.9471
273	74.444	0	0	0	1.383	0	0	0	19.63	0.004	95.461	B-core	791.3345
274	84.499	0	0	0	0.06	0	0.028	0.019	11.831	0	96.437	B-core	877.1826
275	85.807	0	0.003	0	0.183	0	0	0.16	11.893	0.011	98.057	B-core	878.2702
276	82.757	0	0	0	0.143	0	0	0.444	14.433	0.042	97.819	C-core	851.4971
277	82.505	0	0.028	0	0.208	0	0.007	0	14.491	0	97.239	C-core	850.6021
278	60.886	0	0	0	0.053	0	0	0	35.904	0	96.843	C-core	629.0526
279	59.211	0	0	0	0.249	0	0.001	0.174	34.433	0	94.068	C-core	632.2989
280	66.91	0	0	0	0	0	0	0	28.474	0	95.384	C-core	701.4803
281	66.102	0.008	0	0.003	0.276	0	0	0.223	28.86	0.004	95.476	C-core	696.089
282	80.605	0	0	0	0.3	0.018	0.008	0.272	13.751	0.057	95.011	C-core	854.2647
283	81.022	0	0	0	0.203	0	0	0.005	13.181	0.006	94.417	C-core	860.0788
230	57.222	0.007	0	0.005	0.953	0	0	0.154	34.278	0	92.619	A-core	625.377
231	58.87	0.001	0.028	0.012	0	0	0	0.271	33.844	0.005	93.031	A-core	634.9634
232	82.021	0	0	0.004	0.032	0	0	0	18.339	0	100.396	A-core	817.2678
233	59.932	0	0.013	0	0	0	0.023	0.287	33.457	0	93.712	A-core	641.7458
234	73.595	0	0	0	0	0	0	0	23.174	0	96.769	A-core	760.5225
235	89.866	0	0.002	0	0.332	0	0	0	7.179	0.048	97.427	A-core	926.024
236	89.435	0	0	0	0.023	0	0	0	7.145	0	96.603	A-core	926.0199
237	85.992	0	0	0	0	0.042	0.014	0.079	12.05	0.023	98.2	A-core	877.0935
238	85.69	0	0	0.004	0	0.047	0	0	11.91	0	97.651	A-core	877.9713
239	94.081	0	0.039	0	0	0	0	0	5.363	0	99.483	A-core	946.0702
240	89.369	0	0	0.018	0.272	0	0	0	5.684	0.011	95.354	A-core	940.2018
241	91.555	0	0.006	0	0.065	0	0	0	5.354	0.043	97.023	A-core	944.7523
242	92.24	0	0	0	0	0	0	0.092	5.656	0	97.988	A-core	942.2244

SITE 6

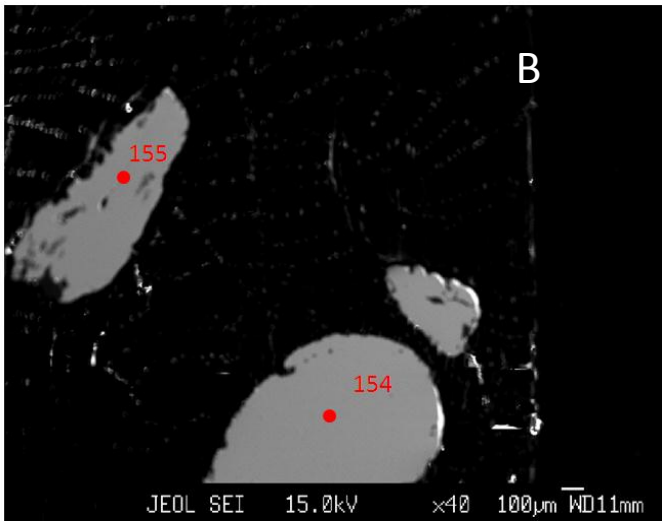
B
155
154
JEOL SEI 15.0kV x40 100µm WD11mm

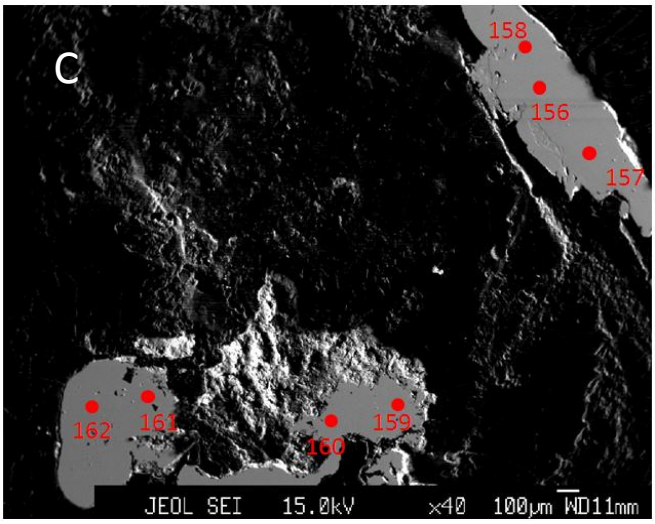
C
158
156
157
162
161
160
159
JEOL SEI 15.0kV x40 100µm WD11mm

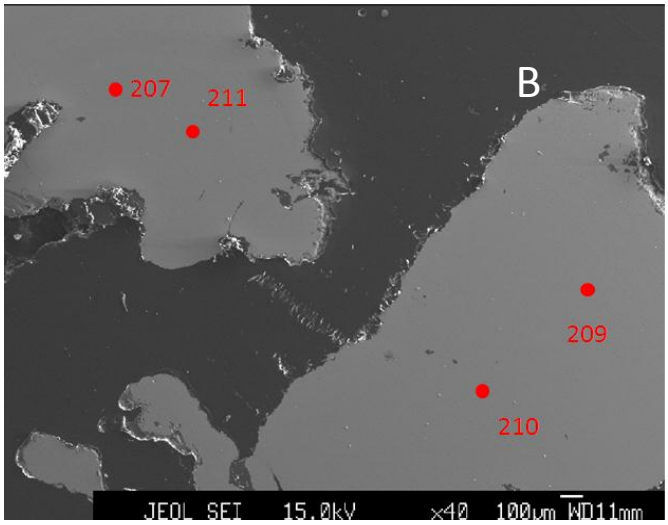
B
207
211
209
210
JEOL SEI 15.0kV x40 100µm WD11mm

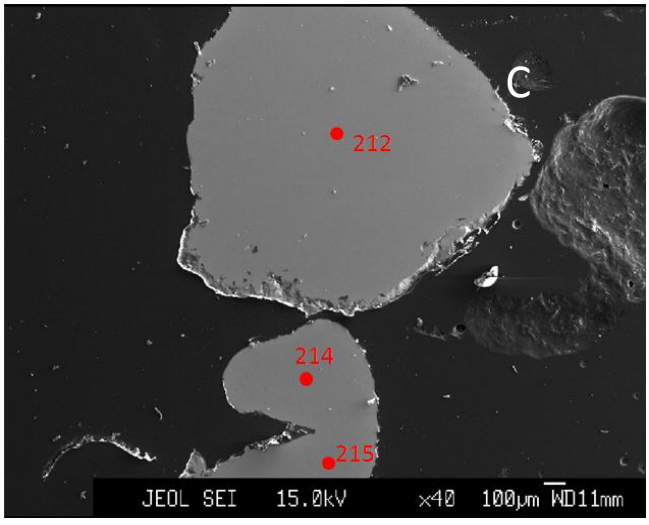
C
212
214
215
JEOL SEI 15.0kV x40 100µm WD11mm

Site 6	Wt%	Wt%	Wt%	Wt%	Wt%	Wt%	Wt%	Wt%	Wt%	Wt%	Wt%		
No.	Au	S	As	Fe	Hg	Sb	Ni	Pb	Ag	Cu	Total	Comment	
154	76.755	0	0.007	0	0.42	0	0	0	19.239	0	96.421	A-core	799.5812
155	76.532	0	0.032	0	0.37	0	0.03	0.13	19.667	0	96.764	A-core	795.5592
156	84.939	0	0	0	0.17	0.04	0	0.018	12.188	0.018	97.378	C-core	874.5148
157	84.092	0	0.003	0	0.25	0	0.00	0	12.162	0	96.514	C-core	873.6468
158	0.248	0	0	0	0.02	0.75	0.01	92.60	0	0.02	93.655	Inclusion	
159	97.38	0	0	0.006	0	0	0.02	0	0.872	0	98.278	C-core	991.1249
160	85.772	0	0	0	0.123	0	0	0.012	11.087	0	96.994	C-core	885.5346
162	86.527	0	0	0	0	0	0	0	11.624	0	98.151	C-core	881.5702
163	84.751	0.03	0	0.02	0	0.00	0	0	11.708	0	96.508	C-core	878.622
207	80.989	0	0	0.1	0.2	0	0.041	0	15.152	0	96.379	A-core	842.3981
208	81.267	0	0.006	0.02	0.03	0	0	0	15.108	0	96.424	dup (207)	843.2374
209	86.536	0	0.017	0	0	0	0	0	9.365	0	95.918	A-core	902.3472
210	89.825	0	0	0.03	0	0	0	0	9.481	0.043	99.376	A-core	904.5274
211	78.89	0	0.003	0.01	0	0	0	0.316	14.664	0.059	93.939	A-core	843.2563
212	66.224	0	0	0	0.3	0	0	0.221	5.609	0.039	72.385	C-core	921.9161
213	64.027	0	0.018	0	0.46	0	0	0.367	5.624	0.023	70.526	dup (212)	919.2546
214	62.586	0	0	0	0.3	0	0	0.463	6.469	0	69.817	C-core	906.321
215	82.297	0	0	0	0	0	0.04	0.639	8.077	0.078	91.126	C-core	910.627